

NPS ARCHIVE
1959
MITCHELL, L.

BOUNDARY LAYER SUCTION TO CONTROL
BOW VIBRATIONS INDUCED
BY ANTI-PITCHING FINS

LELAND G. MITCHELL
AND
ROSS E. SUGG

BOUNDARY LAYER SUCTION TO CONTROL BOW VIBRATIONS
INDUCED BY ANTI-PITCHING FINS

by

LELAND G. MITCHELL, LIEUTENANT, UNITED STATES NAVY

B.S., U. S. Naval Academy

(1952)

and

ROSS E. SUGG, LIEUTENANT, UNITED STATES NAVY

B.S., U. S. Naval Academy

(1952)

SUBMITTED IN PARTIAL FULFILLMENT OF THE REQUIREMENTS

FOR THE DEGREE OF NAVAL ENGINEER

AND THE DEGREE OF

MASTER OF SCIENCE IN NAVAL ARCHITECTURE

AND MARINE ENGINEERING

at the

MASSACHUSETTS INSTITUTE OF TECHNOLOGY

May, 1959

BOUNDARY LAYER SUCTION TO CONTROL BOW VIBRATIONS
INDUCED BY ANTI-PITCHING FINS

By Leland G. Mitchell, Lt., U.S.N. and Ross E. Sugg, Lt., U.S.N.

Submitted to the Department of Naval Architecture and Marine Engineering on May 25, 1959 in partial fulfillment of the requirements for the Master of Science degree in Naval Architecture and Marine Engineering and the Professional degree, Naval Engineer.

ABSTRACT

Interest in the use of anti-pitching fins on ships has been increasing in recent years. It has been found that although bow anti-pitching fins appreciably reduce pitch amplitudes, serious transverse bow vibrations have accompanied their use. These vibrations are especially serious when the ship operates in heavy seas and appear to be induced when the ship's bow is pitching down.

One explanation of the cause of these vibrations is that they result from flow separation on the top surface of the fin when the hydrodynamic angle of attack exceeds the angle of breakdown. This causes asymmetric impulses to be transmitted to the ship's bow structure causing it to vibrate at resonant frequency.

This thesis investigated using boundary layer suction to delay boundary layer breakdown and extend the angle of breakdown beyond the hydrodynamic angle of attack which could be expected. A model of a 17,800 ton passenger ship was instrumented for measuring transverse bow vibrations and applying boundary layer suction to a fin mounted on the bow. Runs were made in regular waves at the MIT towing tank with a fin having an aspect ratio equal to 4 mounted on the base line of the model. In addition, runs were made with a larger fin having an aspect ratio equal to 2 mounted 3 inches below the base line. It was found for the AR4 fin that very small vibrations occurred in moderate waves and that violent vibrations were recorded only when pitch amplitudes were sufficient for the fin to approach or penetrate the free surface. Accompanying the violent vibrations were large air bubbles formed in the top surface of the fin which then collapsed and passed down the side of the ship. Only minor vibrations were recorded for the AR2 fin on which no bubble formation was observed and the fin did not approach the free surface. The application of boundary layer suction appeared to have no measurable effects upon the recorded vibrations for either fin.

In addition, fin lift curves were experimentally determined for several suction rates and the results were compared with a theoretical calculation of hydrodynamic ship fin angle of attack. These calculations and measurements showed that boundary suction could be expected to prevent flow separation and delay the angle of breakdown on a ship operating in only moderate seas and would not be effective in heavy seas. Transverse bow vibrations could be expected at pitch amplitudes sufficient to cause the fin to approach emergence at the free surface.

Thesis Supervisor: Martin A. Abkowitz, Ph.D.
Title: Associate Professor of Naval Architecture

ACKNOWLEDGEMENTS

The authors wish to gratefully acknowledge the following people:

Professor Martin A. Abkowitz, Thesis Supervisor, for his many recommendations and interest in our thesis. His encouragement helped lift our spirits when our disappointments overshadowed our enthusiasm.

Mr. J. E. Kerwin for his assistance and cooperation in conducting our experimental work at the M.I.T. Towing Tank.

Mr. Ray E. Johnson for his help and recommendations in the construction of the fins and for his guidance in the use of the equipment in the M.I.T. Propeller Tunnel.

TABLE OF CONTENTS

	<u>Page</u>
Abstract	ii
Acknowledgements	iii
Table of Contents	iv
List of Figures	vi
List of Tables	viii
Nomenclature	x
I. Introduction	1
II. Procedure	5
A. Theoretical calculations of heave and pitch at constant speed with no hydrofoil	5
B. Calculation of the effects of the hydrofoils	11
C. Calculation of wave heights at which model bow immerses and the fin emerges for $\lambda/L = 1.25$	13
D. Calculation of fin lift coefficients as a function of angle of attack	13
E. Effective aspect ratio = 4 fin (AR = 4.0)	14
F. Effective aspect ratio = 2 fin (AR = 2.0)	16
G. Calibration of fins in Propeller Tunnel	17
III. Results	20
A. AR = 4.0 fin	20
B. AR = 2.0 fin	20
C. Theoretical calculations	21
D. Motion picture data	21
IV. Discussion of Results	22
A. The effect of boundary layer control on model bow vibrations for the AR = 4.0 fin	22

TABLE OF CONTENTS (Continued)

	<u>Page</u>
B. The AR = 2.0 fin	24
C. The effect of boundary layer control on fin lift curves . .	26
D. Motion measurements of the model with fins installed . . .	27
1. Motions as a function of wave length	27
2. Motions as a function of wave height	28
E. Theoretical calculations	29
V. Conclusions	30
VI. Recommendations	31
VII. Appendix	51
A. Details of procedure	52
A. Manufacture and installation of fins	52
B. Details of model instrumentation	56
C. Description of the apparatus for calibrating fins . . .	59
D. Details of Towing Tank instrumentation	61
B. Summary of data and calculations	64
A. Theoretical motion calculation for Model B prototype . .	64
B. Adjustment of radius of gyration of the model	97
C. Sample calculation of lift coefficient	99
D. Sample calculation of the hydrodynamic fin angle of attack from ship motions	100
E. Sample calculation of bow immersion	102
C. Supplementary discussion	104
A. Boundary layer separation	104
B. Vortex ventilation	105
D. Bibliography	107

LIST OF FIGURES

<u>Figure</u>	<u>Title</u>	<u>Page</u>
I	Description of notations	32
II	Model B prototype section area vs. distance of section from \bar{X}	33
III	Circular cylinder $\frac{\omega_e^2 B}{2g}$ vs. K_L	34
IV	Model B prototype SK_2K_L vs. ζ for $\lambda/L = 1.25$	35
V	Theoretical graphical solution of fin angle of attack vs. wave height	36
VI	Strain gage calibration curves and correction curves for tube	37
VII	MIT Model B pitch vs. λ/L AR = 4.0	38
VIII	MIT Model B heave vs. λ/L AR = 4.0	39
IX	Bow vibrations with model in water as a result of a light tap on bow	40
X	Vibrations of the bow for fin (eff. AR = 4.0) mounted on the base line in waves of $\lambda = 5.0$ Ft. and $2h = 2.5$ in. without (A) and with (B) boundary layer control	40
XI	Vibrations of the bow for fin (eff. AR = 4.0) mounted at the base line in waves of $\lambda = 6.0$ Ft. and $2h = 2.3$ in. without (A) and with (B) boundary layer control.	41
XII	Vibrations of the bow under the same conditions ($\lambda = 6.0$ Ft. and $2h = 2.0$ in.) for (A) fin of eff. AR = 4.0 and 2.12% of the waterplane area with no boundary layer control, (B) fin (A) with boundary layer control, and (C) fin of eff. AR = 1.37 and 5.95% of the waterplane area with no boundary layer control. Both fins were mounted at the baseline of the model.	42
XIII	NACA-0018 foil - angle of attack vs. lift coefficient eff. AR = 4.0	43
XIV	Heave as a function of wave height for $\lambda = 600$ Ft. and constant speed. AR = 2.0 fin.	44
XV	Pitch as a function of wave height for $\lambda = 600$ Ft. and constant speed. AR = 2.0 fin.	45

LIST OF FIGURES (Continued)

<u>Figure</u>	<u>Title</u>	<u>Page</u>
XVI	NACA-0018 foil - angle of attack vs. lift coefficient. Eff. AR = 2.0	46
XVII	Vibrations of the bow for fin (eff. AR = 2.0) mounted 3 inches below the base line in waves of $\lambda = 6.0$ Ft. and $2h = 2.0$ in. without (A) and with (B) boundary layer control	47
XVIII	Vibrations of the bow for fin (eff. AR = 2.0) mounted 3 inches below the base line in waves of $\lambda = 6.0$ Ft. and $2h = 0.8$ in. without (A) and with (B) boundary layer control	48
XIX	View of AR = 4.0 fin showing full bubble formation for $\lambda = 6.0$ Ft. and $2h = 2.3$ in.	49
XX	Lift curve for effective AR = 3.0 fin	50
XXI	Sketch showing construction of the AR = 4.0 fin	53
XXII	View of AR = 4.0 fin installed on model	54
XXIII	View of interior of the model	54
XXIV	Sketch showing construction of the AR = 2.0 fin	55
XXV	Model in the Towing Tank with "fishing pole" attached	57
XXVI	Fin of eff. AR = 2.0 installed on the model with the arrangement used for introducing dye ahead of the fin	57
XXVII	View of dynamometer end of Towing Tank	58
XXVIII	Baldwin Strain Indicator and fin mounted on apparatus used to measure the lift versus angle of attack	58
XXIX	Sketch of strain gage arrangement	59
XXX	Sketch of calibration apparatus	60
XXXI	Photographic method used to determine pitch and heave of model	62
XXXII	Description of notation used in the calculation of model radius of gyration	97

LIST OF TABLES

<u>Table</u>	<u>Title</u>	<u>Page</u>
I	Properties of hull	64
II	Calculation of values of sines and cosines for equation (1) for heave	65
III	Calculation of values of sines and cosines for equation (1) for pitch	65
IV	Ship speed and frequency	66
V	K_4 Values	66
VI	K_2 Values	67
VII	Calculation of I in equations (2) and (3)	67
VIII	Calculation of II in equations (2) and (3)	68
IX	Calculation of III in equations (2) and (3)	68
X	Calculation of IV in equations (2) and (3)	69
XI	Calculation of V in equations (2) and (3)	70
XII	Calculation of $\int \frac{B}{2} \sin \frac{2\pi x}{\lambda} \left(\xi + \frac{1}{\pi} \frac{dS}{d\xi} \right) dx$ in equation (3)	70
XIII	Calculation of $\int \frac{B}{2} (1 + K_2 K_4) \sqrt{\frac{2S}{\pi}} \sin \frac{2\pi x}{\lambda} \left(\xi + \frac{1}{\pi} \frac{dS}{d\xi} \right) dx$ in equation (3)	71
XIV	Calculation of $\int \frac{B}{2} (1 + K_2 K_4) S \sin \frac{2\pi x}{\lambda} \left(\xi + \frac{1}{\pi} \frac{dS}{d\xi} \right) dx$ in equation (3)	72
XV	Calculation of $\int \frac{B}{2} (1 + K_2 K_4) \frac{1}{\sqrt{2\pi S}} \frac{dS}{d\xi} \cos \frac{2\pi x}{\lambda} \times \left(\xi + \frac{1}{\pi} \frac{dS}{d\xi} \right) dx$ in equation (3)	72
XVI	Calculation of $\int \frac{B}{2} (1 + K_2 K_4) \frac{dS}{d\xi} \cos \frac{2\pi x}{\lambda} \left(\xi + \frac{1}{\pi} \frac{dS}{d\xi} \right) dx$ in equation (3)	73
XVII	Pitch and heave constants	73
XVIII	Calculation of values to determine a, d, D, A in equation (1)	74

LIST OF TABLES (Continued)

<u>Table</u>	<u>Title</u>	<u>Page</u>
XIX	Calculation of values of coefficient b in equation (1)	74
XX	Calculation of values for determining coefficients c and g in equation (1)	75
XXI	Calculation of values for determining coefficient e in equation (1)	75
XXII	Calculation of heaving force and pitching moment in equation (1)	76
XXIII	Final calculation of values of coefficients of equation (1)	77
XXIV	Calculation of heave and pitch for ship without fins	79
XXV	Calculation of effect of hydrofoil on the ship motions for effective fin $AR = 4.0$	81
XXVI	Calculation of effect of hydrofoil on the ship motions for effective fin $AR = 2.0$	86
XXVII	Summary of theoretical calculations	90
XXVIII	Wave conditions for $AR = 4.0$ fin	91
XXIX	Summary of results for model with $AR = 4.0$ fin for varying wave lengths	92
XXX	Summary of results for model with $AR = 4.0$ fin	93
XXXI	Summary of results for $AR = 2.0$ fin for $\lambda = 600$ Ft.	94
XXXII	Summary of results for $\lambda = 600$ Ft. at varying wave heights for $AR = 2.0$ fin	95
XXXIII	Summary of descriptive data for NACA-0018 air foils used in this thesis	96
XXXIV	Summary of descriptive data for model and ship ($\lambda = 100$)	96
XXXV	Strain readings and resultant lift coefficients	99

NOMENCLATURE

<u>Symbol</u>	<u>Meaning</u>
a, b, c	Coefficients of Eqs. (1)
d, e, g	Coefficients of Eqs. (1)
A, B, C	Coefficients of Eqs. (1)
D, E, G	Coefficients of Eqs. (1)
A	Projected total area of fin
\bar{A}	Ratio of waves made by ship to amplitude of heaving motion
AR	Aspect ratio of hydrofoil
B	Local beam
c	Wave celerity
C_L	Lift coefficient
C_S	Section inertia coefficient
C.G.	Center of gravity
E.H.P.	Effective towed horsepower
F_h	Heaving force
F	Exciting force
F'	Lifting force contributed by fin which is $= f(V_w/V_s)$
g	Acceleration of gravity
h	Wave amplitude
J	Longitudinal moment of inertia of ship about C.G.
K_2	Added mass coefficient in two dimensional vertical flow about a ship section
K_h	Correction coefficient for the effect of free water surface
l	Lever arm of the hydrofoil
L	Ship length

NOMENCLATURE (Continued)

<u>Symbol</u>	<u>Meaning</u>
LBP	Length between perpendiculars
LCB	Longitudinal center of buoyancy
\bar{M}	Pitching moment vector
M	Exciting moment
M'	Pitching moment contributed by fin which is $= f(V_w/V_s)$
m	Mass of the ship
m _i	Virtual mass of the hydrofoil
N(ξ)	Vertical damping force per unit body length per Ft. per sec.
P, Q	Groupings of coefficients for Eqs. (4) and (5)
R, S	Groupings of coefficients for Eqs. (4) and (5)
S	Local section area
s	Station spacing
s'	Projected area of fin over which boundary layer control is applied
SM	Simpson's Multiplier
V _e	Velocity of wave encountered
V _m	Model speed
V _s	Ship speed
V _w	Vertical wave orbital velocity
x	Horizontal coordinate with respect to wave nodal point
y	Draft of ship
z	Vertical coordinate
\bar{z}	Complex amplitude of the heaving motion
α	Angle of attack

NOMENCLATURE (Continued)

<u>Symbol</u>	<u>Meaning</u>
α_0	Angle of installation of hydrofoil
θ	Pitch angle
$\bar{\theta}$	Complex amplitude of pitching motion
λ	Wave length
ξ	Longitudinal coordinate with respect to the C.G.
ρ	Water density
ω_e	Frequency of wave encounter

I. INTRODUCTION

In recent years, several types of ships have been constructed with anti-pitching fins installed on their bow sections. Experimental studies (3) have demonstrated that these fins can effectively provide sufficient damping to reduce pitch at resonance up to 67 per cent, depending upon the geometric characteristic of the fins, the ship form, and the wave conditions in which the tests are conducted. The ships on which bow fins have been installed have been plagued by various degrees of transverse bow vibrations and in at least one case, these vibrations were of such severity that the fins were removed.

Reference (3) suggests that the transverse bow vibrations are caused by asymmetrical flow separation on the top surface of the fin which occurs as the bow pitches down. The flow separation results in air bubbles which collapse at slightly different times on each side of the bow. The collapse of these bubbles causes asymmetrical impulses on the bow structure which makes it vibrate at damped resonant frequency. Reference (3) also suggests that boundary layer suction may be applied to the top surface of the fin to prevent the separation of flow over the fin surface.

It is the purpose of this thesis to investigate the effects of using boundary layer suction to control bow vibrations induced by anti-pitching fins. Although considerable information on boundary layer control appears in NACA literature, almost all of this is for air foils tested in wind tunnels at Reynolds numbers considerably above those used in ship model testing. However, in (14) boundary layer control by suction was applied to model roll stabilization fins to compensate

for "scale effects." "Scale effects" are caused by a practical requirement that small geometrically similar models cannot be tested in water while maintaining both constant Froude and Reynolds numbers. Since for ship model testing, equivalency of Froude number is maintained between ship and model, model tests are therefore conducted at Reynolds numbers considerably lower than those that occur for the ship prototype. Applied to this situation, "scale effects" would cause flow separation on model fins to occur sooner and reduce the fin angles of breakdown and maximum lift coefficients. Therefore, without boundary layer control, flow separation on the model fins can be expected to occur in more moderate wave conditions than would occur in the ship prototype. Reference (14) demonstrated that boundary layer suction can be used to increase the maximum lift coefficient and angle of breakdown for hydrofoils tested at low Reynolds numbers. If it is assumed that flow separation phenomenon induces undesirable bow vibrations on ship anti-pitching fins, it should be possible to test the model in wave conditions that produce these vibrations when suction is not used. By then applying suction to reestablish unseparated flow, the undesirable bow vibrations should be reduced or eliminated.

Because of "scale effects" and correspondingly greater lift and angles of breakdown for ship fins, the breakdown on the ship could be expected in more severe wave conditions. However, by properly positioning suction slots and controlling suction rates, results similar to those obtained from model tests should be expected when the ship operates in heavy seas.

For this thesis, a wooden model of a 481.9 Ft., 17,800 ton passenger ship ($\lambda = 100$), on which severe transverse bow vibrations

induced by anti-pitching fins have actually occurred, was used. The bow was cut at the quarter point and was remounted on a steel bar tuned to vibrate at the same scaled transverse frequency as actually occurred on the ship prototype. These vibrations were measured by strain gages attached to the bar.

In this thesis two fins were used. One fin had an effective aspect ratio of 4 and an area equal to 2.12 per cent of the waterplane area. This fin was mounted at the forward perpendicular at, and parallel to, the base line. A series of runs was made in regular waves at varying wave heights and wave lengths. At each wave condition, runs were made with and without boundary layer control and the model motions, as well as bow vibrations, were measured. In all runs made with this fin a constant towing force was used which corresponded to a ship still water speed of 17.5 knots.

A second fin was constructed with an effective aspect ratio of 2 and an area equal to 8.7 per cent of the waterplane area. This fin was suspended at a prototype depth of 25 feet below the base line. All runs made with this fin were in regular waves having a wave length to model length ratio (λ/L) equal 1.25 at varying wave heights. These runs were made at constant speed corresponding to a ship speed of 11 knots. As with the small fin, model motions and bow vibrations were measured in each wave condition, both with and without boundary layer suction.

In order to determine the influence of various suction rates on fin lift and angle of breakdown, each fin was calibrated in the propeller tunnel by measuring the lift as a function of angle of attack at

varying suction rates. Combining this information with a theoretical calculation of hydrodynamic angles of attack for the fin when installed upon the model, the wave conditions at which boundary layer suction may be effective could be predicted.

Since the theoretical calculation also included a calculation of ship heave and pitch, a comparison of computed and measured model motions could be made.

II. PROCEDURE

A. Theoretical calculations of heave and pitch at constant speed with no hydrofoil.

The sample calculations for $\lambda/L = 1.25$ at a constant speed are given in Appendix B.

In reference (10) the equations of motion for a ship are given as:

$$\begin{aligned} a\ddot{Z} + b\dot{Z} + cZ + d\ddot{\theta} + e\dot{\theta} + g\theta &= F_e j\omega_e t \\ A\ddot{\theta} + B\dot{\theta} + C\theta + D\ddot{Z} + E\dot{Z} + GZ &= M_e j\omega_e t \end{aligned} \quad (1)$$

where F and M are vectorial quantities representing exciting forces and moments due to waves; ω_e is the angular frequency of wave encountered; Z and θ are linear and angular displacements respectively. The sign convention used is given in Figure I for the formulas (1).

- a is the mass of the ship plus the virtual mass accelerated in the vertical direction.
- b is the damping due to heave velocity.
- c is buoyancy, lack or excess, at a position in heave.
- d is the mass accelerated in the vertical direction due to pitching.
- e is the vertical damping due to pitching angular velocity.
- g is the buoyancy, lack or excess, at a position in pitch.
- A is the mass moment of inertia of the ship plus that of the vertical mass due to pitching around the C.G.
- B is the moment of the damping around the C.G. due to pitching angular velocity.
- C is the moment around the C.G. due to buoyancy, lack or excess, at a position in pitch.

D is the mass moment of inertia accelerated around the C.G. in heaving.

E is the damping moment of inertia around the C.G. due to heaving velocity.

G is the moment around the C.G. due to lack or excess of buoyancy at a position in heave.

Calculation of F:

According to reference (10), the maximum heaving force F occurs when the wave crest is at station 11 and is given as

$$F = 2\rho gh \left[I - \frac{\pi^2}{2\lambda} II + \frac{4\pi}{\lambda^2} III + \frac{\pi V_s}{4c} IV - \frac{4V_s}{3\lambda c} V \right] \quad (2)$$

where

$$\begin{aligned} I &= \int \frac{B}{2} \sin \frac{2\pi x}{\lambda} dx \\ II &= \int \frac{B}{2} (1 + K_2 K_4) \sqrt{\frac{2S}{\lambda}} \sin \frac{2\pi x}{\lambda} dx \\ III &= \int \frac{B}{2} (1 + K_2 K_4) S \sin \frac{2\pi x}{\lambda} dx \\ IV &= \int \frac{B}{2} (1 + K_2 K_4) \frac{1}{\sqrt{2\pi S}} \frac{dS}{d\xi} \cos \frac{2\pi x}{\lambda} dx \\ V &= \int \frac{B}{2} (1 + K_2 K_4) \frac{dS}{d\xi} \cos \frac{2\pi x}{\lambda} dx \end{aligned}$$

and

B is the local beam in feet.

x is the distance in feet from the wave nodal point as given in Figure I.

λ is the wave length in feet.

S is the local sectional area in Ft.²

ξ is the distance from the C.G. of the section.

V_s is the ship speed in Ft. per sec.

c is the wave celerity given by the formula $c = \sqrt{\frac{g\lambda}{2\pi}}$

h is the wave height in feet.

K₂ is the added mass coefficient in two dimensional vertical flow.

K₄ is the correction for free water surface.

The values of B and S were taken from a body plan of Model B and are tabulated in Table I.

The values of $\sin \frac{2\pi x}{\lambda}$ and $\cos \frac{2\pi x}{\lambda}$ were calculated for a wave length of 600 Ft. with the wave crest located at station 11. These values are listed in Table II.

The locations of the LCG and the LCB were assumed to be at the midship section for all calculations. This is an approximation but calculations have verified that they are within one foot of the midship section.

The values of $\frac{dS}{d\xi}$ were taken from Figure II by drawing tangents at the different sections. These figures are given in Table X.

The local values of C_s were obtained from Figure XII of reference (18). K₂ was calculated by using the formula: $K_2 = C_s \frac{\pi B^2}{8S}$. These figures are listed in Table VI. The values of K₄ were read from Figure III which was drawn using data given in reference (10).

The value of V_s was taken as the ship speed in waves of $\lambda = 600$ Ft. and $2h = 16.67$ Ft. for a tow rope force equivalent to a speed of 17.5 Kts. in still water. V_s was 11 knots for the ship with small fins installed under the above conditions.

All integrations were performed using Simpson's First Rule over the

even stations, giving a value of 48.19 Ft. for the station spacing. A sample of the computations of the heaving force for a constant speed for $\lambda/L = 1.25$ is given in Table XXII.

Calculations of M:

According to reference (10), the maximum pitching moment when the wave nodal point is at station 11 is given as

$$M = \rho g h \left[\int (I) \left(\xi + \frac{1}{\pi} \frac{dS}{d\xi} \right) dx - \frac{\pi^2}{2\lambda} \int (II) \left(\xi + \frac{1}{\pi} \frac{dS}{d\xi} \right) dx + \right. \\ \left. \frac{4\pi}{\lambda^2} \int (III) \left(\xi + \frac{1}{\pi} \frac{dS}{d\xi} \right) dx + \frac{\pi V_s}{4e} \int (IV) \left(\xi + \frac{1}{\pi} \frac{dS}{d\xi} \right) dx - \right. \\ \left. \frac{4V_s}{3\lambda c} \int (V) \left(\xi + \frac{1}{\pi} \frac{dS}{d\xi} \right) dx \right] \quad (3)$$

where the nomenclature is the same as was used for the force equation (2).

It is noted that the forces are not the same as were previously calculated since the wave nodal point and not the crest is at station 11. The difference is due to the new values of $\sin \frac{2\pi x}{\lambda}$ and $\cos \frac{2\pi x}{\lambda}$ which are given in Table III.

To calculate the moments, the terms I, II, III, IV and V calculated previously were divided by their respective $\sin \frac{2\pi x}{\lambda}$ and $\cos \frac{2\pi x}{\lambda}$ and were multiplied by the new values. Then they were multiplied by $\left(\xi + \frac{1}{\pi} \frac{dS}{d\xi} \right)$ and summed by Simpson's First Rule. This procedure saved much time. A sample of the calculations for M are given in Table XXII. It should be noted here that in future calculations, since the moments lead the forces by 90° in phase, their values will be multiplied by the imaginary unit vector (j).

Calculations for the coefficients of formula (1).

A sample calculation of all the coefficients is found in Table XXIII.

$$a = m + \rho \int SK_2 K_4 d\xi$$

m is the mass of the ship equal to 1,238,260 Lbs. sec.²/Ft.

The local values of $SK_2 K_4$ are given in Table XVIII.

$$b = \int N(\xi) d\xi$$

where $N(\xi)$ is given as $\rho g^2 \bar{A}^2 / \omega_e^3$ and $\bar{A} = 2e^{-\frac{\omega_e^2 S}{gB}} \times$

$\sin(\omega_e^2 B/2g)$. The ratio S/B is given in Table I.

$$c = \rho \int g B d\xi$$

"c" is independent of speed and wave length.

$$d = D = \rho \int (SK_2 K_4) \xi d\xi$$

This value has been calculated by multiplying respective values

of $(SK_2 K_4)$ with their relative ξ and summing.

$$e = \int N(\xi) d\xi - 2V_s \rho \int (SK_2 K_4) d\xi - V_s \rho \int \xi d(SK_2 K_4)$$

$N(\xi)$ had been calculated for "b." The same values were multiplied by their local ξ and summed. The second term was obtained by multiplying the values of the second term of "a" by V_s and summing. The third term was obtained by adding the values of

$\frac{\partial SK_2 K_4}{\partial \xi} d\xi$. This was accomplished by reading off the local slopes from Figure IV and multiplying them by ξ .

$$g = \rho g \int B \xi d\xi - V_s b$$

$$A = J + \rho \int SK_2 K_4 \xi^2 d\xi$$

J is the mass moment of inertia around its C.G. It was obtained by multiplying the mass by the square of the radius of gyration.

The second term was obtained by multiplying the values used for "d" by ξ^2 .

$$B = \int N(\xi) \xi^2 d\xi - 2V_s(D) - V_s \rho \int \xi^2 d(SK_2 K_4)$$

1880 1881 1882 1883 1884

1885 1886 1887 1888 1889
1890 1891 1892 1893 1894
1895 1896 1897 1898 1899

1900 1901 1902 1903 1904
1905 1906 1907 1908 1909

1910 1911 1912 1913 1914
1915 1916 1917 1918 1919
1920 1921 1922 1923 1924

1925 1926 1927 1928 1929
1930 1931 1932 1933 1934
1935 1936 1937 1938 1939
1940 1941 1942 1943 1944

1945 1946 1947 1948 1949
1950 1951 1952 1953 1954
1955 1956 1957 1958 1959
1960 1961 1962 1963 1964

1965 1966 1967 1968 1969

The first term was obtained by multiplying the values of the first term of "e" by ξ and summing. The second term was obtained by multiplying the values used in the determination of "D" by $2V_S$. The third term was obtained by multiplying the third term of "e" by ξ and summing.

$$C = \rho g \int B \xi^2 d\xi - V_S(E)$$

The first term is constant. It was calculated in Table XX.

The computation of the second term is obtained by multiplying "E" by V_S .

$$D = d$$

This has been calculated before.

$$E = \int N(\xi) \xi d\xi - V_S \rho \int \xi d(SK_2K_4)$$

Both parts were taken from the calculation of "e."

$$G = \rho S \int B \xi d\xi$$

This is equal to the first term of "g"

Solutions for the motions at constant speed.

From reference (10) the heave vector is

$$\bar{Z} = \frac{\bar{M}Q - \bar{F}S}{QR - PS} \quad (4)$$

and the pitch vector is

$$\bar{\theta} = \frac{\bar{F}R - \bar{M}P}{QR - PS} \quad (5)$$

where \bar{F} and \bar{M} are the previously calculated force and moment vectors.

In addition

$$\begin{aligned} P &= -a\omega_e^2 + jb\omega_e + c \\ Q &= -d\omega_e^2 + je\omega_e + g \\ R &= -D\omega_e^2 + jE\omega_e + G \\ S &= -A\omega_e^2 + jB\omega_e + C \end{aligned} \quad (6)$$

Sample calculations of \bar{Z} and $\bar{\theta}$ have been presented in Table XXIV.

B. The calculation of the effects of the hydrofoils

The effect of the hydrofoil on the forces, moments and the coefficients of formula (1) was calculated. From this the new heave and pitch amplitudes were obtained. It was assumed that the lift coefficient varies linearly with the angle of attack up to the stall angle predicted for the particular hydrofoil.

The lift force " F_L " of the hydrofoil was calculated by

$$F_L = 1/2 \rho \frac{\partial C_L}{\partial \alpha} \left(\theta - \frac{\dot{Z}}{V_s} - \frac{\dot{\theta} l}{V_s} + \frac{V_w}{V_s} \right) A V_s^2 \quad (7)$$

where A is the projected area of the hydrofoil, $\frac{\partial C_L}{\partial \alpha}$ is the linearized slope of the lift coefficient curve and

$$\frac{\partial C_L}{\partial \alpha} = \frac{\left(\frac{\partial C_L}{\partial \alpha} \right)_{\infty}}{1 + \frac{\left(\frac{\partial C_L}{\partial \alpha} \right)_{\infty}}{\pi A R}} \quad (8)$$

where $\left(\frac{\partial C_L}{\partial \alpha} \right)_{\infty}$ is the slope of the infinite aspect ratio fin taken from (8).

The term in parenthesis of equation (7) is the hydrodynamic angle of attack.

θ is the pitch angle of the ship.

\dot{Z} is the heave velocity.

$\dot{\theta}$ is the angular pitch velocity.

l is the distance between the hydrofoil and the C.G. of the ship and is equal to 240.9 Ft.

V_w is the vertical orbital velocity of the wave and is given in reference (9) as

$$V_w = - \frac{2 \pi h c}{\lambda} e^{\frac{2 \pi y}{\lambda}} \cos \left[\frac{2 \pi}{\lambda} (x - \omega t) + \frac{\pi}{2} \right] \quad (9)$$

This is given for the origin at the wave crest at station 11.

It should be noted that, as in (5), the horizontal component

of orbital wave velocity was neglected.

The moment M_l of the hydrofoil about C.G. was obtained by multiplying F_l by the moment arm.

In the sample calculations of Table XXV, the following points are noted:

"a" of equation (1) had to be increased by the virtual mass of the hydrofoil. The virtual mass is given in reference (5) as

$$m_i = \rho \frac{2\pi a^2 b^2}{a^2 + b^2} \quad (10)$$

where a and b are the half span and the half chord respectively. This value multiplied by the square of "l" gives the increase in the mass moment of inertia corresponding to coefficient "A" in equation (1).

The coefficient for g, e, b, C, B, E, a and A, being scalar quantities were added to their counter parts taken from previous calculations. Since the terms containing V_w were actually vectorial quantities, this had to be taken into consideration when adding to "F" and "M" of equations (1).

The summary of the results of the theoretical calculations are found in Table XXVII.

A study of equations (1) and (2) reveals that the final resulting motions are a linear function of wave height at any one wave length and model speed. Therefore, for a wave length of 600 feet and with the assumption that the lift curve of the ship fin is linear throughout the range of the calculation, the theoretical angle of attack for the fin was calculated for varying wave heights by vectorily adding each term of equation (7). In this calculation, the effect of changing the wave height was to linearly change the magnitudes of the vectors in equation (7) while retaining the same phase relationships between them.

A sample of the graphical procedure used and the resulting curves of fin angles of attack as a function of wave height are found in Figure V. This procedure was repeated for each fin by using measured amplitudes of pitch and heave while retaining the same phase relationships as theoretically computed.

C. Calculation of wave heights at which model bow submerges and the fin emerges for $\lambda/L = 1.25$.

A sample calculation of this procedure is included in Appendix B. In this calculation the instantaneous values of wave height (h_B), pitch (θ_1) and heave (Z) were vectorially added at the forward perpendicular of the ship. This can be expressed as an equation:

$$\overline{h_B} - \overline{\theta_1} - \overline{Z} = H_B \quad (11)$$

Where:

H_B is the instantaneous draft of bow as measured from the load waterline

h_B is the instantaneous wave height at the forward perpendicular measured from LWL and is equal to

$$h_B = |h| \left(\cos \omega_{et} + \frac{2\pi x}{\lambda} \right) \quad (12)$$

The origin is at the wave crest at station 11 and

$$\theta_1 = |\theta| \cos (\omega_{et} + \text{phase of pitch}) \quad (13)$$

$$Z = |Z| \cos (\omega_{et} + \text{phase of heave}) \quad (14)$$

D. Calculation of fin lift coefficients as a function of angle of attack.

A sample calculation appears in Appendix B.

The lift force, as measured in micro-inches per inch on the Baldwin strain indicator as the difference from "zero" angle of attack, was found experimentally for each angle of attack for each run. After averaging the

readings, correcting for hose influence and converting micro-inches per inch to pounds of lift, the following equation was used:

$$C_L = \frac{L}{\frac{1}{2}\rho AV^2} \quad (15)$$

L = measured lift in pounds

ρ = mass density of water in which the test was conducted
in $\frac{\text{Lb. sec.}^2}{\text{Ft.}^4}$

A = projected total surface area of the fin in Ft.^2

V = velocity of water flow during the test in Ft./sec.

E. Effective aspect ratio 4 fin (AR = 4.0 fin).

A complete description of the manufacture and installation of the AR4 fin is given in Appendix A. This fin was a NACA airfoil 0018 having an effective aspect ratio of 4 and a projected area equal to 2.12 per cent of the waterplane area. This airfoil was selected primarily because much of the calculated data appearing in (14) could be used directly. From (13) it also appeared to be a good compromise of all the characteristics desired. It is a symmetrical foil having a relatively high lift drag ratio and a reasonably high maximum lift coefficient and a sufficient thickness to chord ratio to make it structurally feasible for installation on a ship. The fin area was selected in order to give an approximate reduction in pitch amplitude equal to 10%.

After the fin and pump were installed and the hose and electrical connections made, the model was then weighed and ballasted. This was done with the electrical cables attached and the tubing filled with water. All model tests were made at a model displacement equal to 39.21 pounds which corresponded to a full load ship displacement equal to 17,800 tons. The model was then placed in the water and the weight locations were

adjusted for zero trim and list. Finally, the radius of gyration of the model was adjusted to be equal to 25 per cent of the model length. The method used for this adjustment is explained in Appendix B.

The model was then attached to the towing cord and the pan weights and accelerating distances were adjusted until the still water model speed corresponded to a ship speed of 17.5 knots. This is 1.06 times the ship's service speed and equal to the full speed of the ship when utilizing its reserve power. All subsequent runs with this fin were made using the same towing force.

The model was tested in regular waves which, scaled to ship dimensions, are listed in Table XXVIII. At each wave condition, runs were made both with and without boundary layer suction.

Because it was not known what influence on bow vibrations would result from boundary layer suction, it was decided to explore the effect of suction at several wave lengths and at several wave heights in each wave length. In this way it was hoped that at each wave length a range of wave heights could be defined over which bow vibrations would be reduced or eliminated by applying suction. Suction was applied at the rate of 0.6 GPM to the upper surface of the fin for a distance of 0.6 inches from the leading edge. This suction rate was the highest obtainable for this fin and was the only control rate used. The transverse bow vibrations and model speeds were recorded with the Sanborn Recorder for each run.

In order to determine what influence, if any, boundary layer control had on heave and pitching motions, photographs were taken both with and without suction during runs denoted by an asterisk in Table XXVIII. The model motions were measured from photographic negatives as described in (19). Finally a series of runs was made during which high speed motion

pictures were taken of the flow over the fin surface in order to visually study flow distribution.

The procedure followed when making runs was as follows:

(1) The wavemaker was adjusted for proper wave length and wave height with the assistance of calibration curves in the towing tank. These adjustments were checked by using one channel of the Sanborn Recorder to record the readings from the wave measuring device at the tank. When the correct wave condition was achieved, the proper wavemaker setting was recorded and subsequently used whenever tests were run at the same wave condition.

(2) On runs where suction was to be applied, the pump motor was started.

(3) The wavemaker was started, and the model was released when the first wave was approximately 20 feet from the beach. During each run, one man walked along the towing tank, holding the fishpole while carefully not permitting the electrical connections to influence the model motions. The other man operated the towing dynamometer, the Sanborn Recorder, and the camera equipment.

(4) The Sanborn Recorder was started (paper speed = 25mm/sec.) in order to record transverse bow vibrations and model speed. As the model passed the glass walled section of the tank the cameras were operated, either for taking motion measurements or motion pictures.

(5) Upon completion of each run, the model was returned to the opposite end of the tank, the data was recorded, and the measurements were identified. The measured model speed used was the average speed of the model while passing the glassed wall section of the tank.

F. Effective aspect ratio equal 2 fin (AR = 2.0 fin).

Because of the inconclusive results obtained using the small fin, it

was decided to fabricate a large fin having a considerably longer chord. This was done on the basis of several runs made using an available aluminum fin having an effective aspect ratio of 1.37 and an area equal to 5.95 per cent of the waterplane area. The AR2 fin is described in detail in Appendix A. It was an NACA-0018 foil having an effective aspect ratio of 2 and an area equal to 8.7 per cent of the waterplane area of the model. The aspect ratio was reduced from that of the smaller fin in order to keep the span at a reasonable length while retaining a relatively large area and chord length. In addition, the fin was suspended at a distance of 3 inches (corresponds to 25 feet for the ship) below the base line. (See Table XXXIII for a summarized comparison of the two fins.)

All measurements taken with this fin were conducted at a ship wave length and speed equal to 600 feet and 11 knots respectively. The wave conditions were varied by varying the wave height in 1.66 foot increments from 5 feet to 20 feet. At each condition measurement of bow vibrations and model motions were made, both with and without boundary layer control. These measurements were carried out in the same manner as previously described except that maintaining a constant speed meant that the pan weights had to be readjusted for each wave condition. The maximum suction rate obtainable with this fin equaled 1.35 GPM and was the only rate used throughout the tests.

G. Calibration of fins in Propeller Tunnel.

In order to study the influence of suction on the model motions, curves of lift versus angle of attack for both fins were required. In addition, the influence of suction on fin angles of breakdown was needed so an evaluation could be made of the effectiveness of employing boundary layer suction to reduce bow vibrations.

After some thought it was decided to construct an apparatus that could be suspended in the propeller tunnel at MIT (11), which would measure lift force as a function of fin angle of attack. This apparatus is described in detail in Appendix A. It measured the vertical shear forces in the bar. It should be noted that this apparatus did not measure the true lift, but it measured only vertical components of lift and drag. Neglecting the horizontal components was justified on the basis that these components were small and have been neglected in the theoretical calculation. In addition, present facilities are not easily adaptable to more accurate measurements. Other errors introduced by bar flexibility, the failure to simulate the exact flow pattern around the model bow, by making the measurements at a different depth of submergence and by the suction hose arrangement, all contributed to reducing the overall accuracy of the measurements. Although a greater accuracy would have been desirable, the results appeared to adequately justify the "crudeness" of the apparatus. Future experimental work can be devised for more accurate quantitative results.

A fairing was installed to divide the flow pattern so that it would be similar to that of the model. The fairing also surrounded the loop of suction hose between the end of the horizontal bar and the fin. The water level was required to be such that the entire apparatus was submerged in order to prevent surface eddies from influencing the readings. The suction hose connection induced a shear force in the bar which was a function of fin angle of attack. Its magnitude was measured by varying the angle of the fin while the fin was submerged in place in still water. This was called the hose correction and was algebraically added as a correction to the final lift measurements. The separate influence of the fairing and pivot arrangement on lift at various angles of attack was

checked but found to be negligible.

The apparatus was calibrated by hanging known weights on the fin end of the horizontal bar and simultaneously recording the reading on the Baldwin Strain Indicator. A straight line plot resulted from recording measured readings as a function of the magnitude of the weight attached.

Next, the apparatus was placed in the tunnel and a "zero" reading was taken in still water. The flow rate was then adjusted to a water velocity equal to 1.1 knots (corresponds to a ship speed equal to 11 knots). The angle of attack of the fin was adjusted until the strain measured equaled the "zero" reading. This fin position was taken as zero angle of attack.

At least two runs were made at each suction rate by changing the angle of attack in 5° increments from zero to 45° and recording the strain in the bar at each angle. One man was stationed at the top of the tunnel to vary the fin angle of attack and to read the strain indicator. The other man regulated the tunnel water velocity and suction rate. The suction rate was measured by calibrating the sight glass on the vacuum pump receiver. The difference in indicated strain from the "zero" reading could then be converted into pounds of lift by using Figure VI. Conversion of the strain measurements to curves of lift coefficient vs. angle of attack is described in detail in Appendix B.

III. RESULTS

A. AR = 4.0 Fin.

Figure VII is a plot of the measured pitch versus λ/L with and without boundary layer control.

Figure VIII is a plot of the measured heave versus λ/L with and without boundary layer control.

Figure IX shows the recorded transverse vibrations of the bow in water resulting from a light tap.

Figures X, XI and XII show the vibrations of the bow for selected wave conditions with and without boundary layer control.

Figure XIII shows the plot of lift coefficient versus fin angle of attack measured in the propeller tunnel, for various boundary layer suction rates.

Table XXVIII presents the ranges of wave heights for various wave lengths where vibrations were observed for the AR₄ fin.

Tables XXIX and XXX summarize the results obtained for the AR₄ fin.

B. AR = 2.0 Fin.

Figure XIV is a plot of the measured heave versus wave height for the fin with and without boundary layer control. These measured values are also compared with the computed values.

Figure XV is a plot of the observed pitch versus wave height with and without boundary layer control. These measured values are compared with computed values.

Figure XVI shows the plot of lift coefficient versus fin angle of attack, measured in the propeller tunnel, for various amounts of boundary layer control.

Figures XVII and XVIII show the vibrations of the bow for selected wave conditions with and without boundary layer control.

Tables XXXI and XXXII summarize the results obtained for the AR2 fin.

C. Theoretical calculations.

Table XXVII presents the results of the theoretical calculations.

Figure V shows the graphical method used and a plot of the resulting curves for computing fin hydrodynamic angle of attack as a function of wave height for effective $AR = 4.0$ and $AR = 2.0$.

D. Motion picture data.

From viewing some 400 feet of 16 mm. film taken of the fins underwater in various wave conditions, it was observed that there was no indication of boundary layer breakdown on either fin. However when the fin of effective $AR = 4.0$ mounted on the base line came very near the surface or penetrated the surface, a large bubble formed on the top surface (low pressure) of the fin. This bubble subsequently broke up into small bubbles which floated aft and up toward the surface along the bow of the model. The phenomenon occurred with and without boundary layer control. Figures XI and XIX show the phenomenon observed and the accompanying recorded transverse bow vibrations.

IV. DISCUSSION OF RESULTS

A. The effect of boundary layer control on model bow vibrations for the AR = 4.0 fin.

Referring to Figure I of reference (14) a fin having an $AR = 4.0$ could be expected to breakdown at about an angle of attack of 8° ($N_{Re} = 1.756 \times 10^4$) if no boundary layer control were used. Experimentally as shown in Figure XIII there is a definite angle of breakdown at about 18° , however, the slope of the lift curve is slowly decreasing as it approaches this angle of breakdown. This can be attributed to a laminar separation which occurs before turbulent separation. This result is in agreement with experiments conducted at a similar Reynolds number (Figure XX). The angles of breakdown indicated in reference (14), at low Reynolds numbers, are extrapolated curves derived from NACA tests which were conducted at much higher Reynolds numbers where it was found that the slope of the lift curve was relatively constant up to angles of attack approaching angle of breakdown.

By applying boundary layer suction to this fin at the rate of 0.6 GPM, the angle of breakdown was extended to approximately 21° (Figure XIII). These tests show that boundary layer suction at this rate increases the angle of breakdown by only 3° . However, the slope of the lift curve has been improved and the resulting lift is greater. The straighter lift curve is a result of suction delaying laminar separation on the top surface. The increased angle of attack can be attributed to a delay in laminar separation at the leading edge.* Increased pumping rates extended the straight line portion of the lift curve and resulted in increased values of the lift coefficient and angles of breakdown. The measured

* Refer to Appendix C.

slopes corresponded closely to those predicted by calculation. For the model tests the pumping rate was limited to the maximum of 0.6 GPM because of the small size of the fin and the tubing installed in the model.

As noted in Table XXVIII tests were made at five different wave lengths at various wave heights where it was hoped that the hydrodynamic angle of attack would be from 18° to 21° . In this range, boundary layer control was expected to be effective in delaying the fin angle of breakdown. On the assumption that bow vibrations were induced by flow separation in this range boundary layer control would then be expected to reduce or eliminate the vibrations.

Table XXVIII shows that for $\lambda = 400$ Ft. no transverse bow vibrations were apparent; thus it was assumed that flow separation did not occur. At $\lambda = 500$ Ft. vibrations were apparent at double wave heights of 17.5 Ft. and above while very violent vibrations were recorded for $2h = 20.8$ Ft. and above (Figure X). At $\lambda = 600$ Ft. minor vibrations occurred at all wave heights, and above $2h = 19.2$ Ft. violent vibrations again occurred. At $\lambda = 800$ Ft. no vibrations were observed at $2h = 20$ Ft. and minor vibrations occurred at $2h = 21.0$ Ft. and above. At $\lambda = 1,000$ Ft. no vibrations were observed up to $2h = 26.4$ Ft. and above this wave height moderate vibrations were recorded. The application of boundary layer suction did not at any time appear to reduce the above vibrations. This may be for the following reasons: (1) the range over which boundary layer suction was effective in increasing the angle of breakdown was so small (about 3°) for the pumping rate used that wave conditions tested were not in this range. For this fin a theoretical calculation of hydrodynamic angles of attack were calculated only for $\lambda/L = 1.25$; (2) the transition from un-separated to separated flow was so gradual that the separation point could

not be clearly defined to actually differentiate between the angles of breakdown for the suction and no suction tests; (3) the assumed asymmetrical impulses on the bow resulting from flow separation were not of sufficient magnitude to record until the hydrodynamic angle of attack considerably exceeded the angle of breakdown; (4) it is possible that transverse boundary vibrations were not a result of the boundary layer breakdown phenomenon. In high speed motion pictures taken of the flow pattern over the fin, in instances where no vibrations or moderate vibrations were recorded, no indications of bubble formation as a result of separation were observed. In contrast, runs in which violent vibrations were recorded (Figure XXI), it was observed that the fin approached very closely or actually penetrated the surface of the water. Motion pictures taken at these wave conditions showed a definite formation of a bubble and subsequent bubble collapse (Figure XIX). In these cases boundary layer control had no effect in reducing vibrations. This phenomenon is attributed to vortex ventilation which occurs when low aspect ratio fins operate near the surface of the water (17).*

B. The AR = 2.0 Fin.

Since the tests with the AR = 4.0 fin did not conclusively demonstrate the effectiveness of boundary layer suction in reducing transverse bow vibrations assumed to be induced by boundary layer separation, a larger fin with a chord = 4 inches and an area equal to 5.95 per cent of the waterplane area was used to indicate whether more distinct vibrations would be obtained due to the larger forces involved. As shown by Figure XII there was an indication that a larger fin may be more effective in producing positive results. Consequently, the AR = 2.0 fin was manufactured. In order to eliminate the observed effect of vortex ventilation

* Refer to Appendix C.

the fin was mounted 3 inches below the base line of the model. In addition the use of a larger fin resulted in an increase in the maximum rate of pumping (1.35 GPM).

All tests were made at $\lambda/L = 1.25$ (near resonance for the ship) at varying wave heights. Because the hydrodynamic angle of attack varies linearly with wave height when model speed and wave length are constant, a computation for one wave length sufficed to explore a full range of angles of attack where boundary layer control may be effective. All runs were made at a constant speed (11 knots). This speed was used for the theoretical calculations and was the same speed which resulted when the $AR = 4.0$ finned model was tested with a constant tow force at a double wave height equal to 16.67 Ft. at this wave length.

The lift curves shown in Figure XVI indicate that applying a suction of 1.35 GPM increases the angle of breakdown for this fin from 15° to 20° . It was theoretically determined (Table XXXII) that this suction rate should be effective in delaying flow separation for wave heights from $2h = 6.66$ Ft. to $2h = 9.17$ Ft. In the experiment no significant vibrations at all were recorded in the above range. Vibrations were not recorded below wave heights of 11.67 Ft., which corresponds to a hydrodynamic angle of attack of 27° , which is greater than the theoretical angle at which boundary layer control could be expected to be effective. When vibrations were recorded at wave heights above this value (Figure XVII) boundary layer suction had no effect. It is felt that the range of wave conditions at which boundary layer suction would be effective was thoroughly explored; therefore, this strengthens the assumption stated that boundary layer separation, in itself, does not result in forces large enough to cause violent transverse bow vibrations. In these tests,

since the fin was mounted 3 inches below the base line and thus did not penetrate or closely approach the surface of the water, violent vibrations were not recorded. Therefore, although boundary layer separation may cause minor transverse bow vibrations, violent damaging vibrations are believed to be the result of vortex ventilation. The observation of motion pictures taken in all wave heights recorded with this fin showed no indication of bubble formation thus verifying the above statement.

C. The effect of boundary layer control on fin lift curves.

In order to determine the effectiveness of various boundary layer control suction rates on the lift of the fins, lift curves were experimentally determined as shown in Figures XIII and XVI. No attempt was made to optimize the various parameters effecting this curve relating to location of points of suction or suction rates relative to these points. Referring to these figures an increase in suction rate has the effect of extending the straight line portion of the lift curve and thus increasing the maximum lift and the angle of breakdown. This is true in all cases except when suction was taken over the entire fin area. Since measurements were taken at 5° increments it was difficult to determine the exact angle of laminar separation. As discussed in reference (16) for fins tested at a constant Reynolds number suction applied at, or aft of, the middle chord length has the effect of straightening the lift curve, but it does not increase angle of breakdown. The straightening of the curve is attributed to the delay in the point of laminar separation. If boundary layer suction is applied at or near the leading edge of the fin, laminar separation is delayed thus extending the lift curve to a greater angle of breakdown. Since the fins tested had suction areas near the leading edge only, the resulting curves did not have the constant slope expected but

showed the effect of laminar separation, but no clear point of laminar separation was defined, and the slope of the curves slowly decreased until it finally became negative.

Laminar separation is particularly influential in modifying the slope of the lift curve in tests at low Reynolds numbers such as were used in this thesis. At higher Reynolds numbers, there would be a more definite point of laminar separation. As indicated in Figure I of reference (14) for the Reynolds numbers expected on the ship, the angle of breakdown without boundary layer control would be 21.5° for the $AR = 4.0$ fin and 31° for the $AR = 2.0$ fin, and this would primarily be influenced by the point of laminar separation. For application of boundary layer control to ship fins, it is, therefore, necessary to have the suction slots (and related suction flow rates) first on the after part of the fin to increase the lift and at the leading edge of the fin to further increase the lift and the angle of breakdown. It should be noted, however, that if boundary control applied to ship fins succeeded in delaying the angle of breakdown to as much as 40° the double amplitude wave height necessary in 600 Ft. waves to produce this angle of attack for the $AR2$ fin is only 18.35 Ft. It is not uncommon that ships can be expected to operate in waves considerably above this wave height. It can, therefore, be concluded that boundary layer control would probably not be effective in heavy seas and activated fins would probably be a better approach to solve this problem.

D. Motion measurements of the model with fins installed.

1. Motions as a function of wave length.

It can be observed in Figure VII that pitch amplitude is reduced by the $AR = 4.0$ fin at a $\lambda/L = 1.25$ by about 25 per cent. This compares

favorably with a calculated pitch reduction of about 24.5 per cent. The crossover of the curves with and without suction occurs at a $\lambda/L = 1.18$. At wave lengths lower than the crossover point, suction appears to reduce the pitch amplitude. This can be attributed to the increased lift obtainable by employing suction at these wave lengths. At wave lengths above this point the pitch amplitude, when suction was applied, was greater than without suction. This can be explained by the assumption that boundary layer suction is no longer effective and that the angle of breakdown in both cases has been exceeded. Because suction was applied only to the top surface of the fin there is little difference in the pressure distribution on the fins when the ship is pitching down; however, when the ship is pitching up, suction applied to the top surface of the fin tends to reduce the distributed pressure on the high pressure surface (relative to no suction case) thus tends to increase the pitch amplitude. It is therefore recommended that boundary suction be taken on both surfaces of the fin, alternately so that full advantage can be taken of the increased lift obtainable by suction and also that the detrimental effects of suction on the high pressure surface will be eliminated. The experimental accuracy of determining the pitch curves is within $\pm 0.5^\circ$, therefore the difference between the suction and no suction cases may not be as great as the curves demonstrate.

In heave there is no appreciable difference between the suction and no suction cases although there is some improvement by the addition of the fin over the no fin case for λ/L less than 1.25, (Figure VIII).

2. Motions as a function of wave height for AR2 fin.

Referring to Figures XIV and XV both curves (with and without suction) vary approximately linearly with wave height. Because of the

experimental accuracy, stated previously, no definite trends can be detected between these two cases. The experimental accuracy would be improved by using gyroscopes or accelerometers to measure model motions. With this improved accuracy the effects of the boundary layer control could be better ascertained.

It is noted that in the above curves, the slope tends to decrease at $2h = 16.66$ Ft. This is attributed to the increased damping caused by observed bow immersion of the model.

E. Theoretical calculations.

Figure XV shows that for the $AR = 2.0$ fin the amplitude of pitch measured agrees favorably with calculated amplitudes. For heave (Figure XIV) the computed values are consistently about 3 feet less than the measured values of heave. It is believed that this is primarily a result of the speed influence on the damping coefficients for heave, and also the effects of the bulb in determining the inertia coefficient could not be properly evaluated with the data available.

V. CONCLUSIONS

1. Boundary layer control is not effective in eliminating transverse bow vibrations that may be induced by boundary layer separation.

2. Violent damaging vibrations are a result of vortex ventilation.

3. Boundary layer control does delay flow separation; however, the increase in angle of separation is small, thus for wave heights that would be expected by the ship in moderate storms, the increased angle of breakdown resulting from boundary layer control would be exceeded.

4. Boundary layer control increases the maximum lift obtainable for a particular fin.

5. Boundary layer control did not change the model motions beyond the measurable accuracy, thus the results are largely inconclusive.

VI. RECOMMENDATIONS

1. The bow of models used should be "detuned" by using a lighter more sensitive bar, thus making the bow more sensitive to vibratory forces.
2. The location of suction slots and the suction rates should be optimized for fins tested. Tests should be made at various Reynolds numbers to show this influence on lift and hydrodynamic angle of attack.
3. An investigation of the effectiveness of alternate suction on both sides of the fin should be made.
4. Accelerometers or gyroscopes should be used to measure the effect of boundary layer control on model motions.
5. Anti-pitching fins should be mounted as low as possible or aft of the fore foot to prevent vortex ventilation from occurring.
6. A study should be made on the use of fin vents in controlling boundary layer separation.
7. A greater pumping capacity should be incorporated in models for employing boundary layer control.
8. Activated fins should be investigated as a possible solution to the vibrations problem.

$\rightarrow 10,6 \text{ M}$

 $+V_s \cdot C_1 \cdot X$

DESCRIPTION OF INMATE 4/18/59

At

FIGURE II

MODL 3 PROTOTYPE SECTION AREA VS. DISTANCE OF SECTION FROM ∇

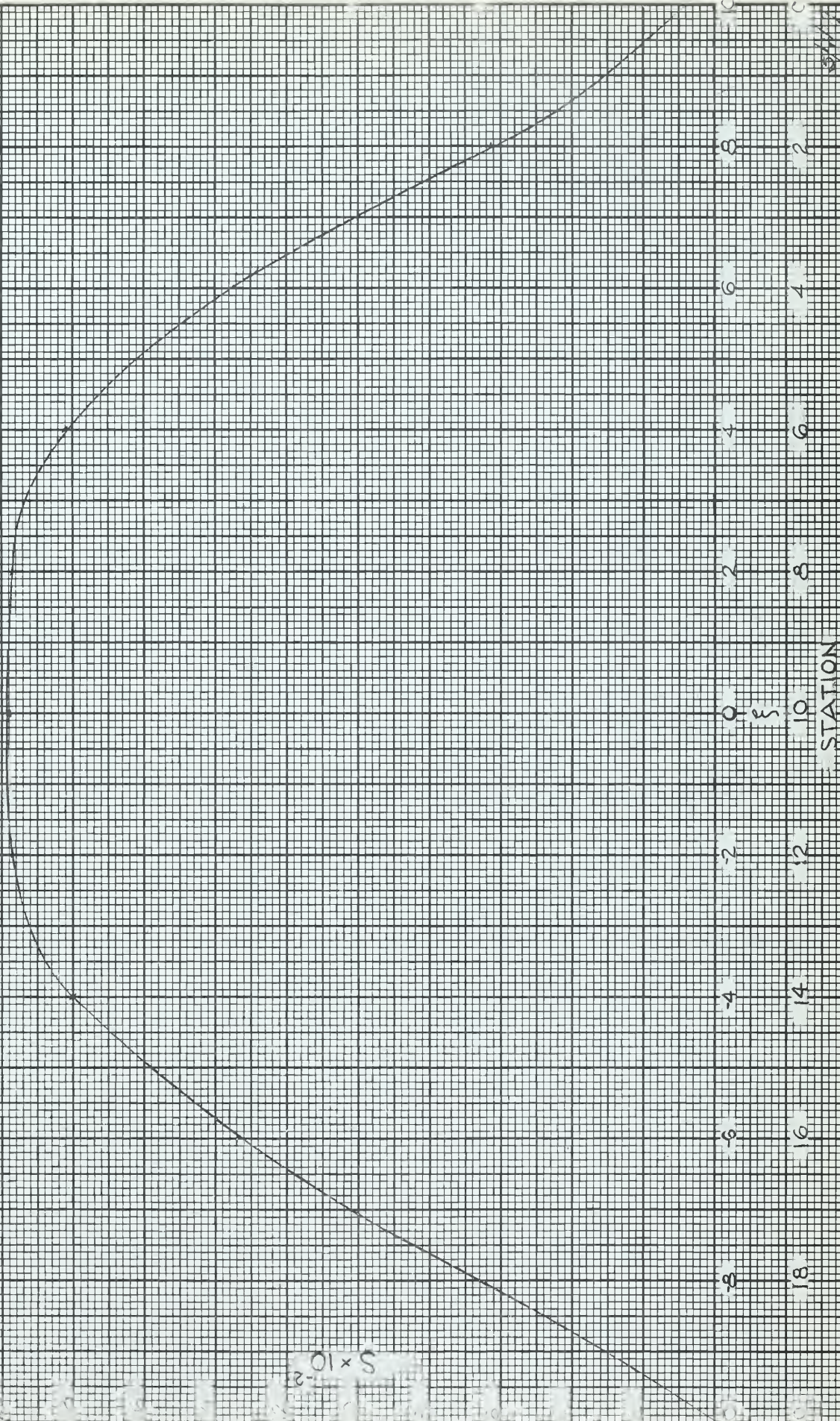
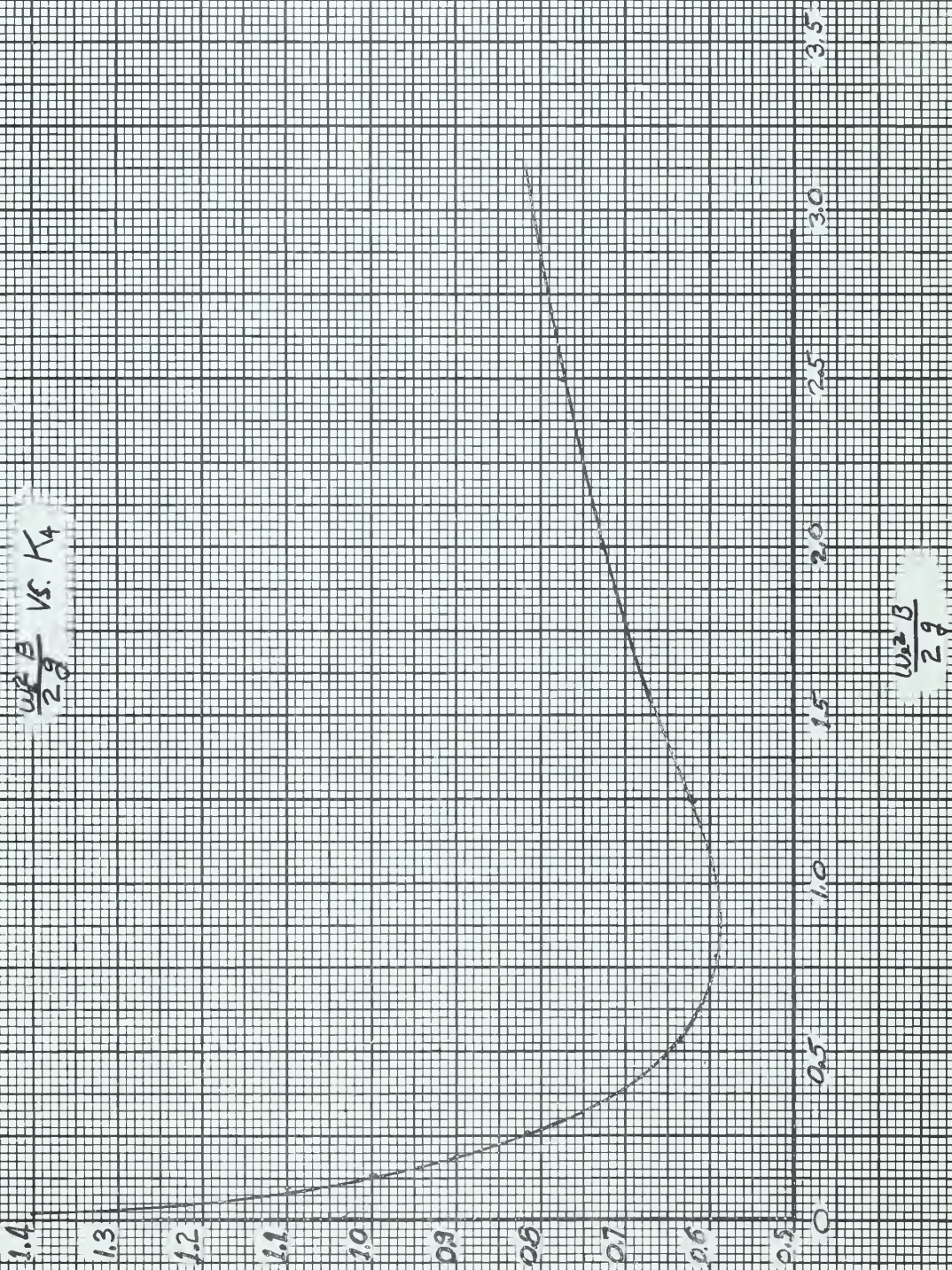


FIGURE III

CIRCULAR CYLINDER

$\frac{w_2 B}{2g}$ VS. K_4



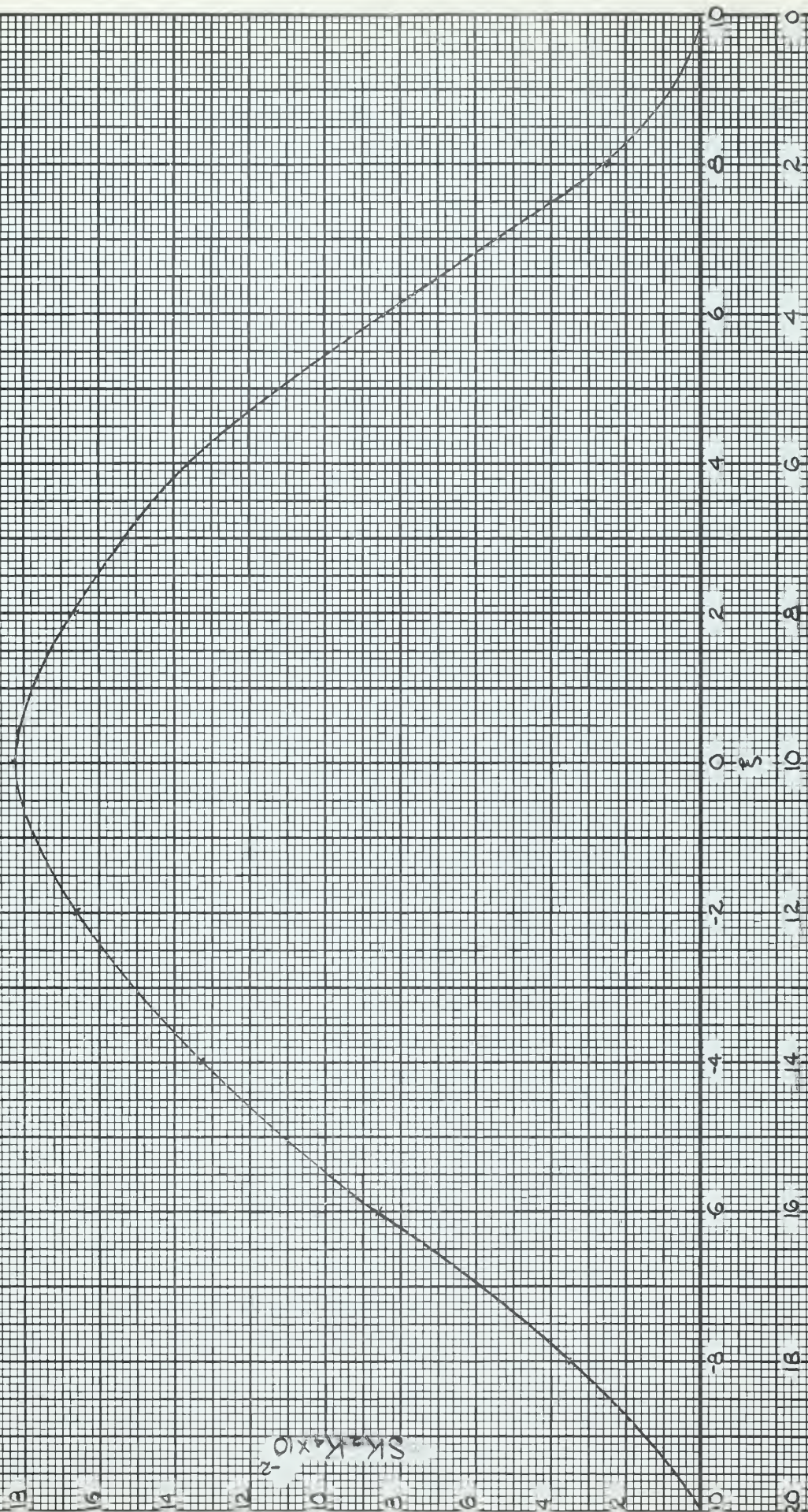
$\frac{w_2 B}{2g}$

4

11/10/57
S.M.

FIGURE IV

MODEL B PROTOTYPE SK_2K_4 vs. $\xi - \Lambda/L = 1.25$



STATION

5/1/79
JCH

FIGURE IV THEORETICAL GRAPHICAL SOLUTION OF FIN ANGLE OF ATTACK vs WAVE HEIGHT

SAMPLE PLOT

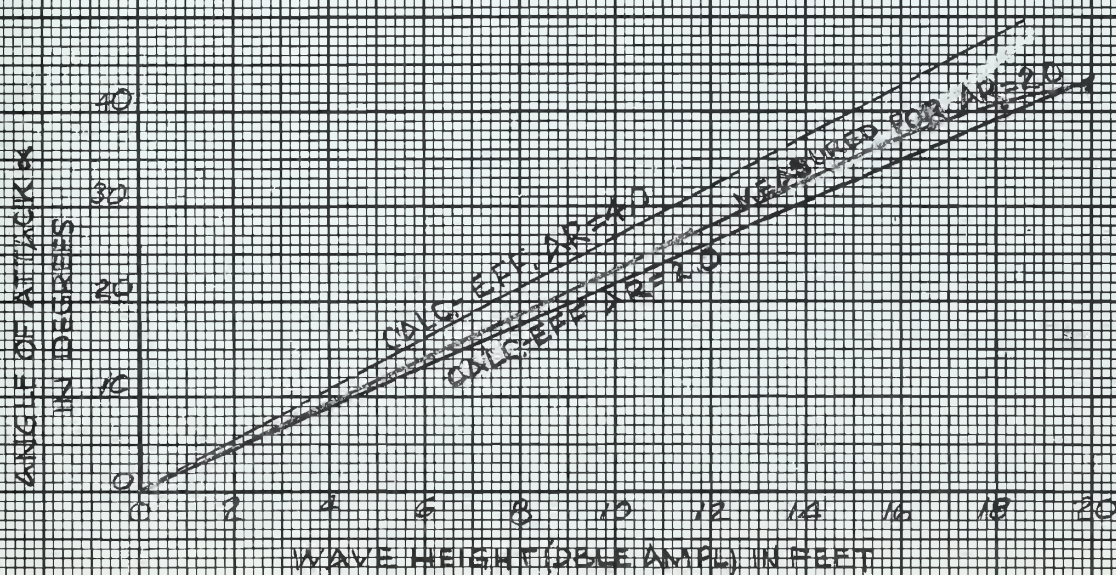
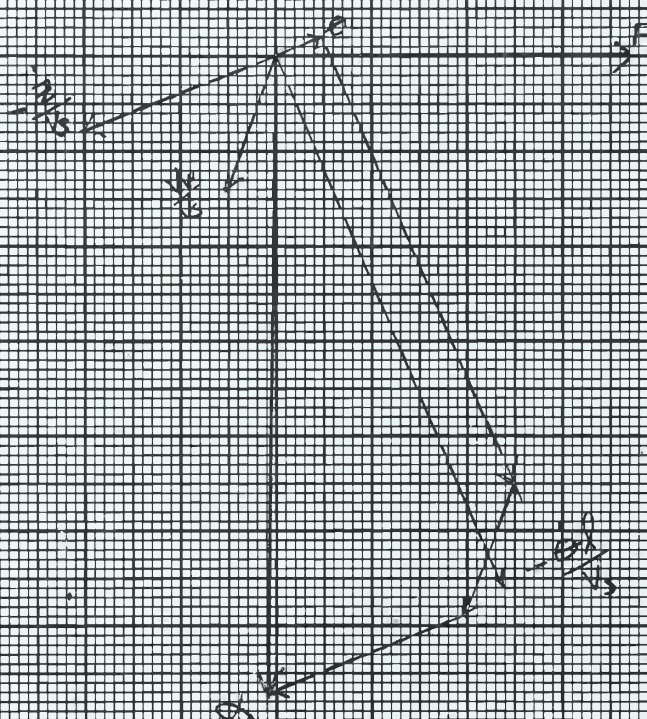
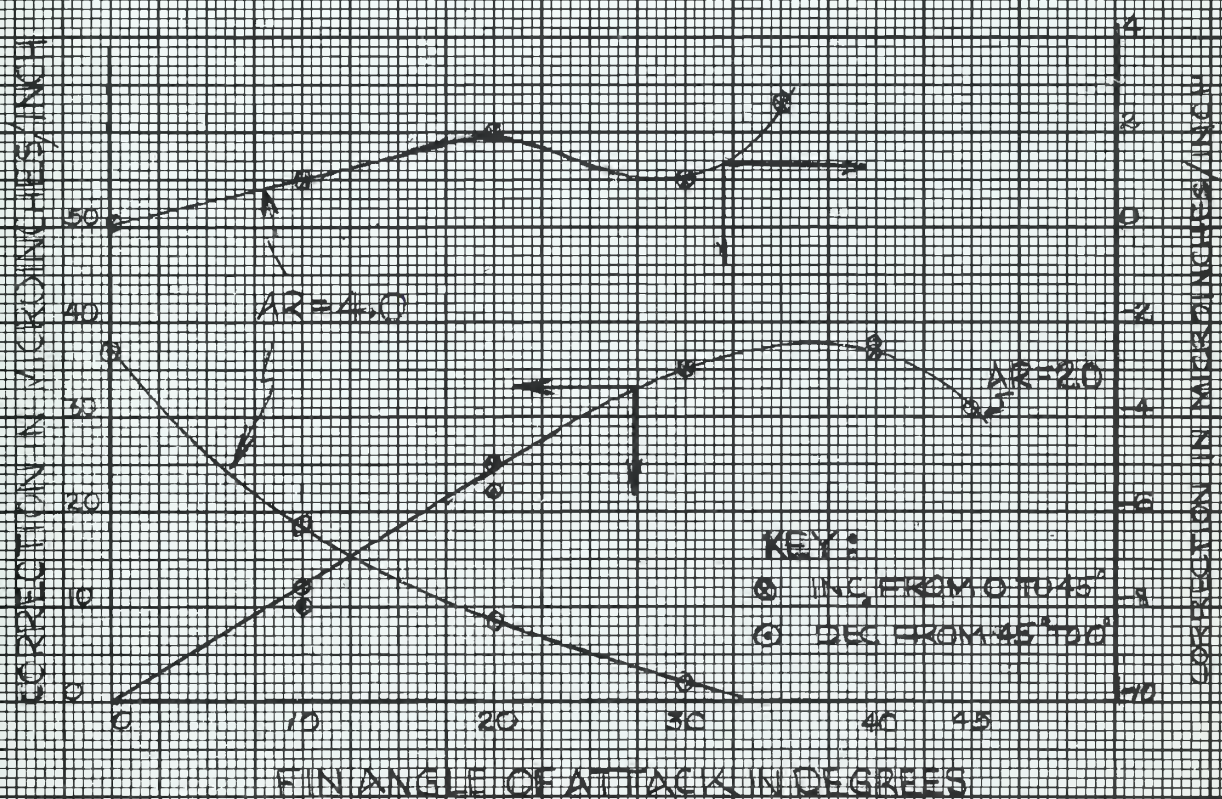
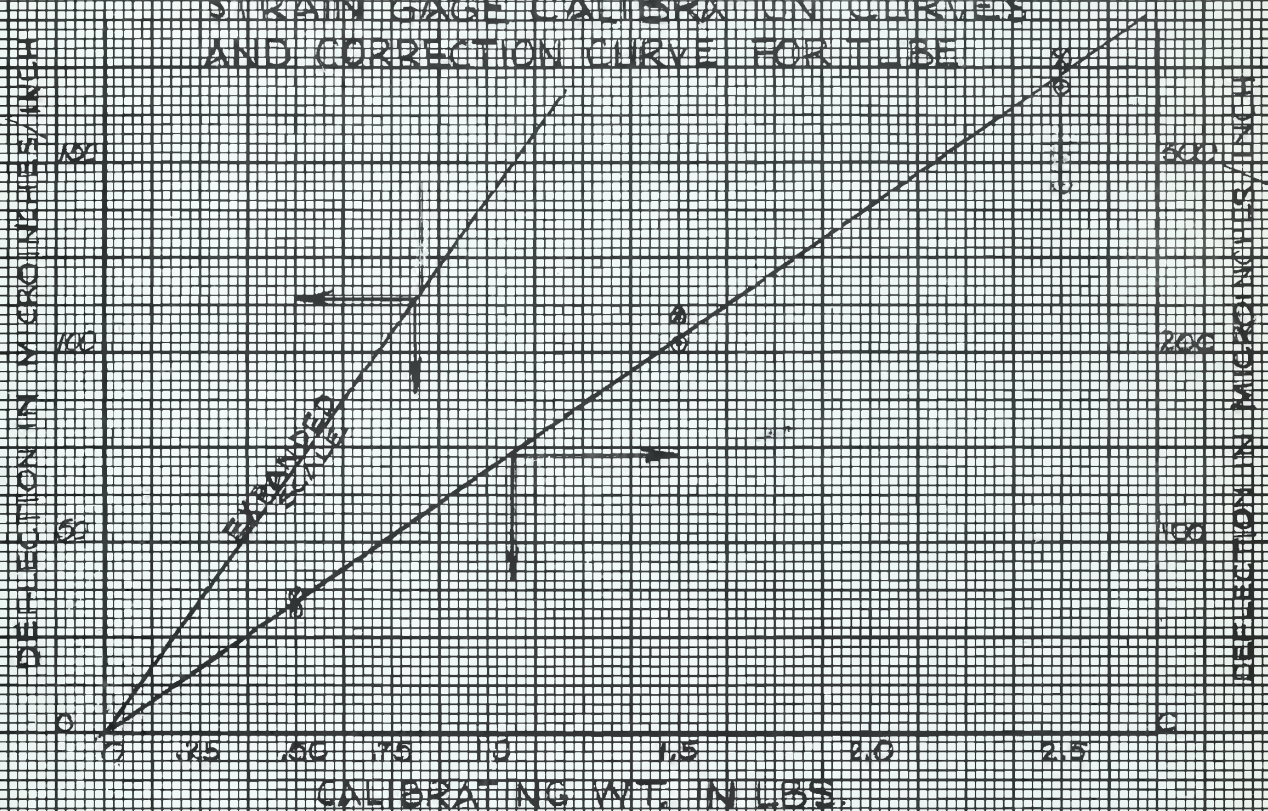
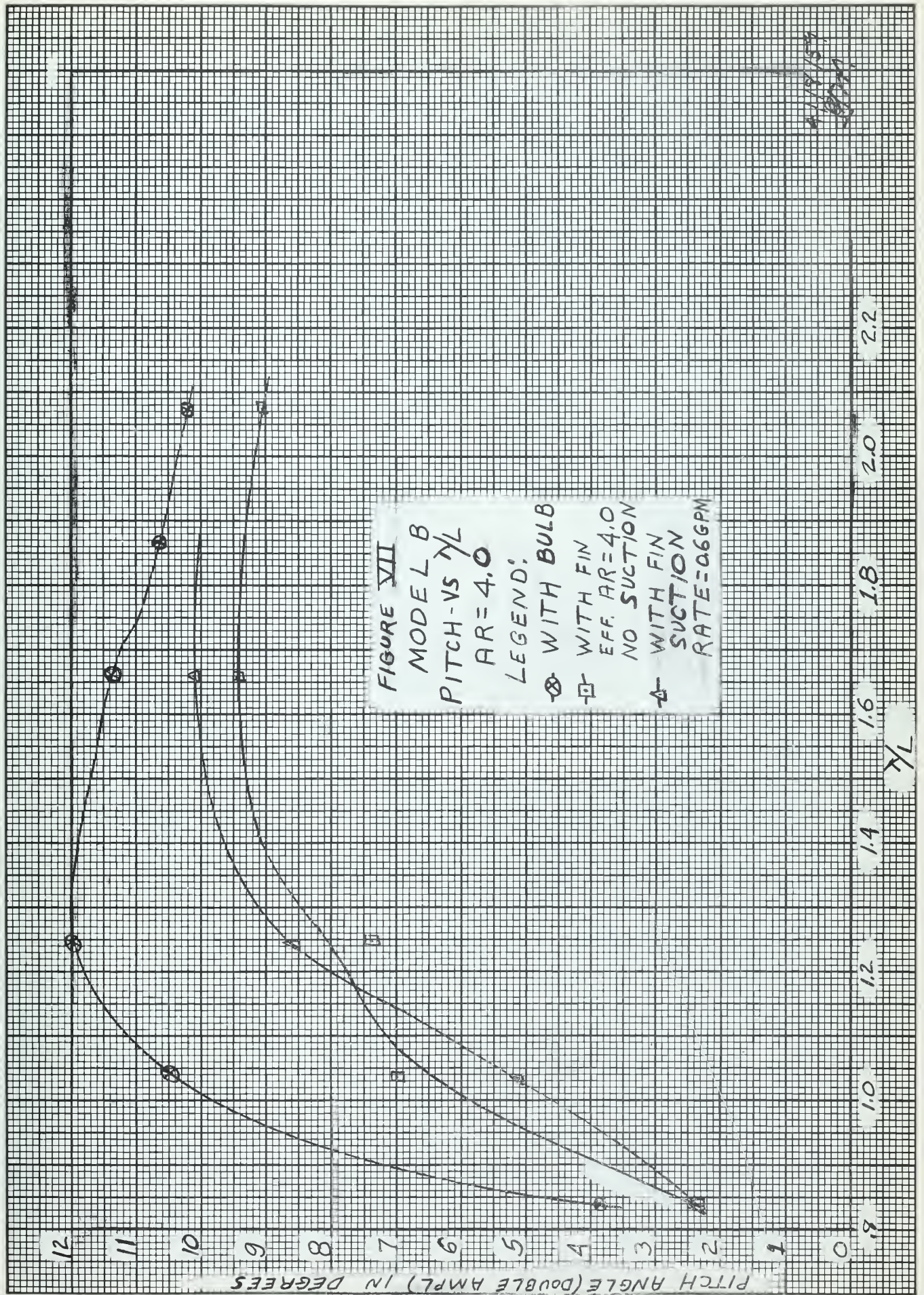


FIGURE III
STRAIN GAGE CALIBRATION CURVES
AND CORRECTION CURVE FOR TLBE





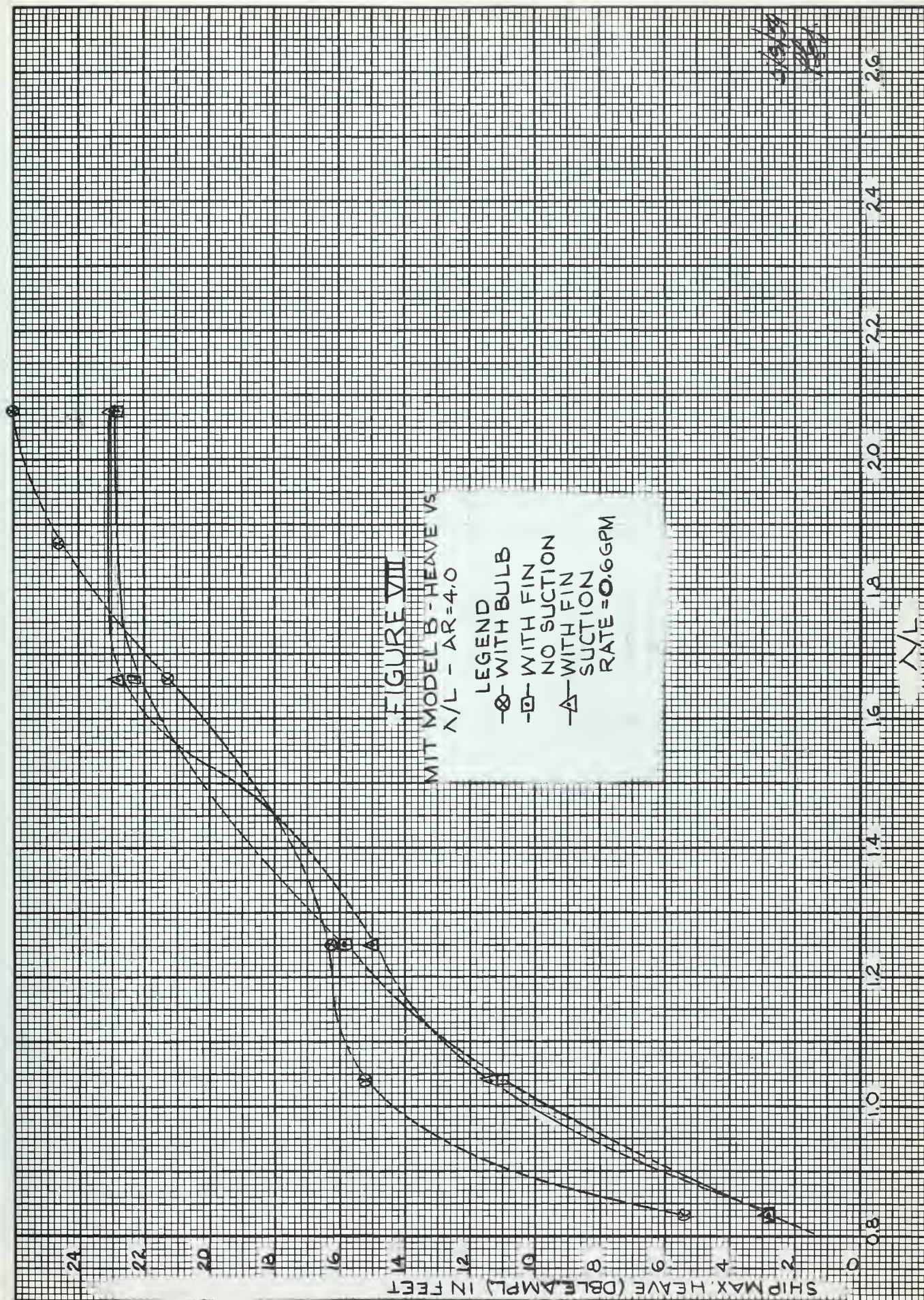


Figure IX. Bow vibrations with model in water as a result of a light tap on the bow.

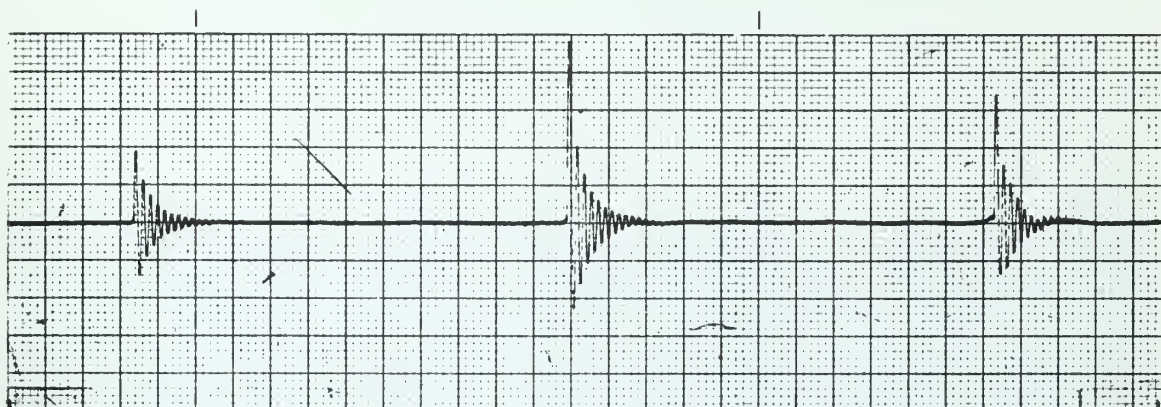


Figure X. Vibrations of the bow for fin (eff. AR: 4.0) mounted on the base line in waves of $\lambda = 5.0$ ft. and $2h = 2.5$ in. without (A) and with (B) boundary layer control.

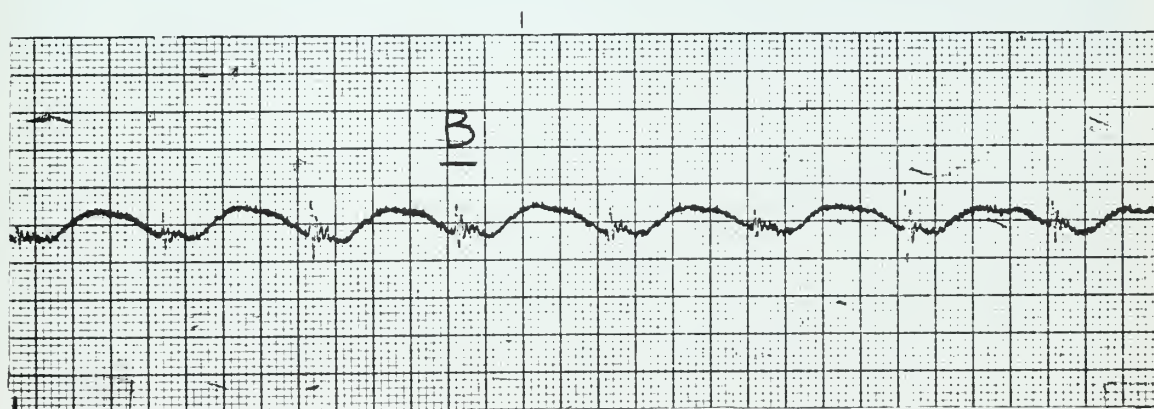
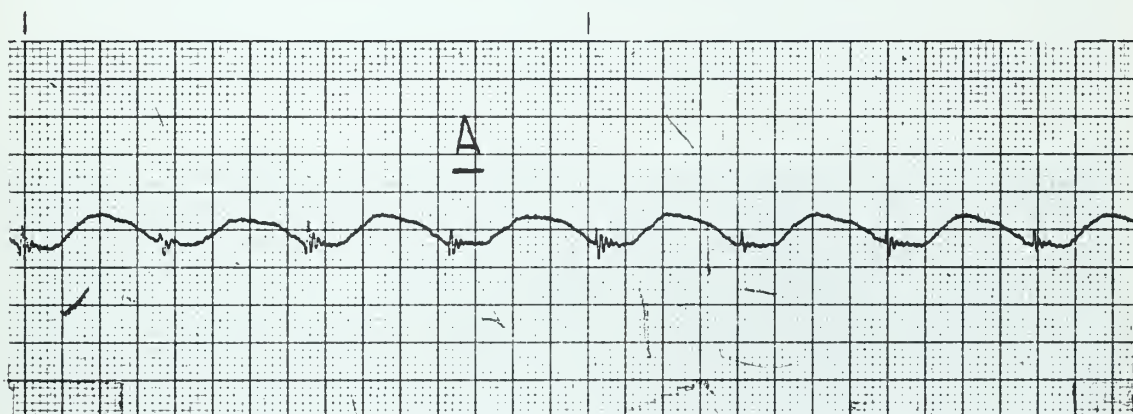


Figure XI. Vibrations of the bow for fin (eff. $AR=4.0$) mounted at the base line in waves of $\Lambda=6.0$ ft. and $2h=2.3$ in. without (A) and with (B) boundary layer control.

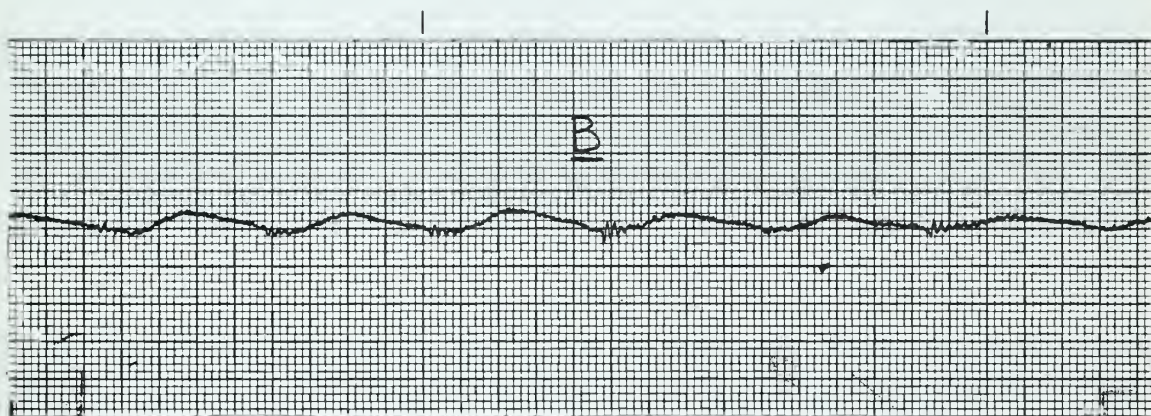


Figure XII. Vibrations of the bow under the same wave conditions ($\lambda = 6.0$ ft. and $2h = 2.0$ in.) for (A) fin of eff. AR = 4.0 and 2.12% of the water plane area with no boundary layer control, (B) fin (A) with boundary layer control, and (C) fin of eff. AR = 1.37 and 5.95% of the water plane area with no boundary layer control. Both fins were mounted at the base line of the model.

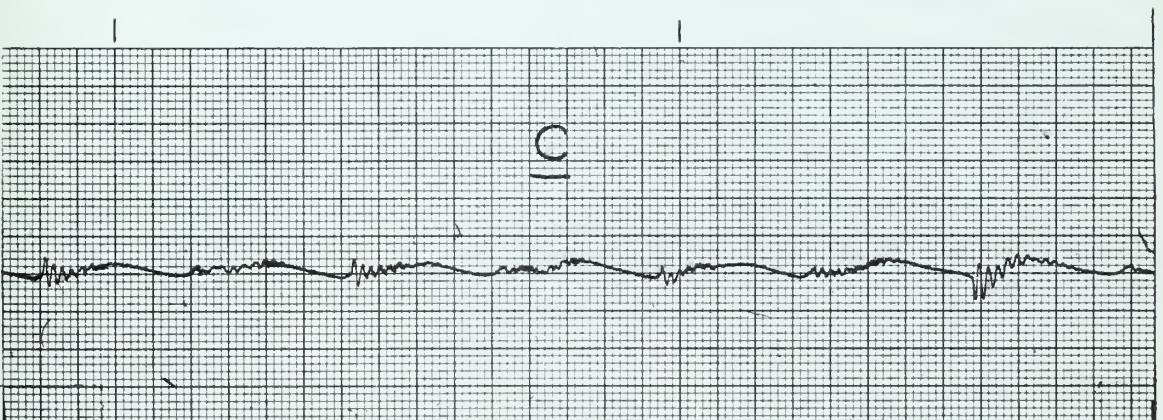
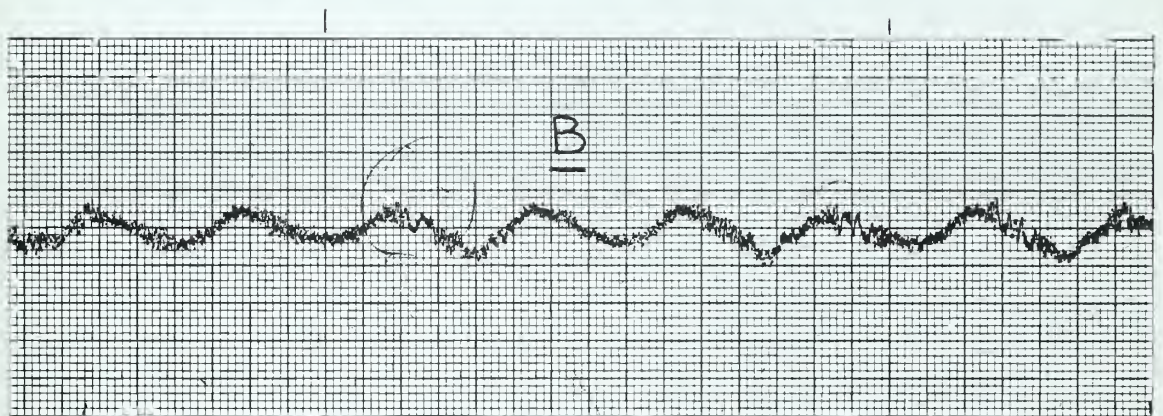


FIGURE XII
NACA-0018 FOIL - ANGLE OF
ATTACK VS LIFT COEFFICIENT

EFF. A.R. = 4.0

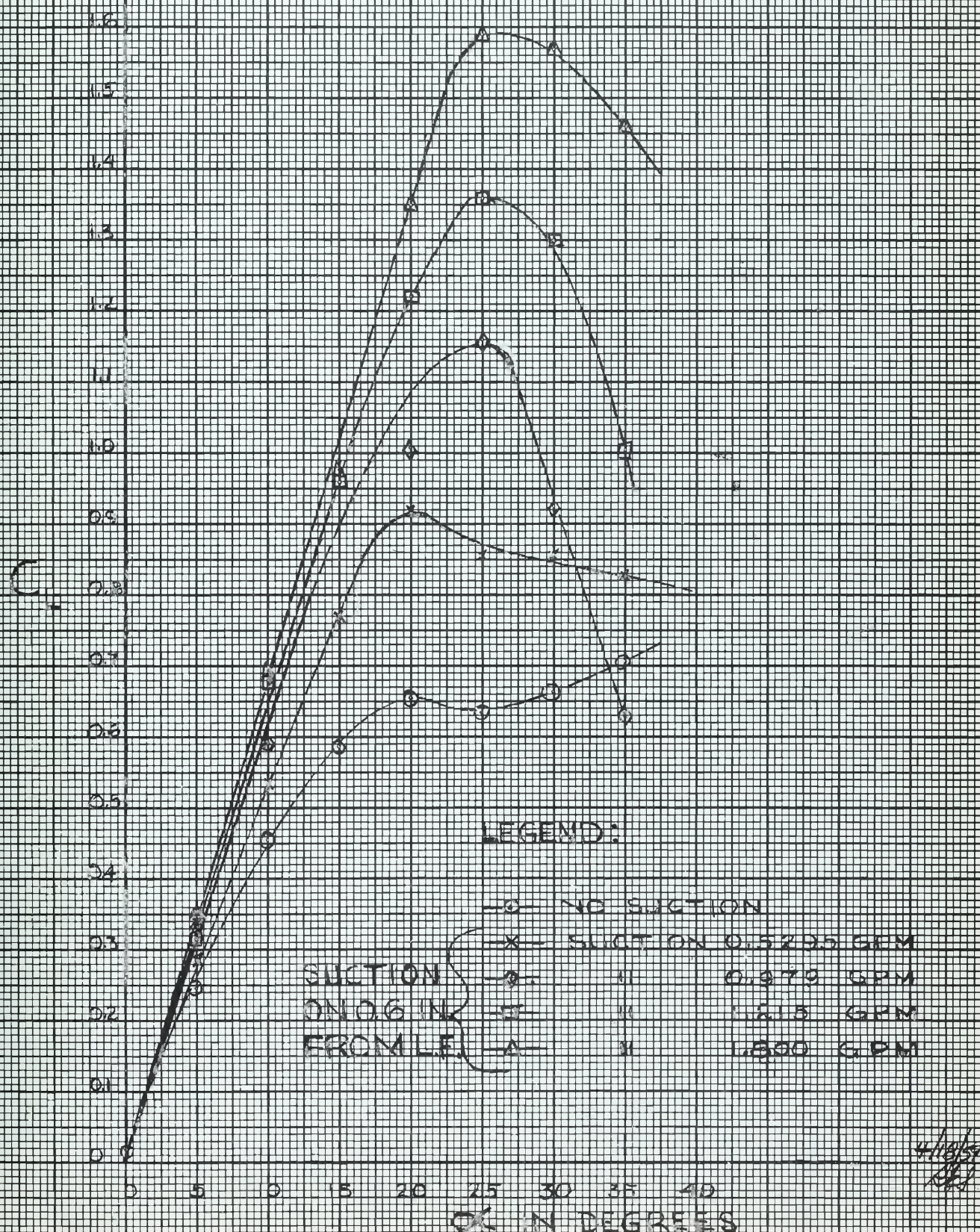
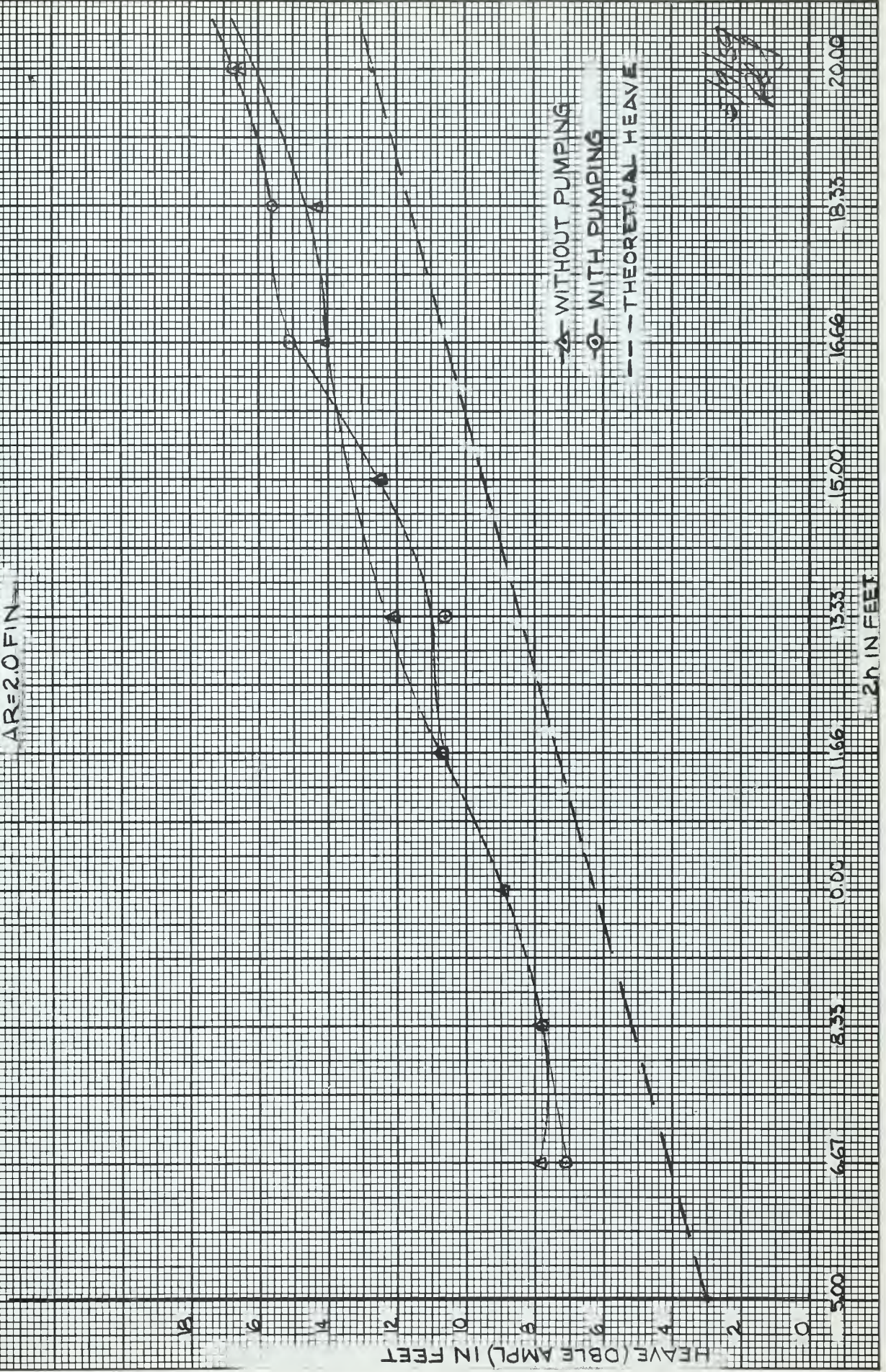


FIGURE XIV

HEAVE AS A FUNCTION OF WAVE HEIGHT FOR $\lambda=600$ FT. AND CONSTANT SPEED

$\Delta R=2.0$ FIN



5/11/59
R.S.J.

PITCH (DOUBLE AMPL) IN DEGREES

FIGURE XV
PITCH AS A FUNCTION OF WAVE HEIGHT FOR

$\lambda = 600$ FT AND CONSTANT SPEED

$AR = 2.0$ F/N

LEGEND:
A WITHOUT PUMPING
O WITH PUMPING
--- THEORETICAL PITCH

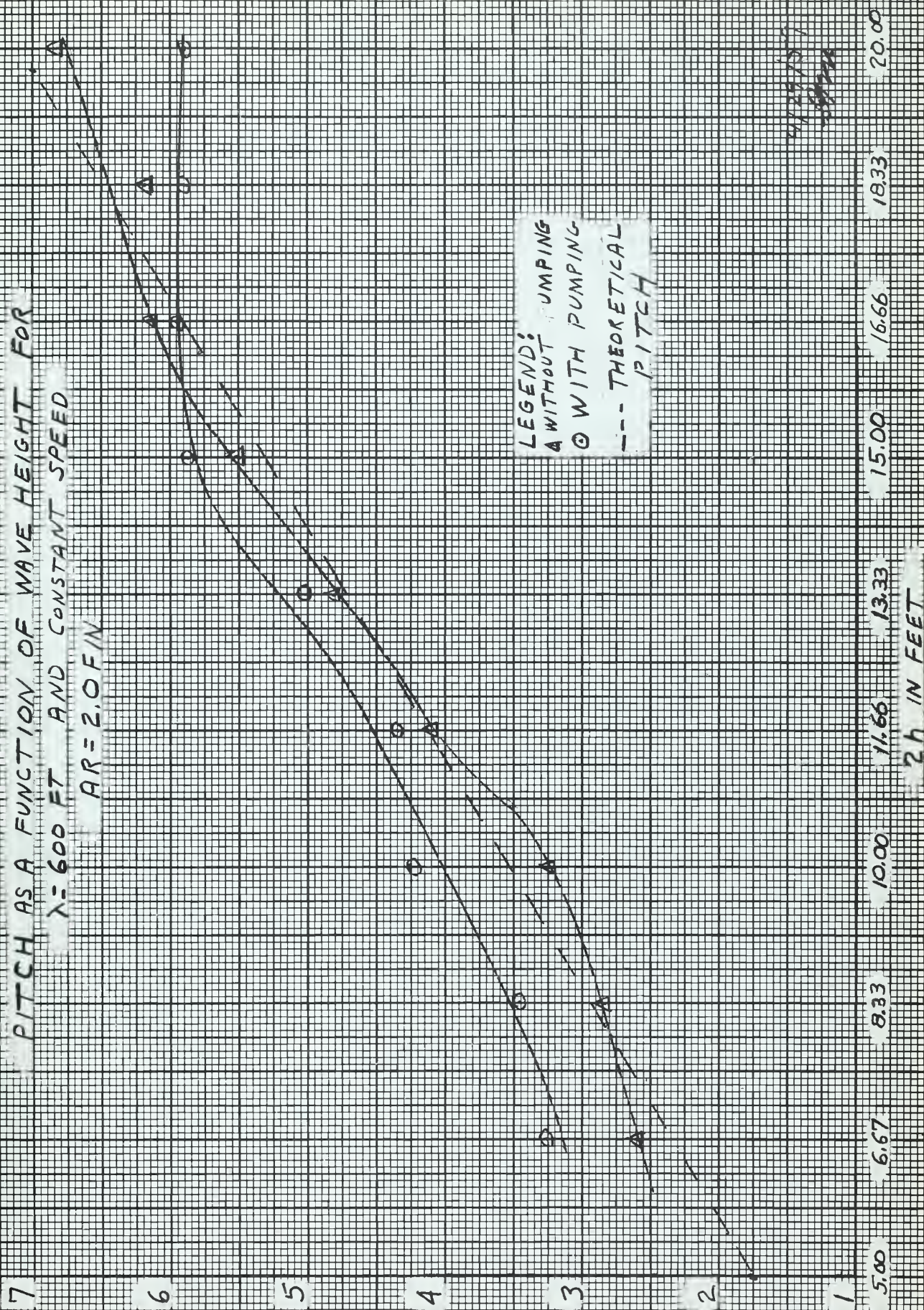
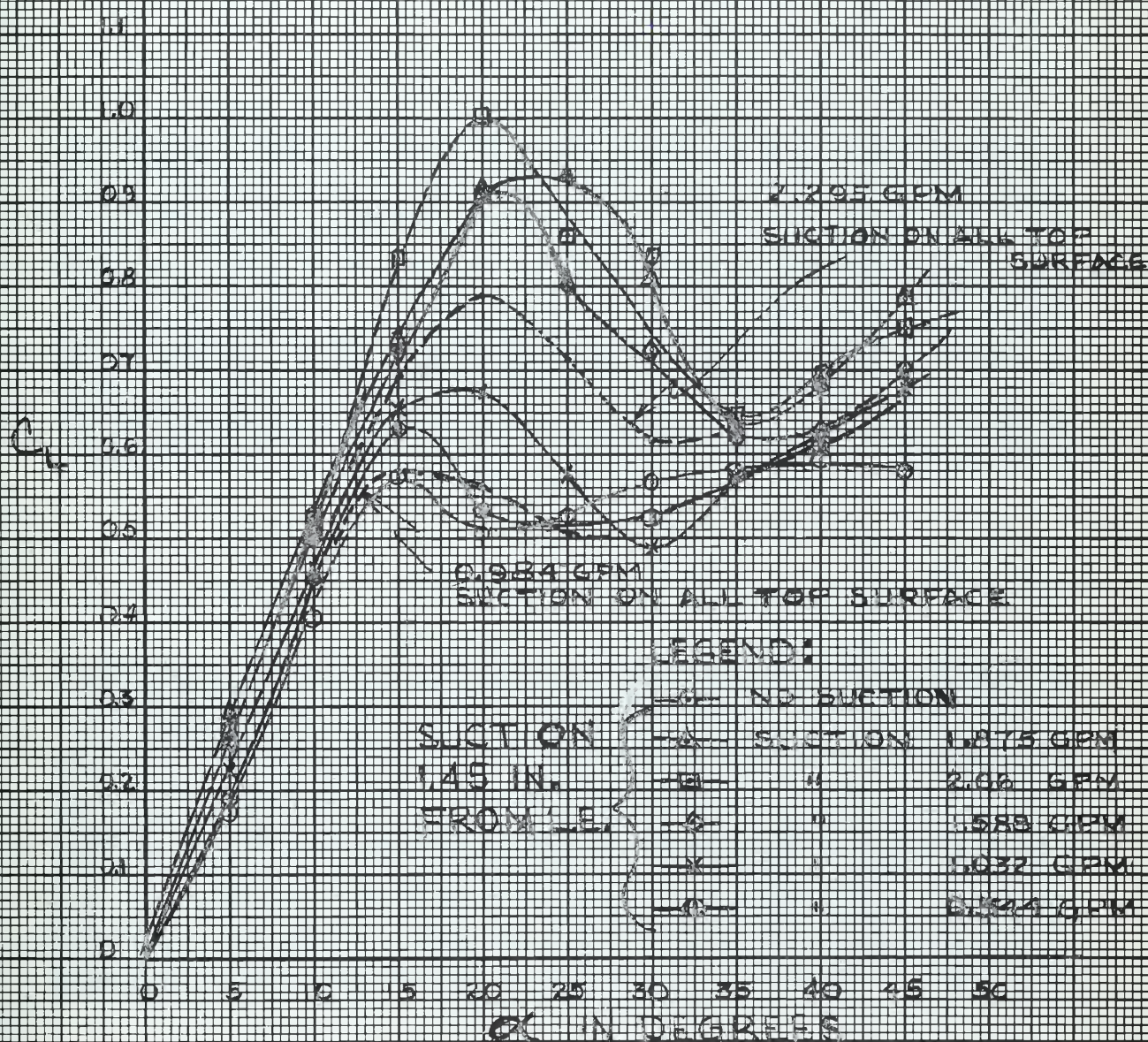


FIGURE XVI
NACA-0018 FOIL - ANGLE OF ATTACK VS
LIFT COEFFICIENT

EFF. AR = 2.0



4/19/59
HSL

Figure XVII. Vibrations of the bow for fin (eff. $AR = 2.0$) mounted 3 inches below the baseline in waves of $\lambda = 6.0$ ft. and $2h = 2.0$ in. without (A) and with (B) boundary layer control.

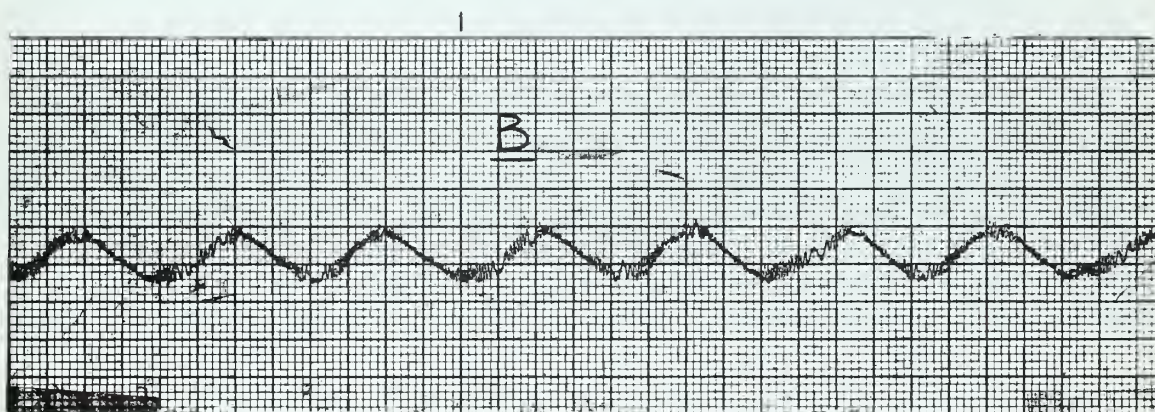
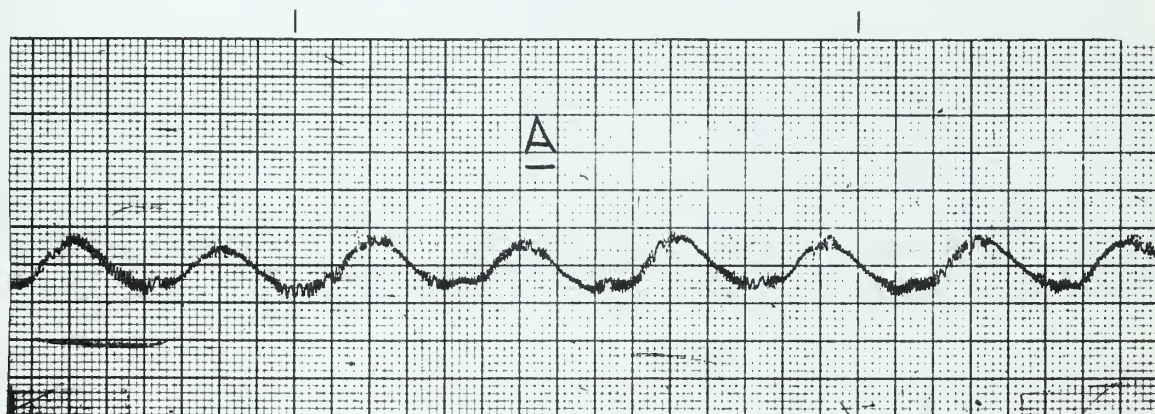


Figure XVIII. Vibrations of the bow for fin (eff. $AR=2.0$) mounted 3 in. below the baseline in waves of $\lambda=6.0$ ft. and $2h=0.8$ without (A) and with (B) boundary layer control.

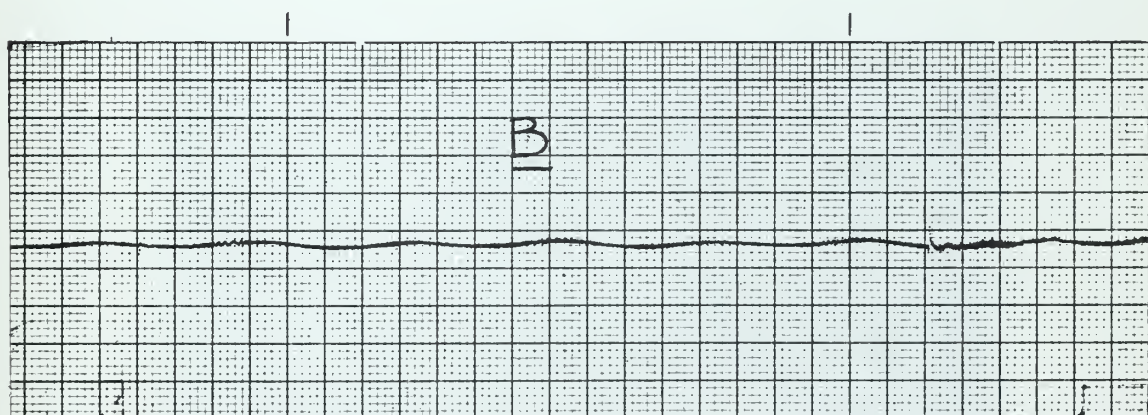
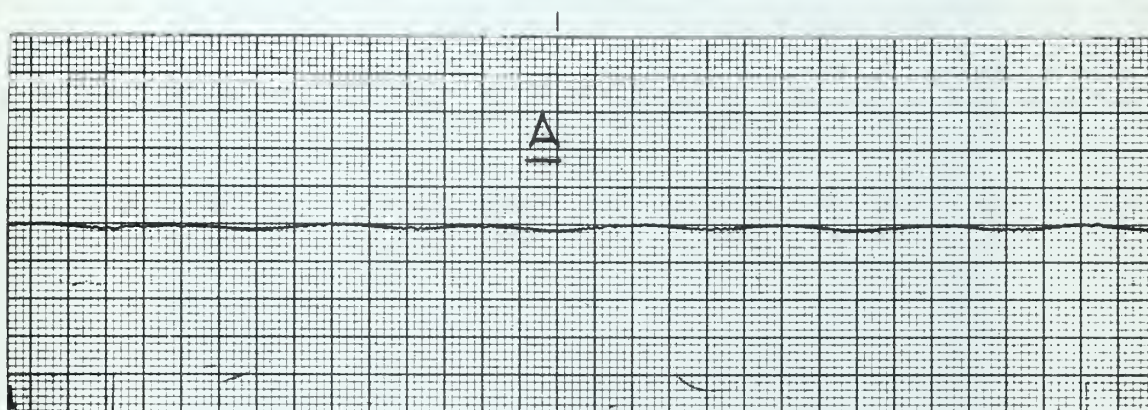
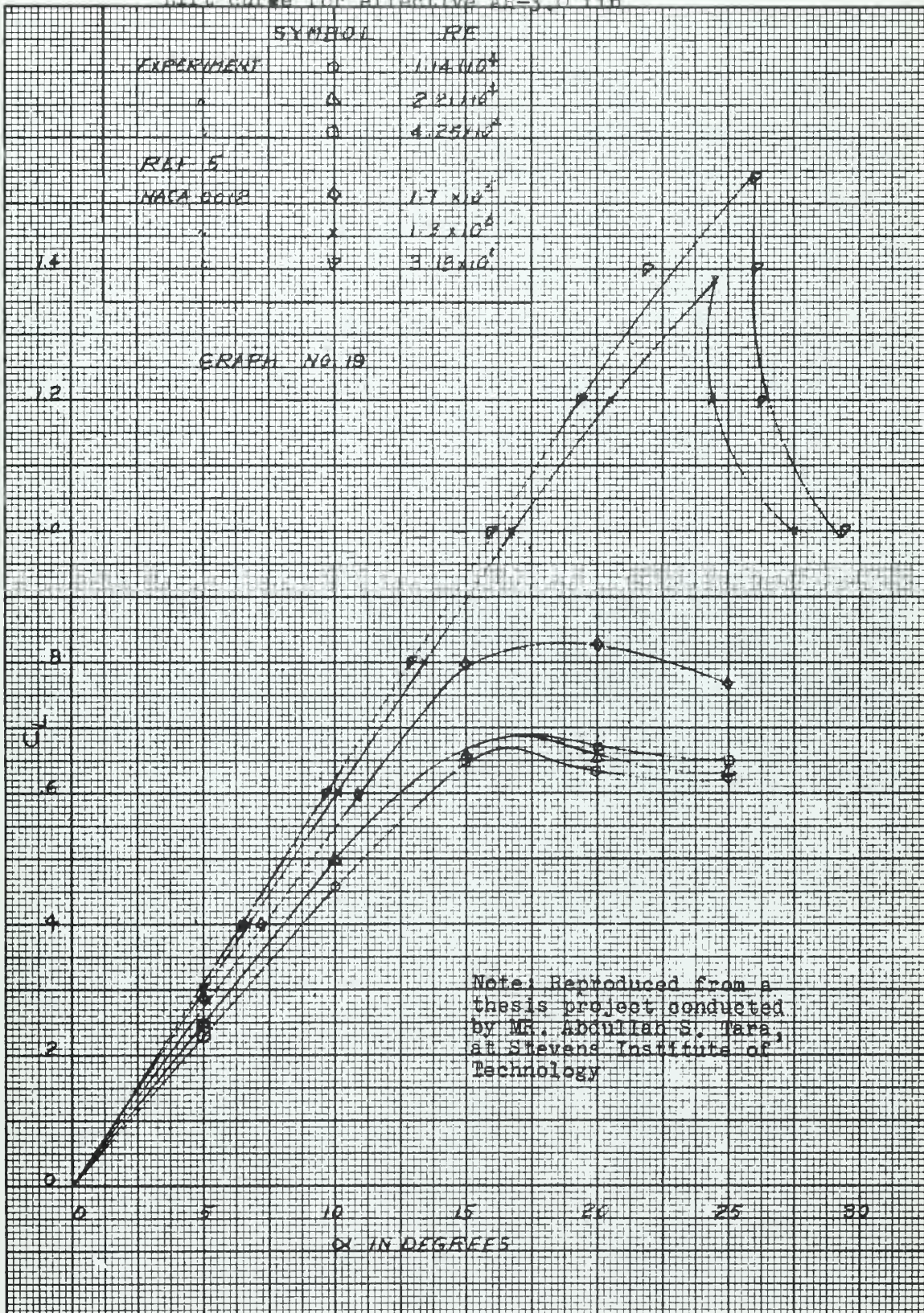


Figure XIX
View of AR= 4.0 fin showing full bubble formation for
 $\lambda = 6.0$ Ft. and $2h = 2.3$ in.



Figure XX
Lift curve for effective AR=3.0 fin



VII. APPENDIX

APPENDIX A

DETAILS OF PROCEDURE

A. Manufacture and installation

The fin with an effective $AR = 4$ was manufactured from solid brass bar stock to conform with the section shape for the NACA-0018 airfoil. The dimensions of this section were reduced by 0.02 inches to allow for the thickness of the perforated brass sheet which formed the surface of the fin. The brass sheet was first formed around the solid section. The end pieces and the center section were then cut from the solid airfoil section and were soldered as ribs into the perforated sheet. The fin had a projected area of 7.83 square inches, a total span of 5.60 inches and a chord length of 1.4 inches.

The brass sheeting was perforated with 24 staggered rows of holes per inch along the span of the fin. The holes in each row were 0.023 inches in diameter and were spaced to provide 18 holes per inch along the chord of the fin. The holes in the way of the end pieces were sealed for a distance of 0.118 inches at the fin tips. For a distance of about 0.2 inches from the trailing edge the upper and lower edges of the fin were sealed together by solder. The fin was mounted on the model at the forward perpendicular with the chord parallel to the base line. The model had a bulbous bow which made a good platform upon which to mount the fin. A $\frac{1}{8}$ inch hole was drilled in the model at an angle of 50° to accommodate the $7/16$ inch steel tube which was soldered to the fin. This tube was used to take a suction on the fin surface.

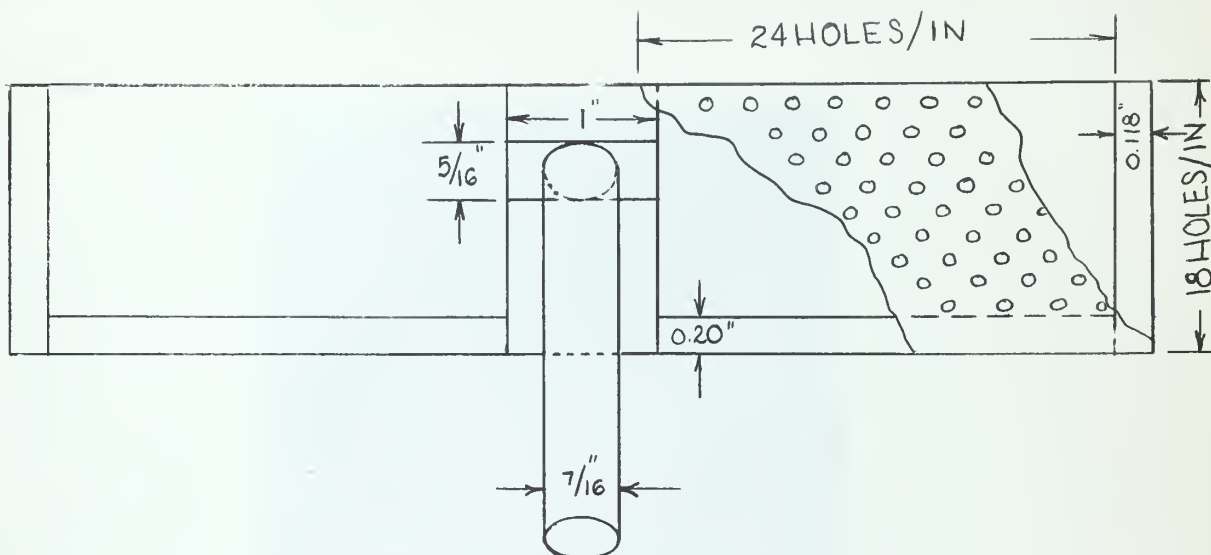


FIGURE XXI. Sketch showing construction of the $AR = 4.0$ fin

Figure XXII shows the small fin in position on the model. The fin, as stated previously, was mounted with the chord parallel to the base line of the model for zero installed angle of attack. The experimental work was conducted with the holes in the high pressure surface sealed with a mixture of paraffin and beeswax. The holes in the low pressure surface were left open for 0.60 inches from the leading edge of the fin. Figure XXIII shows the boundary layer control pump arrangement inside the model. This pump was used to take a suction on the fin via the indicated tubing. The discharge from the pump was piped overboard through a $\frac{1}{2}$ inch rubber tube.

The fin with effective $AR = 2$ was manufactured from 1 inch plexi-glass stock to conform with the section shape for the NACA-0018 airfoil. The dimensions of the low pressure side of the section were reduced by 0.02 inches to allow for the thickness of the perforated brass sheet.

Figure XXII
View of $AR=4.0$ fin installed on model



Figure XXIII
View of the interior of the model



The fin had a projected area of 32 square inches with a total span of 8 inches and with a chord length of 4 inches. A $\frac{1}{2}$ inch section was provided in the center to mount the fin on the model. The upper part of the fin was hollowed by milling $\frac{1}{4}$ inch from the thickest section. This provided a chamber inside the fin from which a suction could be taken from the low pressure surface through a $\frac{1}{2}$ inch aluminum tube. (See Figure XXIV). After hollowing out the inside of fin, the perforated brass sheet was shaped to conform with the section and was cemented to the low pressure surface with Duco cement. The trailing part of the low pressure surface was then covered with thin strips of rubber tape to a point 1.45 inches from the leading edge.

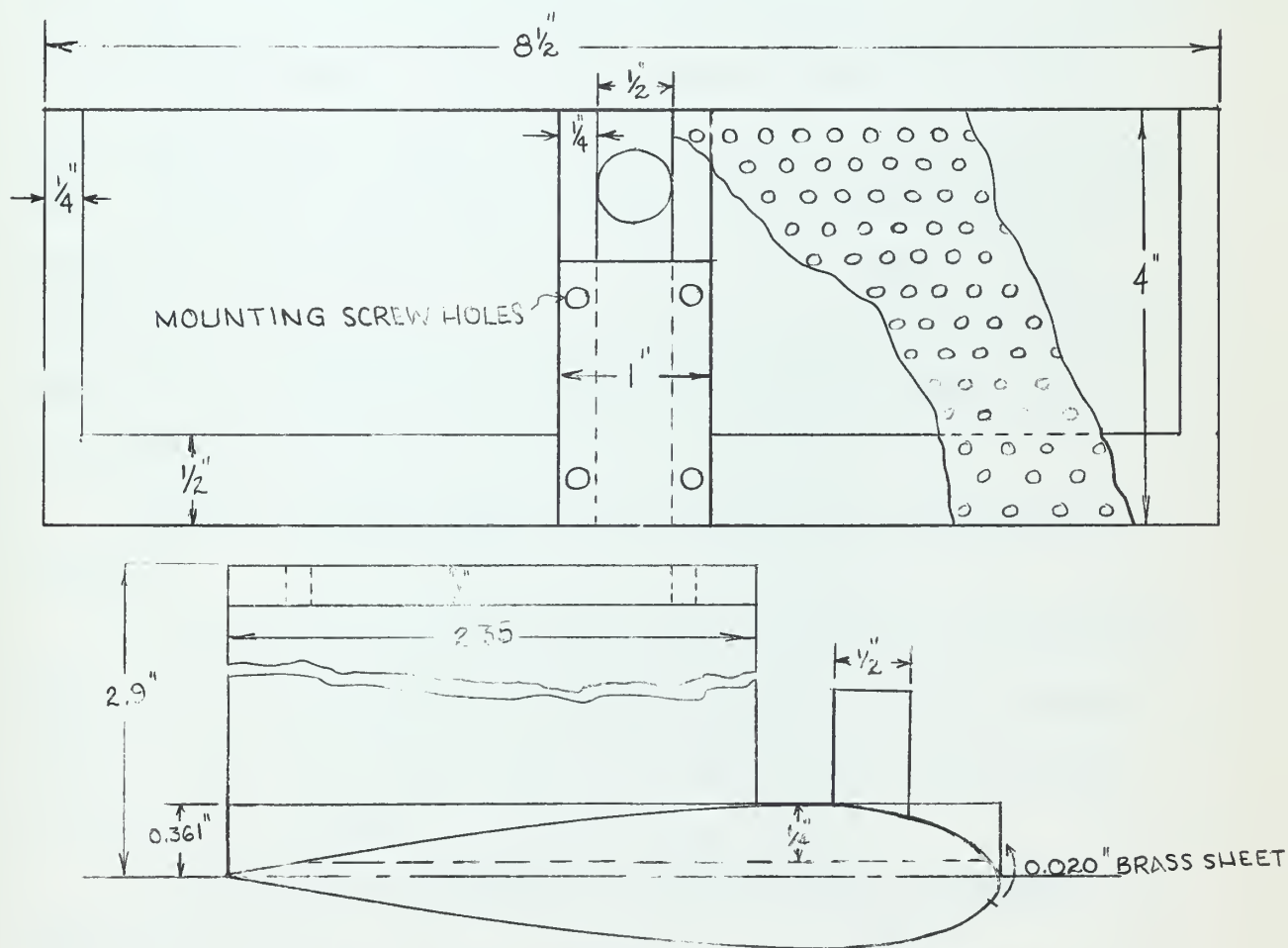


FIGURE XXIV. Sketch showing construction of the AR = 2.0 fin

When installed, the fin was mounted approximately 3 inches below base line and parallel to it. A sheet metal fairing was formed around the vertical leading edge of the supporting strut and tube connection so that the low pressure surfaces on each side of the model were separated from one another, (see Figure XXVI). The $\frac{1}{2}$ inch aluminum tube on the fin was connected by a short length of $\frac{1}{2}$ inch rubber tubing to the $7/16$ inch steel tube that passed through the hole in the model. The arrangement of tubes and pump as shown in Figure XXIII was the same as for the AR4 fin.

B. Details of model instrumentation

The model used for this thesis was MIT Model B. It is a model of a 17,800 ton ocean going passenger ship operating in the North Atlantic, ($\lambda = 100$)(Table XXXIV). Figure XXIII shows an interior view of the model with the covers removed. Figure XXV shows the model in the towing tank. It should be noted that a standard towing bracket is used to tow the model. The vertical wood stick having a white stripe on a black background was marked in one inch increments and was installed amidships. This stick provided the record of model motions that could be seen in the photographs.

Referring to Figure XXIII the following items are installed in the model:

1. The steel bar with four strain gages connected in a full bridge which measured the transverse bow vibrations [see Figure II, reference (15)]. The bow was "tuned" (15) to vibrate in water at approximately 23 vibrations per second.

2. The inboard arrangement of the $7/16$ inch steel and $\frac{1}{2}$ inch rubber tubing used for taking a suction on the fin surface.

Figure XXV
Model in the Towing Tank with "fishing pole" attached.



Figure XXVI
Fin of eff. AR 2.0 installed on the model with arrangement used for introducing dye ahead of the fin.



Figure XXVII
View of the dynamometer end of the Towing Tank

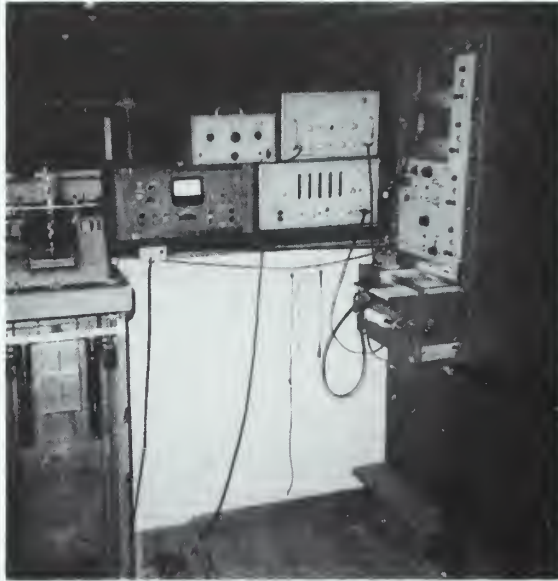


Figure XXVIII
Baldwin Strain Indicator and fin mounted on the apparatus used to measure the lift versus angle of attack.



3. The suction pump which was an Eastern Industries Model A-1 pump. It has a maximum capacity of 4.5 GPM and is driven by a 115 volt AC-DC motor.

C. Description of the apparatus for calibrating fins

Four SR-4 Type A-7 strain gages, connected in a full bridge, were attached to a $1" \times \frac{1}{4}"$ aluminum bar, (Figure XXVIII). This arrangement compensated for temperature variations and measured only vertical shear forces in the bar.

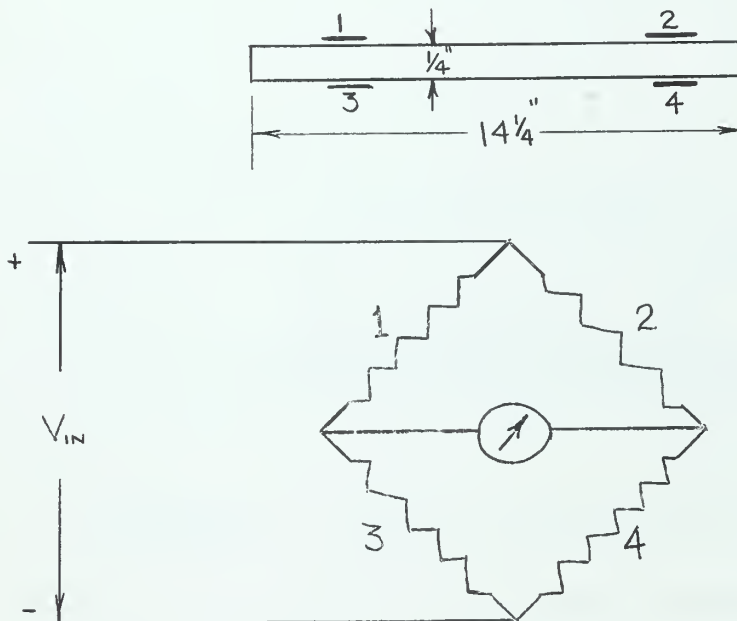


FIGURE XXIX. Sketch of strain gage arrangement

The strain gages were waterproofed by layers of a paraffin and beeswax mixture covered by the thick layer of vaseline. This method, carefully done, was found to be very effective.

The apparatus resembled a large "L" with the fin attached to the end of the horizontal aluminum bar which, in turn, was attached to a vertical $1\frac{1}{4}$ inch diameter steel bar 33 inches long. The fin angle of

attack was indicated by putting 5° scribe marks on a copper sheet, the center of which was the center of rotation. Pumping, or suction, in this case, was accomplished by connecting $\frac{1}{2}$ inch rubber tubing from the fin to a $\frac{7}{16}$ inch steel tube tied to the aluminum bar. The steel tube in turn was connected to the vacuum pump by $\frac{1}{2}$ inch rubber tube. Figure XXX is a sketch of the arrangement.

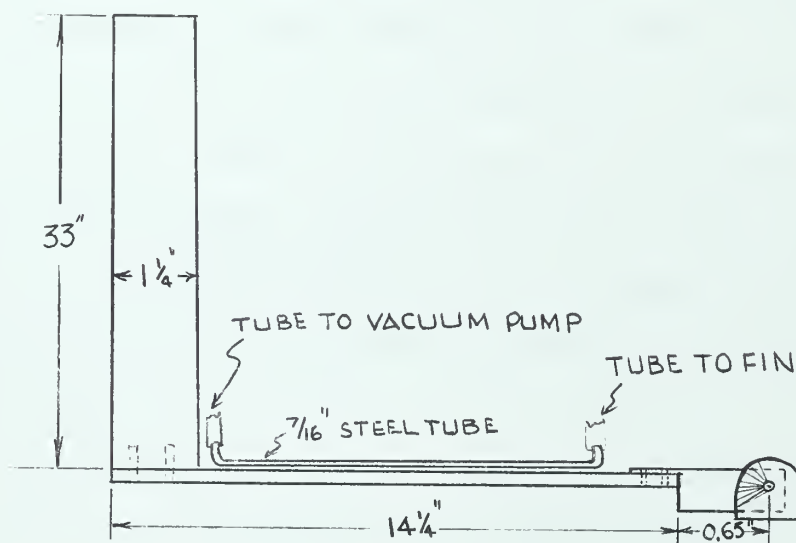


FIGURE XXX. Sketch of calibration apparatus

A sheet metal fairing was constructed to separate the two ends of the fin to simulate the same water flow pattern that occurred on the model.

When taking lift measurements, the apparatus was clamped by a vise at the top of the propeller tunnel so the fin was suspended in the center of the test section.

The lift force on the fin was measured by the strain gages which were connected to a Type K Baldwin Strain Indicator. The suction was accomplished by the use of the vacuum pump available near the propeller

tunnel. The operation of the propeller tunnel is described in (11).

D. Details of Towing Tank instrumentation

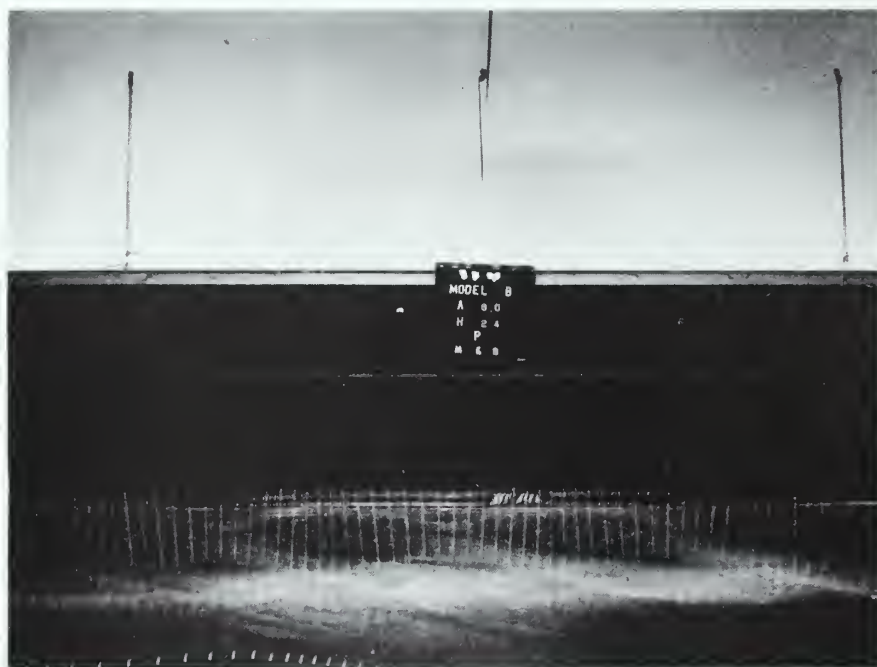
A general description of the towing tank is given in (4). Because the MIT towing tank does not, at the present time, have a towing carriage, a "fishpole" arrangement as shown in Figure XXV was used. The electrical connections for the pump motor and the strain gages were led through long cables from a 115 volt, 60 cycle, AC wall socket and the Sanborn Recorder respectively, via the "fishpole" to the model.

The speed and the transverse bow vibrations of the model were recorded on each of two channels of the Sanborn Recorder installed at the tank. The Sanborn Recorder is constructed so a full bridge strain gage arrangement can be connected directly to it. The speed signal from the photoelectric cell is fed to the recorder through the electronic E-Put meter and an integrator.

The photographic procedure for determining model heave and pitch is described in (19). The Graphic View II Camera by Graphlex, Inc. was carefully mounted at the side of the tank and focused on the model attached to the towing cord. Kodak Royal Pan 4" x 5" sheet film was used and the lens opening was set at f-32. During each run, the towing tank was darkened, the camera shutter was opened, and as the model passed the camera a stroboscope with strobolume was used to obtain a series of pictures of the model motions as it moved across the negative. (Figure XXXI). The photographs were then processed and the motions were measured from the negatives.

When motion pictures of the fin were taken, a super speed 16 mm. Bell and Howell Film Automatic Cine Camera was used. This camera takes movies at the rate of 100 frames per second. Lighting was provided by

Figure XXXI
Photographic method used to determine pitch and
heave of the model



a battery of four flood lamps mounted so they illuminated the water behind the glass panel in the side of the towing tank. During each run, one man with the camera sat behind this glass and photographed the fin as it passed through the illuminated area.

APPENDIX B

SUMMARY OF DATA AND CALCULATIONS

A. Theoretical motion calculation for Model B prototype

TABLE I

Properties of Hull

LBP	481.9 Ft.
Max. Beam	69.6 Ft.
Max. Draft	28.677 Ft.
Displacement	17,800.0 Tons
Radius of gyration	0.25 L = 120.2 Ft.
Designed speed	17.5 Kts.
LCB as % LBP from XX	0.

<u>Station</u>	<u>S</u>	<u>B</u>	<u>S/B</u>
0	95.9	0.87	109.6
2	621.0	28.2	21.05
4	1351.0	55.0	24.55
6	1830.0	67.7	27.05
8	1970.0	69.6	28.35
10	1980.0	69.6	28.45
12	1963.0	69.6	28.08
14	1798.0	69.2	26.00
16	1340.0	60.4	22.20
18	647.0	39.1	16.59
20	7.95	6.1	1.305

TABLE II

Calculation of values of sines and cosines
for equation (1) for heave

$\lambda = 600$ Ft.

Heave (wave crest at station 11)

Station	x	$\frac{2\pi x}{\lambda}$	Deg.	$\sin \frac{2\pi x}{\lambda}$	$\cos \frac{2\pi x}{\lambda}$
0	415	4.345	248.9	-.93358	-.35837
2	366.8	3.840	219.9	-.64279	-.76604
4	318.6	3.335	191.1	-.19766	-.98027
6	270.4	2.831	162.2	.30542	-.95213
8	222.2	2.326	133.2	.72897	-.68455
10	174.09	1.823	104.4	.96815	-.25038
12	125.91	1.308	75.5	.96815	.25038
14	77.75	0.814	46.6	.72657	.68709
16	29.55	0.309	17.7	.30348	.95275
18	-18.62	-0.195	-11.17	-.19366	.98107
20	-66.80	-0.699	-40.00	-.64412	.76492

TABLE III

Calculation of values of sines and cosines
for equation (1) for pitch

$\lambda = 600$ Ft.

Pitch (wave nodal point at station 11)

Station	x	$\frac{2\pi x}{\lambda}$	Deg.	$\sin \frac{2\pi x}{\lambda}$	$\cos \frac{2\pi x}{\lambda}$
0	265	2.773	158.96	.35891	-.9337
2	216.8	2.269	130.06	.76530	-.64368
4	168.6	1.764	101.12	.98124	-.19281
6	120.4	1.260	72.23	.95231	.30514
8	72.2	.755	43.28	.68561	.72797
10	24.09	.252	14.44	.24925	.96844
12	-24.09	-.252	-14.44	-.24925	.96844
14	-72.2	-.755	-43.28	-.68561	.72797
16	-120.4	-1.260	-72.23	-.95231	.30514
18	-168.6	-1.764	-101.12	-.98124	-.19281
20	-216.8	-2.269	-130.06	-.76530	-.64368

TABLE IV

Ship speed and frequency

$$\lambda = 600 \text{ Ft.}$$

V_s	11.0 (Equivalent to model speed using small fins and constant tow force of 17.5 knot still water speed)
V_s fps	18.579
C	-55.50
ω_e	0.7770
ω_e^2	.60372

TABLE V

K_L Values

(Refer to figure No.)

Station	$\frac{\omega_e^2 B}{2g}$	K_L
0	.00815	$\rightarrow \infty$
2	.264	.815
4	.515	.640
6	.635	.609
8	.652	.602
10	.652	.602
12	.652	.602
14	.649	.603
16	.566	.624
18	.366	.725
20	.057	1.210

TABLE VI

K₂ Values

$$C_s = f\left(\frac{S}{BH}, BH\right) \left[\text{Figure XII, reference (6)} \right]$$

$$K_2 = C_s \left(\frac{\pi B^2}{8S} \right)$$

Station	BH	$\frac{S}{BH}$	B/H	C _s	B ²	$\frac{B^2}{S}$	$\frac{\pi B^2}{8S}$	K ₂
0	24.95	3.830	.030		.757	.00793	.00311	.05
2	808.69	.768	.983	0.96	795.2	1.280	.503	.483
4	1577.20	.856	1.917	1.11	3025.0	2.239	.879	.976
6	1941.43	.943	2.361	1.25	4583.3	2.504	.983	1.229
8	1995.90	.987	2.427	1.40	4844.2	2.458	.965	1.351
10	1995.90	.992	2.427	1.45	4844.2	2.446	.961	1.529
12	1995.90	.983	2.427	1.39	4844.2	2.468	.969	1.347
14	1984.44	.906	2.413	1.17	4788.6	2.663	1.046	1.224
16	1732.09	.774	2.106	0.97	3648.2	2.722	1.069	1.037
18	1121.27	.578	1.360	0.79	1528.8	2.360	.927	.732
20	174.93	.045	0.213		37.21		1.838	1.15

TABLE VII

Calculation of I in equations (2) and (3)

$$\lambda = 600 \text{ Ft.} \quad \text{Heave}$$

$$I = \int \frac{B}{2} \sin \frac{2\pi x}{\lambda} dx$$

Station	(1) $\frac{B}{2}$	(2) $\sin \frac{2\pi x}{\lambda}$	(3) = (1)x(2)	(4) SM	(3)x(4)
0	0.435	-.93358	-.4061	1	-.4061
2	14.10	-.64279	-9.0633	4	-36.2532
4	27.50	-.19766	-5.4356	2	-10.8712
6	33.85	.30542	10.3385	4	41.3540
8	34.80	.72897	25.3682	2	50.7364
10	34.80	.96815	33.6916	4	134.7664
12	34.80	.96815	33.6916	2	67.3832
14	34.60	.72657	25.1393	4	100.5572
16	30.20	.30348	9.1651	2	18.3302
18	19.55	-.19366	-3.7861	4	-12.1444
20	3.05	-.64412	-1.9646	1	-1.9646

Sum = 351.50

TABLE VIII

Calculation of II in equations (2) and (3)

$$\lambda = 600 \text{ Ft.} \quad \text{Heave}$$

$$II = \int \frac{B}{2}(1+K_2K_4) \sqrt{\frac{2S}{\pi}} \sin \frac{2\pi x}{\lambda} dx$$

Station	(1) $\frac{B}{2} \sin \frac{2\pi x}{\lambda}$	(2) K_2K_4	(3) $\frac{2S}{\pi}$	(4) $(1) \times (2) \times (3)$	(5) SM $(4) \times (5)$
0	-.4061	0	60.95	-3.166	1
2	-9.0633	.394	395.329	-250.789	4
4	-5.4356	.625	860.047	-259.244	2
6	10.3385	.748	1164.978	617.148	4
8	25.3682	.813	1254.102	1629.056	2
10	33.6916	.920	1260.468	2296.419	4
12	33.6916	.810	1249.646	2155.706	2
14	25.1393	.738	1144.607	1478.541	4
16	9.1651	.647	853.044	441.074	2
18	-3.7861	.530	412.389	-117.650	4
20	-1.9646	1.39	5.060	-10.612	1
Sum =					24014.104

TABLE IX

Calculation of III in equations (2) and (3)

$$\lambda = 600 \text{ Ft.} \quad \text{Heave}$$

$$III = \int \frac{B}{2}(1+K_2K_4) S \sin \frac{2\pi x}{\lambda} dx$$

Station	(1) $\frac{B}{2} \sin \frac{2\pi x}{\lambda}$	(2) $1+K_2K_4$	(3) S	(4) $(1) \times (2) \times (3)$	(5) SM $(4) \times (5)$
0	-.4061	1	95.5	-38.782	1
2	-9.0633	1.394	621.0	-7845.863	4
4	-5.4356	1.625	1351	-11933.180	2
6	10.3385	1.748	1830	33071.207	4
8	25.3682	1.813	1970	90605.316	2
10	33.6916	1.920	1980	128081.987	4
12	33.6916	1.810	1963	119707.266	2
14	25.1393	1.738	1798	78558.401	4
16	9.1651	1.647	1340	20227.191	2
18	-3.7861	1.530	647.8	-3752.532	4
20	-1.9646	2.390	7.95	-37.328	1
Sum =					1349609.87

TABLE X

Calculation of IV in equations (2) and (3)

$$\lambda = 600 \text{ Ft.} \quad \text{Heave}$$

$$IV = \int \frac{B(1+K_2K_4)}{2} \frac{1}{\sqrt{2\pi S}} \frac{dS}{d\xi} \cos \frac{2\pi x}{\lambda} dx$$

Station	(1) $\frac{dS}{d\xi}$	(2) $\frac{B}{2}$	(3) $\cos \frac{2\pi x}{\lambda}$	(4) $A=(2)x(3)$	(5) $(1)x(4)$	(6) $\sqrt{2\pi S}$
0	-8.302	0.435	-.35837	-.1559	1.294	24.494
2	-13.502	14.10	-.76604	-10.801	145.835	62.50
4	-13.709	27.50	-.98027	-26.957	369.553	92.15
6	-6.439	33.85	-.95213	-32.229	207.522	107.20
8	-1.039	34.80	-.68455	-23.822	24.751	111.20
10	0	34.80	-.25038	-8.713	0	111.70
12	1.246	34.80	.25038	8.713	10.856	111.10
14	6.231	34.60	.68709	23.773	148.129	106.30
16	12.879	30.20	.95275	28.773	370.567	91.73
18	14.956	19.55	.98107	19.179	286.841	63.80
20	6.640	3.05	.76492	2.330	15.471	7.06

Station	(7) $\frac{1}{\sqrt{2\pi S}}$	(8) $(5)x(7)$	(9) $(1+K_2K_4)$	(10) $(8)x(9)$	(11) SM	$(10)x(11)$
0	.04083	.0528	1.0	.0528	1	.0528
2	.0160	2.333	1.394	3.2522	4	13.2088
4	.0108	3.991	1.625	6.4854	2	12.9708
6	.00933	1.936	1.748	3.3841	4	13.5364
8	.008992	.223	1.813	.4043	2	.8086
10	-	0	1.920	0	4	0
12	.008992	.0976	1.810	.1766	2	.3532
14	.00940	1.3920	1.738	2.4119	4	9.6772
16	.010901	4.0395	1.647	6.6530	2	13.3060
18	.010567	4.4948	1.530	6.8770	4	27.5080
20	.14160	2.1907	2.390	5.2358	1	5.2358

Sum = 96.6576

TABLE XI

Calculation of V in equations (2) and (3)

$$\lambda = 600 \text{ Ft.} \quad \text{Heave}$$

$$V = \int \frac{B}{2}(1+K_2K_4) \frac{dS}{d\xi} \cos \frac{2\pi x}{\lambda} dx$$

Station	(1) $\frac{dS}{d\xi}$	(2) $(1+K_2K_4)$	(3) $(1) \times (2)$	(4) SM	(3) x (4)
0	1.294	1.0	1.294	1	1.294
2	145.835	1.394	203.293	4	813.172
4	369.553	1.625	600.524	2	1201.048
6	207.522	1.748	362.748	4	1450.992
8	24.751	1.813	44.873	2	89.746
10	0	1.920	0	4	0
12	10.856	1.810	19.649	2	39.298
14	148.129	1.738	257.448	4	1029.792
16	370.567	1.647	610.324	2	1220.648
18	286.841	1.530	438.867	4	1755.468
20	15.471	2.390	369.757	1	<u>369.757</u>
Sum				=	7971.215

TABLE XII

Calculation of $\int \frac{B}{2} \sin \frac{2\pi x}{\lambda} \left(\xi + \frac{1}{\pi} \frac{dS}{d\xi} \right) dx$ in equation (3)
 $\lambda = 600 \text{ Ft.}$ Pitch

Station	(1) ξ	(2) $\frac{1}{\pi} \frac{dS}{d\xi}$	(3) $(1)+(2)$	(4) $\sin \frac{2\pi x}{\lambda} (F)$	(5) $\sin \frac{2\pi x}{\lambda} (M)$
0	240.95	-2.643	238.31	-.93358	.35891
2	192.76	-4.298	188.46	-.64279	.76530
4	144.57	-4.364	140.21	-.19766	.98124
6	96.38	-2.049	94.33	.30542	.95231
8	48.19	-0.331	47.86	.72897	.68561
10	0	0	0	.96815	.24925
12	-48.19	.397	-47.79	.96815	-.24925
14	-96.38	1.983	-94.40	.72657	-.68561
16	-144.57	4.099	-140.47	.30348	-.95231
18	-192.57	4.761	-188.00	-.19366	-.98124
20	-240.95	2.114	-238.84	-.64412	-.76530

TABLE XII (Continued)

Station	(6) (5)/(4)	(7) (3)x(4) from Table	(8) (6)x(7)	(3)x(8)
0	-.3844	-.4061	0.1561	37.2002
2	-1.1906	-36.2532	43.1630	8134.4990
4	-4.9643	-10.8712	53.9679	7566.8393
6	3.1180	41.3540	128.9418	12163.0800
8	.9405	50.7364	47.7176	2283.7643
10	.2574	134.7664	34.6889	0
12	-.2574	67.3832	-17.3444	828.8889
14	-.9436	100.5572	-94.8857	8957.2101
16	-3.1379	18.3302	-57.5183	8079.5956
18	5.0668	-12.1444	-61.5332	11568.2416
20	1.1881	-1.9646	-2.3341	<u>557.7644</u>
Sum =				60177.085

TABLE XIII

Calculation of $\int \frac{B}{2}(1+K_2K_4) \sqrt{\frac{2S}{\pi}} \sin \frac{2\pi x}{\lambda} \left(\xi + \frac{1}{\pi} \frac{dS}{d\xi} \right) dx$ in equation (3)

$\lambda = 600$ Ft.

Pitch

Station	(1) (4)x(5) Table	(2) (6) Table	(3) (3) Table	(1)x(2)x(3)
0	-3.144	-.3844	238.31	288.117
2	-1003.156	-1.1906	188.46	225089.086
4	-518.488	-4.9643	140.21	360890.725
6	2468.592	3.1180	94.33	726063.670
8	3258.112	.9405	47.86	146655.005
10	9185.676	.2574	0	0
12	4311.412	-.2574	-47.86	53035.430
14	5914.164	-.9436	-94.40	526809.121
16	882.148	-3.1379	-140.47	388835.007
18	-470.600	5.0668	-188.00	448274.720
20	-10.612	1.1881	-238.84	<u>3011.323</u>
Sum =				2,878,952.21

TABLE XIV

Calculation of $\int \frac{B(1+K_2K_4)}{2} S \sin \frac{2\pi x}{\lambda} \left(\xi + \frac{1}{\pi} \frac{dS}{d\xi} \right) dx$ in equation (3)

$\lambda = 600$ Ft. Pitch

Station	(1) (4)x(5) Table	(2) (6) Table	(3) (3) Table	(1)x(2)x(3)
0	-38.782	-.3844	238.31	3552.68
2	-31383.452	-1.1906	188.46	7041833.91
4	-23866.360	-4.9643	140.21	16597660.20
6	132284.828	3.1180	94.33	38932695.44
8	181210.632	.9405	47.86	8153276.20
10	512347.948	.2574	0	0
12	239414.532	-.2574	-47.79	2974821.31
14	314233.604	-.9436	-94.40	27990621.41
16	40454.382	-3.1379	-140.47	17843441.57
18	-15010.128	5.0668	-188.00	14307055.68
20	-37.328	1.1881	-238.84	10609.27

Sum = 133,851,467.00

TABLE XV

Calculation of $\int \frac{B(1+K_2K_4)}{2} \frac{1}{\sqrt{2\pi S}} \frac{dS}{d\xi} \cos \frac{2\pi x}{\lambda} \left(\xi + \frac{1}{\pi} \frac{dS}{d\xi} \right) dx$ in equation (3)

$\lambda = 600$ Ft. Pitch

Station	(1) (10)x(11) Table	(2) $\cos \frac{2\pi x}{\lambda}$ (F)	(3) $\cos \frac{2\pi x}{\lambda}$ (M)	(4) (3)/(2)	(5) (3) Table	(6) (1)x(5)	(4)x(6)
0	0.0528	-.35837	-.93370	2.6054	238.31	12.583	32.784
2	13.2088	-.76604	-.64368	.8403	188.46	2489.330	2091.784
4	12.9708	-.98027	-.19281	.1967	140.21	1818.636	357.726
6	13.5364	-.95213	.30514	-.3203	94.33	1276.889	-408.988
8	.8086	-.68455	.72797	-1.0634	47.86	38.700	-41.154
10	0	-.25038	.96844	-3.8680	0	0	0
12	.3532	.25038	.96844	3.8680	-47.79	-16.879	-65.271
14	9.6772	.68709	.72797	1.0595	-94.40	-913.528	-967.883
16	13.3060	.95275	.30514	.3203	-140.47	-1869.094	-598.863
18	27.5080	.98107	.19281	-.1965	-188.00	-5171.504	1016.201
20	5.2358	.76492	.64368	-.8415	-238.84	-1250.518	1052.311

Sum = 2,468.65

TABLE XVI

Calculation of $\int \frac{B}{2}(1+K_2K_4) \frac{dS}{d\xi} \cos \frac{2\pi x}{\lambda} \left(\xi + \frac{1}{\pi} \frac{dS}{d\xi} \right) dx$ in equation (3)

$\lambda = 600$ Ft.

Pitch

Station	(1) (3)x(4)Table	(2) (3)Table	(3) (4)Table	(1)x(2)x(3)
0	1.294	238.31	2.6054	800.952
2	813.172	188.46	.8403	128775.992
4	1201.048	140.21	.1967	33107.287
6	1450.992	94.33	-.3203	-43872.344
8	89.746	47.86	-1.0634	-4567.771
10	0	0	-3.8680	0
12	39.298	-47.79	3.8680	-7267.806
14	1029.792	-94.40	1.0595	-102996.501
16	1220.648	-140.47	.3203	-54920.147
18	1755.468	-188.00	-.1965	64850.573
20	369.757	-238.84	-.8415	74306.970
Sum				= 88,222.200

TABLE XVII
PITCH AND HEAVE CONSTANTS

$$\frac{\pi^2}{2} = \frac{(3.1416)^2}{1200} = 0.008225$$

$$\frac{4\pi}{\lambda^2} = \frac{(4)(3.1416)}{36 \times 104} = 0.349 \times 10^{-4}$$

$$\frac{\pi V_s}{4C} = \frac{(3.1416)(18.579)}{(4)(-55.5)} = -0.2629$$

$$\frac{4V_s}{3C\lambda} = \frac{(4)(18.579)}{(3)(-55.5)(600)} = -7.439 \times 10^{-4}$$

$$\rho g = 64 \text{ LB/Ft.}^3$$

$$h = 2 \times 1/2 \text{ in.} = \frac{200}{2 \times 12} \text{ Ft.} = 8.333$$

TABLE XVIII

Calculation of values for determining a, d, D, A in equation (1)

$$\lambda = 600 \text{ Ft.}$$

Heave

$$a = m + \rho \int SK_2 K_4 d\xi \quad d = D = \rho \int (SK_2 K_4) \xi d\xi$$

$$A = J + \rho \int SK_2 K_4 \xi^2 d\xi$$

Station	(1) S	(2) K ₂ K ₄	(3) (1)x(2)	(4) SM	(5) (3)x(4)	(6) ξ	(7) (5)x(6)	(6)x(7)
0	95.5	0	0	1	0	240.95	0	0
2	621.0	.394	244.67	4	978.68	192.76	188650.36	36364243.39
4	1351.0	.625	844.37	2	1688.74	14.57	244462.00	35341871.34
6	1830.0	.748	1368.84	4	5475.36	96.38	527715.20	50861190.98
8	1970.0	.813	1601.61	2	3202.22	48.19	154314.98	7436438.89
10	1980.0	.920	1821.60	4	7286.40	0	0	0
12	1963.0	.810	1590.03	2	3180.06	-48.19	-15324.71	7384977.27
14	1798.0	.783	1326.92	4	5307.68	-96.38	-511554.20	49303593.80
16	1340.0	.647	866.98	2	1733.96	-144.57	-250678.60	36240605.20
18	647.0	.530	342.91	4	1371.64	-192.76	-264397.33	50965229.33
20	7.95	1.39	11.05	1	11.05	-240.95	-2662.50	641529.37

Sum = 30,235.79

Sum = -60,397.28

Sum = 274,539,678.0

TABLE XIX

Calculation of values of coefficient (b) in equation (1)

$$\lambda = 600 \text{ Ft.}$$

Heave

$$b = \int N(\xi) d\xi$$

$$N(\xi) = \rho g^2 \frac{\bar{A}^2}{\omega_e^3}$$

$$\bar{A} = 2e \frac{-\omega_e^2 S}{gB} \sin \frac{\omega_e^2 B}{2g}$$

Station	(1) $\frac{\omega_e^2 B}{2g}$	(2) $\sin \frac{\omega_e^2 B}{2g}$	(3) $\frac{\omega_e^2 S}{gB}$	(4) $\frac{-\omega_e^2 S}{e gB}$	(5) (2)x(4)	(6) $(5)^2 = \frac{\bar{A}^2}{4}$	(7) SM	(6)x(7)
0	.008	.008	2.055	.128	.00102	.00010404x10 ⁻²	1	.000104x10 ⁻²
2	.264	.2610	.395	.674	.1759	3.098x10 ⁻²	4	12.392x10 ⁻²
4	.515	.4925	.460	.632	.3113	9.672x10 ⁻²	2	19.344x10 ⁻²
6	.635	.5930	.507	.602	.3570	12.745x10 ⁻²	4	50.980x10 ⁻²
8	.652	.6068	.532	.588	.3568	12.745x10 ⁻²	2	25.490x10 ⁻²
10	.652	.6068	.533	.587	.3562	12.674x10 ⁻²	4	50.696x10 ⁻²
12	.652	.6068	.526	.590	.3580	12.816x10 ⁻²	2	25.632x10 ⁻²
14	.649	.6044	.487	.614	.3711	13.764x10 ⁻²	4	55.056x10 ⁻²
16	.566	.5360	.416	.660	.3538	12.535x10 ⁻²	2	25.070x10 ⁻²
18	.366	.3570	.311	.732	.2613	6.828x10 ⁻²	4	27.352x10 ⁻²
20	.057	.057	.024	.9764	.0557	.310x10 ⁻²	1	.310x10 ⁻²

Sum = 292.322x10⁻²

TABLE XX

Calculation of values for determining coefficients c and g in equation (1)

$$\lambda = 600 \text{ Ft.}$$

Heave

$$c = \int \rho g B d\xi \quad g = \rho g \int B \xi d\xi - V_s b$$

Station	(1) B	(2) SM	(3) (1)x(2)	(4) ξ	(5) (3)x(4)	(4)x(5)
0	0.87	1	0.87	240.95	209.63	50510.35
2	28.20	4	112.8	192.76	21743.33	4191244.29
4	55.00	2	110.0	144.57	15902.70	2299053.34
6	67.70	4	270.8	96.38	26099.70	2515489.09
8	69.60	2	139.2	48.19	6708.05	323260.92
10	69.60	4	279.4	0	0	0
12	69.60	2	139.2	-48.19	-6708.05	323260.92
14	69.20	4	276.8	-96.38	-26677.98	2571223.71
16	60.40	2	120.8	-144.57	-17464.06	2524779.15
18	39.10	4	156.4	-192.76	-30147.66	5811262.94
20	6.10	1	6.1	-240.95	-1469.79	354145.90

Sum = 1611.37

Sum = -11804.13

Sum = 20,964,230.6

TABLE XXI

Calculation of values for determining coefficient e of equation (1)

$$\lambda = 600 \text{ Ft.}$$

Heave

$$e = \int N(\xi) \xi d\xi - 2V_s \rho \int (SK_2 K_4) d\xi - V_s \rho \int \xi dSK_2 K_4$$

Station	(1) (6)x(7)Table	(2) ξ	(3) (1)x(2)	(4) (2)x(3)
0	.000104x10 ⁻²	240.95	0	0
2	12.392x10 ⁻²	192.76	2388.30x10 ⁻²	4603.11
4	19.344x10 ⁻²	144.57	2795.60x10 ⁻²	4042.18
6	50.980x10 ⁻²	96.38	4913.45x10 ⁻²	4735.15
8	25.490x10 ⁻²	48.19	1228.36x10 ⁻²	591.77
10	50.696x10 ⁻²	0	0	0
12	25.632x10 ⁻²	-48.19	-1235.11x10 ⁻²	595.20
14	55.056x10 ⁻²	-96.38	-5306.68x10 ⁻²	5114.89
16	25.070x10 ⁻²	-144.38	-3624.37x10 ⁻²	5239.22
18	27.352x10 ⁻²	-192.76	-5271.99x10 ⁻²	10162.30
20	.310x10 ⁻²	-240.95	-74.69x10 ⁻²	179.97

Sum = -41.87 Sum = 35,263.79

TABLE XXI (Continued)

$$V_s \rho \int \xi^2 d(SK_2 K_L) = V_s \rho \int \xi^2 \frac{\partial(SK_2 K_L)}{\partial \xi} d\xi$$

Station	(1) $f \left[\frac{\partial(SK_2 K_L)}{\partial \xi} d\xi \right]$	(2) Scale correction $= \frac{400}{48.19} = 8.30$	(3) $(2) \times \xi$	(4) SM	(5) $(3) \times (4)$	$(3) \times (4) \times \xi$
0	-.55	-4.565	-1099.94	1	-1099.94	-265030.54
2	-.95	-7.885	-1519.91	4	-6079.64	-1171911.41
4	-1.50	-12.45	-1799.90	2	-3599.80	-520423.09
6	-1.00	-8.30	-799.95	4	-3199.80	-308396.72
8	-.60	-4.98	-239.79	2	-479.58	-23110.96
10	0	0	0	4	0	0
12	.70	5.81	-279.98	2	-559.96	26984.47
14	.90	7.47	-719.96	4	-2879.84	277558.98
16	1.25	10.375	-1499.91	2	-2999.82	433683.98
18	1.05	8.72	-1680.00	4	-6720.00	1294000.00
20	0.675	5.60	-1350.00	1	-1350.00	325100.00
Sum = -28,968.38						Sum = 68,453.8

TABLE XXII

Calculation of heaving force and pitching moment in equation (1)

HEAVE

$$F = \frac{\rho}{3} 2 \rho g h \left[(I) - \frac{\pi^2}{2\lambda} (II) - \frac{4}{\lambda^2} (III) - \frac{4V_s}{4c} (IV) - \frac{4V_s}{3\lambda c} (V) \right]$$

$$F = (16.06)(1066) \left[351.5 - (8.224 \times 10^{-3})(24014.1) + (0.349 \times 10^{-4})(1349609.87) + (-0.2629)(96.0576) - (-7.445 \times 10^{-4})(7971.215) \right]$$

$$F = \underline{3,112,066.33 \text{ Lbs.}}$$

PITCH

$$M = \frac{\rho}{3} 2 \rho g h \left[(I) \int \left(\xi + \frac{1}{\pi} \frac{dS}{d\xi} \right) dx - \frac{\pi^2}{2\lambda} (II) \int \left(\xi + \frac{1}{\pi} \frac{dS}{d\xi} \right) dx + \frac{4\pi}{\lambda^2} (III) \int \left(\xi + \frac{1}{\pi} \frac{dS}{d\xi} \right) dx + \frac{\pi V_s}{4c} (IV) \int \left(\xi + \frac{1}{\pi} \frac{dS}{d\xi} \right) dx - \frac{V_s 4}{3\lambda c} (V) \int \left(\xi + \frac{1}{\pi} \frac{dS}{d\xi} \right) dx \right]$$

TABLE XXII (Continued)

$$M = 17,119.96 \left[60,177.08 - (.0082)(2,878,952) + (.349 \times 10^{-4})(133,851,467) + (.263)(2468.65) - (88,222.2)(7.44 \times 10^{-4}) \right]$$

$$M = \underline{696,054,431.3 \text{ Ft.-Lbs.}}$$

TABLE XXIII

Final calculation of values of coefficients of equation (1)

CONSTANTS

$$a = m + \rho \int SK_2K_4 d\xi$$

$$m = \frac{(17.800)(2240)}{32.2} = 1,238,260 \frac{\text{Lb. Sec.}^2}{\text{Ft.}}$$

$$\rho \int SK_2K_4 d\xi = (16.06)(1.9876)(302,350.79) \\ = 965,152.30 \frac{\text{Lb. Sec.}^2}{\text{Ft.}}$$

$$a = 2,203,412 \frac{\text{Lb. Sec.}^2}{\text{Ft.}}$$

$$A = J + \rho \int (SK_2K_4) \xi^2 d\xi$$

$$J = mr^2 \quad r = 0.25L$$

$$J = \frac{(1,238,260)(481.9)^2}{(4)^2} = 17,970,867,380 \text{ Lb. Sec.}^2 \text{ Ft.}$$

$$\rho \int SK_2K_4 \xi^2 d\xi = (1.9876)(16.06)(274,539,678) \\ = 8,763,581,125.28 \text{ Lb. Sec.}^2 \text{ Ft.}$$

$$A = 17,970,867,380 + 8,763,581,125$$

$$A = 26,734,448,800 \text{ Lb. Sec.}^2 \text{ Ft.}$$

$$d = D = \rho \int SK_2K_4 \xi d\xi \\ = (1.9876)(16.06)(-67397.28)$$

$$D = -2151388.5$$

TABLE XXIII (Continued)

$$\begin{aligned}
 b &= \int N(\xi) d\xi \\
 &= \frac{4\rho g^2}{\omega^3} (16.06)(2.923) \\
 &= \frac{(4)(1036.84)(31.92)(2.923)}{(.46909)}
 \end{aligned}$$

$$b = 824,895 \frac{\text{Lb. Sec.}}{\text{Ft.}}$$

$$\begin{aligned}
 B &= \int N(\xi) \xi^2 d\xi - 2V_s D - V_s \rho \int \xi^2 d(SK_2 K_4) \\
 \int N(\xi) \xi^2 d\xi &= (8841.135)(31.92)(35263.8) \\
 &= 9,951,762,799.0
 \end{aligned}$$

$$2V_s D = (2)(18.578)(-2151388.5)$$

$$= -79,945,596.66$$

$$\begin{aligned}
 V_s \rho \int \xi^2 d(SK_2 K_4) &= (18.579)(31.92)(68,453.8) \\
 &= 40,595,970.0
 \end{aligned}$$

$$B = 9,991,112,425 \text{ Lb. Sec. Ft.}^2$$

$$\begin{aligned}
 E &= \int N(\xi) \xi d\xi - V_s \rho \int \xi d(SK_2 K_4) \\
 \int N(\xi) \xi d\xi &= (-41.87)(31.92)(8841.135) \\
 &= -11,816,095.2
 \end{aligned}$$

$$\begin{aligned}
 V_s \rho \int \xi d(SK_2 K_4) &= (-18.579)(31.92)(28,968.38) \\
 &= -17,179,408.0752
 \end{aligned}$$

$$E = 5,363,313 \text{ Lb. Sec.}$$

$$\begin{aligned}
 e &= \int N(\xi) \xi d\xi - 2V_s \rho \int (SK_2 K_4) d\xi - V_s \rho \int \xi d(SK_2 K_4) \\
 \int N(\xi) \xi d\xi &= -11,816,095 \\
 V_s \rho \int \xi d(SK_2 K_4) &= -17,179,241 \\
 2V_s \rho \int SK_2 K_4 d\xi &= (2)(18.579)(965,152.3) \\
 &= 35,863,100
 \end{aligned}$$

$$e = -30,499,954 \text{ Lb. Sec.}$$

TABLE XXIII (Continued)

$$c = \rho g \int B d\xi = (31.92)(32.2)(1611.37)$$

$$c = 1,656,198.0 \text{ Lb. Ft.}$$

$$C = \rho g \int B \xi^2 d\xi - V_S E$$

$$= (1027.82)(20,964,230.6) - (18.579)(5,363,146)$$

$$C = 21,447,814,000 \text{ Lb. Ft.}$$

$$g = \rho g \int B \xi d\xi - V_S b = (1027.82)(-11804.13) - (18.579)(824,895)$$

$$g = -27,459,070 \text{ Lb.}$$

$$G = \rho g \int B \xi d\xi$$

$$G = -12,132,520.9 \text{ Lb.}$$

TABLE XXIV

Calculation of heave and pitch for ship without fins

$$\bar{z} = \frac{\bar{MQ} - \bar{FS}}{\bar{QR} - \bar{PS}}$$

$$\theta = \frac{\bar{FR} - \bar{MP}}{\bar{QR} - \bar{PS}}$$

$$P = -a\omega_e^2 + j b \omega_e + c$$

$$Q = -d\omega_e^2 + j e \omega_e + g$$

$$R = -D\omega_e^2 + j E \omega_e + g$$

$$S = -A\omega_e^2 + j B \omega_e + C$$

$$P = (-2,203,386)(.60372) + j(824,895)(0.777) + 1,656,198$$

$$P = 325,954 + j 640,943$$

$$Q = (2,151,388.5)(0.60372) + j(-30,499,954)(0.777) - 27,459,070$$

$$Q = -26,160,234 - j 23,698,464$$

$$R = 1,298,836.26 + j(5,363,146)(.777) - 12,132,520.9$$

$$R = -10,833,684.64 + j 4,167,164$$

$$S = (-26,734,448,000)(.60372) + j(9,991,112,400)(.777) + 21,447,814,000$$

$$S = 5,307,693,000 + j 7,763,094,335$$

$$QR = (-26,160,234 - j 23,698,464)(-10,833,684.64 + j 4,167,164)$$

$$QR = 382,167,120,718,316 + j 147,727,708,603,064$$

TABLE XXIV (Continued)

$$PS = (325,954 + j 640,943)(5,307,693,000 + j 7,763,094,335)$$

$$PS = -3,245.6946 \times 10^{12} + j 5,932.3403 \times 10^{12}$$

$$QR - PS = 3,627.8617 \times 10^{12} - j 5,784.6126 \times 10^{12}$$

$$= \sqrt{46.623123 \times 10^{30}}$$

$$= 6827 \times 10^{12} / \underline{-\tan^{-1} 1.782}$$

$$QR - PS = 6827 \times 10^{12} / \underline{-60.7^\circ}$$

$$\bar{MQ} - \bar{FS} = (j 696,054,431)(-26,160,234 - j 23,698,464)$$

$$- (3,112,066)(5,307,693,000 - j 7,763,094,335)$$

$$= -22.470 \times 10^{12} - j 42,368.209 \times 10^{12}$$

$$= \sqrt{5.049 \times 10^{26} + 17.9506 \times 10^{32}}$$

$$= 42,370 \times 10^{12} / \underline{\tan^{-1} 1885}$$

$$\bar{MQ} - \bar{FS} = 42.370 \times 10^{12} / \underline{270^\circ}$$

$$\bar{Z} = \frac{42370 / 270}{6827 / \underline{-60.7^\circ}}$$

$$\bar{Z} = 6.2062 \text{ Ft.} / \underline{-29.3^\circ}$$

$$2\bar{Z} = \underline{12.41 \text{ Ft.} / \underline{-29.3^\circ}}$$

$$\theta = \frac{\bar{FR} - \bar{MP}}{QR - PS}$$

$$\bar{FR} - \bar{MP} = (3,112,066)(-10,833,684 + j 4,167,164)$$

$$- (j 696,054,431)(325,954 + j 640,943)$$

$$= 412.4161 \times 10^{12} - j 213.9132 \times 10^{12}$$

$$= \sqrt{170,087.015 + 45758.861 \times 10^{12}}$$

$$\bar{FR} - \bar{MP} = 464.7 \times 10^{12} / \underline{\tan^{-1} 0.5186} = 27.4^\circ$$

$$\theta = \frac{464.7 / 27.4^\circ}{6827 / \underline{-60.7^\circ}} = 0.06807 \text{ rad} / \underline{88.1^\circ}$$

$$2\theta = \underline{0.06807 \times 57.319^\circ / 88.1^\circ} = \underline{7.8034^\circ / 88.1^\circ}$$

TABLE XXV

Calculations of effect of hydrofoil on the ship motions for effective
fin AR = 4.0

$$F_L = \frac{1}{2} \rho \frac{\partial C_L}{\partial \alpha} \left(\theta - \frac{-\dot{z} - \dot{\theta} l + V_w}{V_s} \right) A V_s^2$$

$$A = \text{Area of hydrofoil} = \frac{2(1.4)(2.8)(10,000)}{144}$$

$$= 544.44 \text{ Ft.}^2$$

$$V_s = 18.579 \text{ Ft./Sec.}$$

$$\text{For infinite wing section: } \left(\frac{\partial C_L}{\partial \alpha} \right)_{\infty} = 5.73$$

$$\text{For finite aspect ratio: } \frac{\partial C_L}{\partial \alpha} = \frac{\left(\frac{\partial C_L}{\partial \alpha} \right)_{\infty}}{1 + \frac{\left(\frac{\partial C_L}{\partial \alpha} \right)_{\infty}}{\pi A R}}$$

$$\frac{\partial C_L}{\partial \alpha} = \frac{5.73}{1 + \frac{5.73}{(\pi)(4)}} = 3.94$$

$$\lambda = 600 \text{ Ft.}$$

$$F_L = \left(\frac{1}{2} \right) \left(\frac{64}{32.2} \right) (3.9378)(544.4)(18.579)^2 \left[\theta - \frac{-\dot{z} - \dot{\theta} l + V_w}{V_s} \right]$$

$$= 7.3581 \times 10^5 \left(\theta - \frac{-\dot{z} - \dot{\theta} l + V_w}{V_s} \right)$$

$$z = 6.2062 \text{ Ft. } \angle -29.3^\circ$$

$$z = 6.2062 \cos (\omega_\theta t - 29.3^\circ)$$

$$\frac{dz}{dt} = -6.2062 \omega_\theta \sin (\omega_\theta t - 29.3^\circ)$$

$$\theta = 3.9017^\circ \angle 88.1^\circ = 0.06807 \text{ rad } \angle 88.1^\circ$$

$$\theta = 0.06807 \cos (\omega_\theta t + 88.1^\circ)$$

$$\frac{d\theta}{dt} = -0.06807 \omega_\theta \sin (\omega_\theta t + 88.1^\circ)$$

$$\omega_\theta = 0.770 \text{ rad/sec.}$$

TABLE XXV (Continued)

$$\left| \frac{dz}{dt} \right|_{\max} = (6.2062)(0.777) = 4.822 \text{ Ft./sec.}$$

$$\left| \frac{d\theta}{dt} \right|_{\max} = (0.06807)(0.777) = 0.05289 \text{ rad/sec.}$$

$$\tan^{-1} \frac{\dot{z}_1}{V_s} = \frac{4.822}{18.579} = \tan^{-1} 0.25954 = 14.55^\circ = 0.254 \text{ rad}$$

$$\text{Phase} - \frac{\dot{z}}{V_s} = -29.3 + 90 + 180 = 240.7^\circ$$

Assuming fin is mounted at the forward perp.

$$l = \text{distance from CG to fin} = 240.95 \text{ Ft.}$$

$$\therefore \tan^{-1} \left| \frac{\dot{\theta}_1}{V_s} \right| = \frac{(0.05289)(240.95)}{18.579} = 34.5^\circ = 0.603 \text{ rad}$$

$$\text{Phase} - \frac{\dot{\theta}_1}{V_s} = 88.1 + 270 = -1.9^\circ$$

$$v_w = \frac{-2\pi hc}{\lambda} \cdot \frac{2\pi y}{\lambda} \cos \left[\left\{ \frac{2\pi}{\lambda} (x - \omega_\theta t) \right\} + \frac{\pi}{2} \right]$$

$$x = 265 \text{ Ft.}$$

$$\begin{aligned} v_w &= \frac{(2\pi)(100)(55.5)}{(12)(600)} \cdot \frac{-2\pi(28.67)}{600} \cos \left[\frac{2\pi}{600} (265 - \omega_\theta t) + \frac{\pi}{2} \right] \\ &= 4.84 \cdot^{-0.30} \cos \left[2.775 - .010475 \omega_\theta t + 1.5708 \right] \\ &= (4.84)(0.7405) \cos (4.3458 - 0.010475 \omega_\theta t) \end{aligned}$$

$$v_w = 3.584 \cos (249.11^\circ - 0.010475 \omega_\theta t)$$

$$\tan^{-1} \left| \frac{v_w}{V_s} \right|_{\max} = \tan^{-1} \frac{3.584}{18.579} = 10.9^\circ = 0.1902 \text{ rad.}$$

$$\text{Phase} = 249.11^\circ$$

Calculation of virtual mass of fin:

$$m_i = \frac{2 a^2 b^2}{a^2 b^2}$$

TABLE XXV (Continued)

$$\text{Model: } a = \frac{(2)(2.8)}{2}$$

$$a^2 = \frac{(5.6)^2}{4} = \frac{31.36 \text{ in}^2}{4}$$

$$b^2 = \frac{(1.4)^2}{4} \text{ in}^2 = \frac{1.96 \text{ in}^2}{4}$$

$$\text{Ship: } a^2 = \frac{313600}{(144)(4)} = \frac{2177.77}{4}$$

$$b^2 = \frac{19600}{(144)(4)} = \frac{136.11}{4}$$

$$a^2 b^2 = 296,416.3$$

$$m_i = \frac{(1.9875)(2\pi)(296,416.3)}{(16) \sqrt{\frac{136.11}{4} + \frac{2177.77}{4}}}$$

$$m_i = \frac{76,917.17}{(8)} \frac{\text{Lb. sec.}^2}{\text{Ft.}} = \Delta a = 9614.64 \frac{\text{Lb. sec.}^2}{\text{Ft.}}$$

$$\Delta J = m_i l^2$$

$$\Delta J = \frac{(76,917.17)}{8} (240.95)^2 = 558,196,555.9 \text{ Lb. sec.}^2 \text{ Ft.} = \Delta A$$

$$F_1 = 0.73581 \times 10^6 \left(\theta - \frac{\dot{z}}{V_s} - \frac{\dot{\theta}_1}{V_s} + \frac{V}{V_s} \right)$$

$$\Delta g = 0.73581 \times 10^6$$

$$\Delta c = (0.73581 \times 10^6)(240.95) = 177.293 \times 10^6$$

$$\Delta b = -\frac{0.73581}{18.579} \times 10^6 = -0.03960 \times 10^6$$

$$\Delta E = -\frac{177.293 \times 10^6}{18.579} = -9.5426 \times 10^6$$

$$\Delta e = -9.5426 \times 10^6$$

$$\Delta B = (-9.5426 \times 10^6)(240.95) = -2299.28947 \times 10^6$$

$$F' = + 0.0396 \times 10^6 V_w$$

$$M' = 9.5426 \times 10^6 V_w$$

$$V_w = 3.584 \cos (\omega_{\theta} t - 110.89) = 3.584 (\cos 69.11^\circ - j \sin 69.11^\circ)$$

$$V_w = (1 - 1.262 - j 3.355) e^{j \omega_{\theta} t}$$

TABLE XXV (Continued)

$$\begin{aligned}
F' &= \left[-0.049752 - j 0.132858 \right] \times 10^6 e^{j\omega_e t} \\
M' &= \left[-12.04276 - j 32.0154 \right] \times 10^6 e^{j\omega_e t} \\
F &= 3.112066 \times 10^6 - \left[0.0499752 - j 1.32858 \right] \times 10^6 \\
F &= 3.0620908 \times 10^6 - j 0.132858 \times 10^6 \\
M &= j 696.054431 \times 10^6 + \left[-12.04276 - j 32.0154 \right] \times 10^6 \\
M &= -12.04276 \times 10^6 + j 664.03903 \times 10^6 \\
a &= 2.2033 \times 10^6 + 0.00961464 \times 10^6 \\
a &= 2.213 \times 10^6 \\
A &= 26,734.448 \times 10^6 + 558.196556 \times 10^6 \\
A &= 27292.645 \times 10^6 \\
D &= d = -2.151388 \times 10^6 \\
b &= 824,895 + 39600 \\
b &= 864,495 \\
B &= 9991.1124 \times 10^6 + 2290.28947 \times 10^6 \\
B &= 12201.4133 \times 10^6 \\
E &= 5.363146 \times 10^6 + 9.5426 \times 10^6 \\
E &= 14.905746 \times 10^6 \\
e &= -30.499954 \times 10^6 + 9.5426 \times 10^6 \\
e &= -20.957354 \times 10^6 \\
c &= 1.656198 \times 10^6 \\
C &= 21,447.814 \times 10^6 - 177.293 \times 10^6 \\
C &= 21,270.521 \times 10^6 \\
g &= -27.459070 \times 10^6 - 0.73581 \times 10^6 \\
g &= -28.19488 \times 10^6
\end{aligned}$$

TABLE XXV (Continued)

$$G = -12.132521 \times 10^6$$

$$P = -a\omega_e^2 + j b\omega_e + c$$

$$= \left[-(2.213)(0.60372) + j(.864495)(0.777) + 1.656198 \right] \times 10^6$$

$$P = \left[0.320168 + j 0.671713 \right] \times 10^6$$

$$Q = -d\omega_e^2 + j e\omega_e + g$$

$$Q = \left[-26.896044 - j 16.283864 \right] \times 10^6$$

$$R = -D\omega_e^2 + j E\omega_e + G$$

$$R = (-10.833685 + j 11.581765) \times 10^6$$

$$S = -A\omega_e^2 + j B\omega_e + c$$

$$S = (4793.821 + j 9480.495571) \times 10^6$$

$$QR = (479.98566 - j 135.09636) \times 10^{12}$$

$$PS = (-4833.344 + j 6255.4232) \times 10^{12}$$

$$QR - PS = 8312 \times 10^6 \angle -50.41^\circ$$

$$\bar{M}Q = (11137.024 - j 17683.919) \times 10^{12}$$

$$\bar{F}S = (15938.675 + j 28393.241) \times 10^{12}$$

$$\bar{M}Q - \bar{F}S = 46270 \times 10^6 \angle -95.94^\circ$$

$$\bar{F}R = (-31.634997 + j 36.903758) \times 10^{12}$$

$$\bar{M}P = (-449.89936 + j 204.51477) \times 10^{12}$$

$$\bar{F}R - \bar{M}P = 450.7 \times 10^6 \angle -21.85^\circ$$

$$Z = \frac{46270 \angle -95.94^\circ}{8312 \angle -50.41^\circ} = 5.567 \text{ Ft.} \angle -45.53^\circ$$

$$2Z = 11.134 \text{ Ft.} \angle -45.53^\circ$$

$$\theta = \frac{450.7 \angle -21.85^\circ}{8312 \angle -50.41^\circ} = 0.05422 \text{ rad} \angle 28.56^\circ$$

$$2\theta = 6.216^\circ \angle 28.56^\circ$$

TABLE XXVI

Calculations of effect of hydrofoil on ship's motions for effective
fin AR = 2.0

$$F_L = 1/2 \rho A V^2 \left(\theta - \frac{\dot{\theta} l}{V_s} - \frac{\dot{z}}{V_s} + \frac{V_w}{V_s} \right) \frac{\partial C_L}{\partial \alpha}$$

$$\frac{\partial C_L}{\partial \alpha} = \frac{5.73}{1 - \frac{5.73}{(\pi)(2)}} = 2.9962$$

$$A = \frac{(4)(8)}{144} \times 10,000 = 2222.2 \text{ Ft.}^2$$

$$\begin{aligned} F &= (2.9962)(0.9943658)(2222.2)(345.18) \left(\theta - \frac{\dot{\theta} l}{V_s} - \frac{\dot{z}}{V_s} + \frac{V_w}{V_s} \right) \\ &= 2.285 \times 10^6 \left(\theta - \frac{\dot{\theta} l}{V_s} - \frac{\dot{z}}{V_s} + \frac{V_w}{V_s} \right) \end{aligned}$$

Without fins:

$$\left| \frac{dz}{dt} \right|_{\max} = (6.2062)(0.777) = 4.822 \text{ Ft./sec.}$$

$$\left| \frac{d\theta}{dt} \right|_{\max} = (0.06807)(0.777) = 0.05289 \text{ rad/sec.}$$

$$\tan^{-1} \left| \frac{\dot{z}}{V_s} \right| = 14.55^\circ = 0.254 \text{ rad}$$

$$\text{Phase} = 240.7^\circ$$

$$\tan^{-1} \left| \frac{\dot{\theta} l}{V_s} \right| = \frac{(0.05289)(240.95)}{18.579} = 34.5^\circ = 0.603 \text{ rad}$$

$$\text{Phase} = -1.9^\circ$$

$$V_w = \frac{2\pi h c}{\lambda} e^{\frac{2\pi y}{\lambda}} \cos \left[\left\{ \frac{2\pi}{\lambda} (x - \omega_e t) \right\} + \frac{\pi}{2} \right]$$

$$h = \frac{100}{12} = 8.333 \text{ Ft.}$$

$$y = 28.677 + \frac{300}{12} = 53.677 \text{ Ft.}$$

TABLE XXVI (Continued)

$$V_w = 4.84 e^{-0.5621} \cos(\omega_e t + 249.11^\circ) = 2.763 \cos(\omega_e t + 249.11^\circ)$$

$$\tan^{-1} \left| \frac{V_w}{V_s} \right|_{\max} = \frac{2.763}{18.579} = 8.46^\circ = 0.14759 \text{ rad}$$

$$M_i = \frac{\rho 2\pi a^2 b^2}{\sqrt{a^2 + b^2}}$$

$$a = \frac{(8)(100)}{(2)(12)} = 33.333$$

$$a^2 = 1111.1$$

$$b = \frac{(4)(100)}{(2)(12)} = 16.666$$

$$b^2 = 277.755$$

$$m_i = 0.10341 \times 10^6 = \Delta a$$

$$\Delta A = (0.10341)(58,056.9) \times 10^6$$

$$\Delta A = 6,003.567 \times 10^6$$

$$\Delta g = 2.285 \times 10^6$$

$$\Delta C = (240.95)(2.285 \times 10^6) = 550.643 \times 10^6$$

$$\Delta b = \frac{-2.285 \times 10^6}{18.579} = -0.123 \times 10^6$$

$$\Delta e = \Delta E = -\frac{550.643 \times 10^6}{18.579} = -29.6379 \times 10^6$$

$$\Delta B = (-29.6379 \times 10^6)(240.95) = -7141.252 \times 10^6$$

$$a = 0.10341 \times 10^6 + 2.203386 \times 10^6 = 2.3068 \times 10^6$$

$$A = 26,734.448 \times 10^6 + 6003.567 \times 10^6 = 32,738 \times 10^6$$

$$d = D = -2.151388 \times 10^6$$

$$b = 0.824895 \times 10^6 + 0.123 \times 10^6 = 0.947895 \times 10^6$$

$$B = 9,991.1124 \times 10^6 + 7141.252 \times 10^6 = 17,132.364 \times 10^6$$

TABLE XXVI (Continued)

$$\begin{aligned}
 E &= 5.363146 \times 10^6 + 29.6379 \times 10^6 = 35.001 \times 10^6 \\
 e &= -30.499954 \times 10^6 + 29.6379 \times 10^6 = -0.862054 \times 10^6 \\
 c &= 1.656198 \times 10^6 \\
 C &= 21,447.814 \times 10^6 - 550.643 \times 10^6 = 20,897.171 \times 10^6 \\
 g &= -27.45907 \times 10^6 - 2.2853 \times 10^6 = -29.74437 \times 10^6 \\
 F &= 3.112060 \times 10^6 - (0.12304)(0.984152) \times 10^6 - j(0.12304)(2.58177 \times 10^6) \\
 F &= 2.991897 \times 10^6 - j 0.3176609 \times 10^6 \\
 M &= -29.09857 \times 10^6 + j(696.054431 \times 10^6 - 76.54039 \times 10^6) \\
 M &= -29.09857 \times 10^6 + j 619.514040 \times 10^6
 \end{aligned}$$

Calculations of Heave and Pitch

$$z = \frac{\bar{M}Q - \bar{F}S}{QR - PS} \qquad \theta = \frac{\bar{F}R - \bar{M}P}{QR - PS}$$

$$P = -a\omega_e^2 + j b \omega_e + c$$

$$Q = -d\omega_e^2 + j e \omega_e + g$$

$$R = -D\omega_e^2 + j E \omega_e + G$$

$$S = -A\omega_e^2 + j B \omega_e + C$$

$$P = 0.263539 \times 10^6 + j 0.736514 \times 10^6$$

$$Q = -28.74437 \times 10^6 - j 0.6698159 \times 10^6$$

$$R = -10.13252 \times 10^6 + j 27.1950 \times 10^6$$

$$S = 1132.585 \times 10^6 + j 13311.8468 \times 10^6$$

$$QR = 309.46764 \times 10^{12} - j 774.91432 \times 10^{12}$$

$$PS = -9505.8817 \times 10^{12} + j 4342.3548 \times 10^{12}$$

$$QR - PS = 9815.3493 \times 10^{12} - j 5117.2691 \times 10^{12}$$

$$QR - PS = 11080 \times 10^{12} \angle -27.54^\circ$$

TABLE XXVI (Continued)

$$\bar{M}_Q = 1251.32364 \times 10^{12} - j 17788.05 \times 10^{12}$$

$$\bar{F}_S = 7617.2309 \times 10^{12} + j 39467.897 \times 10^{12}$$

$$\bar{M}_Q - \bar{F}_S = -6365.9073 \times 10^{12} - j 57255.94 \times 10^{12}$$

$$\bar{M}_Q - \bar{F}_S = 57630 \times 10^{12} \angle -96.36^\circ$$

$$\bar{z} = \frac{57630}{11080} \angle \frac{-96.36}{-27.54} = 5.2012 \angle -68.82^\circ$$

$$2\bar{z} = 10.4 \text{ Ft.} \angle -68.82^\circ$$

$$\bar{F}_R = -21.676668 \times 10^{12} + j 84.583344 \times 10^{12}$$

$$\bar{M}_P = -588.85218 \times 10^{12} + j 136.01489 \times 10^{12}$$

$$\bar{F}_R - \bar{M}_P = 570.7 \times 10^{12} \angle -5.18^\circ$$

$$\theta = \frac{570.7}{11080} \angle \frac{-5.18^\circ}{-27.54^\circ} = 0.0515 \text{ rad} \angle 22.36^\circ$$

$$2\theta = 5.90^\circ \angle 22.36^\circ$$

TABLE XXVII

Summary of theoretical calculations

<u>Quantity</u>	<u>No Fin</u>	<u>Fin-AR = 2.0</u>	<u>Fin-AR = 4.0</u>	<u>Units</u>
a	2.203×10^6	2.307×10^6	2.213×10^6	$\frac{\text{Lb. sec.}^2}{\text{Ft.}}$
A	26.734×10^9	32.738×10^9	27.293×10^9	Lb. sec. 2 Ft.
b	0.824×10^6	0.948×10^6	0.864×10^6	$\frac{\text{Lb. sec.}}{\text{Ft.}}$
B	9.991×10^9	17.132×10^9	12.201×10^9	Lb. sec. Ft. ²
c	1.656×10^6	1.656×10^6	1.656×10^6	Lb. Ft.
C	21.448×10^9	20.897×10^9	21.270×10^9	Lb. Ft.
d = D	-2.151×10^6	-2.151×10^6	-2.151×10^6	Lb. sec. ²
e	-30.499×10^6	-0.862×10^6	-20.957×10^6	Lb. sec.
E	5.363×10^6	35.001×10^6	14.906×10^6	Lb. sec.
g	-27.459×10^6	-29.744×10^6	-28.195×10^6	Lb.
G	-12.132×10^6	-12.132×10^6	-12.132×10^6	Lb.
F	3.112×10^6	$(2.992 - j0.318) \times 10^6$	$(3.062 - j0.133) \times 10^6$	Lb.
M	$j696.054 \times 10^6$	$(-29.099 + j619.514) \times 10^6$	$(-12.043 + j664.039) \times 10^6$	Ft. Lb.
2Z	$12.41 \text{ Ft.} / \underline{-29.3^\circ}$	$10.40 \text{ Ft.} / \underline{-68.82^\circ}$	$11.134 \text{ Ft.} / \underline{-45.53^\circ}$	
2Θ	$7.8034^\circ / \underline{88.1^\circ}$	$5.90^\circ / \underline{22.36^\circ}$	$6.216^\circ / \underline{28.56^\circ}$	

TABLE XXVIII

Wave conditions for AR = 4.0 fin

<u>Wave length (Ft.)</u>	<u>Double amplitude wave height (Ft.)</u>
400	12.9 (No observed vibrations)
	13.3*
	20.0
	21.7
	23.0
500	13.3
	15.0*
	16.7
	17.5†
	20.8 Ft.**
600	15.8 (Vibrations observed for all
	16.7* wave heights tested)
	17.5
	18.4
	19.2**
800	20.0
	20.0*
	21.6†
	25.0
	23.3*
1000	23.8
	24.3
	24.8
	25.4
	25.8
	26.4
	27.4†
	28.5
	29.4

* Denotes wave conditions at which the model motions were photographed.

† Vibrations observed at this wave height and above.

** Violent vibrations observed at this wave height and above.

TABLE XXIX

Summary of results for model with AR = 4.0 fin for varying wave lengths

	<u>Ship</u>	<u>Model</u>
Reynolds number for fin	1.69 x 10 ⁶	1.765 x 10 ⁴
Speed	11 knots	1.1 knots
Predicted fin angle of breakdown	21.5°	8°
Predicted fin maximum lift coefficient (without suction)	1.25	.65
Double wave height at which fin emerges	17.06 Ft.	2.05 in.
Measured maximum model lift coefficient (assuming constant slope)	<u>Without suction</u> .655	<u>With suction</u> .95
Measured model fin angle of breakdown	21°	18°
Slope of fin lift curve	<u>Predicted</u> 3.93/radian	<u>Measured</u> 3.95/radian
Computed fin angle of attack	<u>From computed amp.</u> 45°	<u>From measured amp.</u> 55°

Computed pitch double amplitude = 6.216°

Computed heave double amplitude = 11.134 Ft.


Ship double wave height = 16.7 Ft.

Suction rate = 0.6 GPM

For $\lambda/L = 1.25$ ($\lambda = 600$ Ft.)

TABLE XXX

Summary of results for model with AR = 4.0 fin

	<u>MODEL</u>						
	Wave length λ (Ft.)	Double computed wave height (in.)	V(KTs)	Double amplitude Pitch (degree) (measured)		Double amplitude Heave (inches) (measured)	
				With suction	Without suction	With suction	Without suction
.831	4.0	1.6	1.65	2.40	2.45	.348	.342
1.04	5.0	1.8	1.35	5.12	7.0	1.375	1.34
1.25	6.0	2.0	1.10	8.65	7.36	1.81	1.91
1.65	8.0	2.4	1.40	10.15	9.48	2.74	2.67
2.08	10.0	2.8	1.50		9.01		2.74


	<u>SHIP</u>						
	Wave length λ (Ft.)	Double computed wave height (Ft.)	V(KTs)	Double amplitude Pitch (degree) (measured)		Double amplitude Heave (Feet) (measured)	
				With suction	Without suction	With suction	Without suction
.831	400	13.3	16.5	2.40	2.45	2.90	2.85
1.04	500	15.0	13.5	5.12	7.00	11.45	11.1
1.25	600	16.7	1.10	8.65	7.36	15.0	15.9
1.66	800	20.0	14.0	10.15	9.48	22.8	22.3
2.08	1000	23.3	15.0		9.01		22.8

TABLE XXXI

Summary of results for AR = 2.0 fin for $\lambda = 600$ Ft.

	<u>Ship</u>	<u>Model</u>
Reynolds number	4.84×10^6	5.05×10^4
Predicted angle of breakdown	31°	14.5°
Predicted fin maximum lift coefficient (without suction)	1.49	.600
Double wave height at which bow emerges	16 Ft.	1.92 in.
Measured model fin angle of breakdown	<u>Without suction</u> 15°	<u>With suction</u> 20°
Measured model maximum lift coefficient	.570	.810
Slope of fin lift curve	<u>Measured</u> 3.02 per radian	<u>Predicted</u> 2.93 per radian

$$\lambda_s = 600 \text{ Ft.}$$

$$\lambda = 6.0$$

$$\text{Ship speed} = 11 \text{ knots}$$

$$\text{Model speed} = 1.1 \text{ knots}$$

$$\text{Suction rate} = 1.35 \text{ GPM}$$

TABLE XXXII

Summary of results for $\Lambda = 600$ Ft. at varying wave heights for AR = 2.0 fin

MODEL

Double wave height (in.)	Pitch double amplitude (degrees)		Pitch* calculated	Heave double amplitude (inches)		Heave* calculated (Ft.)	Computed hydrodynamic angle of attack (degrees)	
	With suction	Without suction		With suction	Without suction		From measured model motions	From computed model motions
.6	2.70	2.90	1.78	.743	.960	.349	16.6	11.7
.8	3.10	2.62	2.36	.852	.948	.48	18.9	15.6
1.0	3.50	2.87	2.94	.948	.948	.612	21.2	19.5
1.2	3.98	3.30	3.54	1.068	1.066	.743	24.35	23.4
1.4	4.30	4.10	4.12	1.25	1.27	.877	28.3	27.3
1.6	5.00	4.85	4.72	1.31	1.44	1.01	32.7	31.2
1.8	5.80	5.55	5.30	1.49	1.58	1.14	36.1	35.1
2.0	5.95	6.05	5.88	1.80	1.68	1.27	38.6	39.0
2.2	5.95	6.45	6.48	1.88	1.73	1.41	40.3	42.9
2.4	5.95	6.70	7.06	2.00	1.94	1.53	42.3	46.8

SHIP

Double wave height (Ft.)	Pitch double amplitude (degrees)		Pitch* calculated (degrees)	Heave double amplitude (Ft.)		Heave* calculated (Ft.)	Computed hydrodynamic angle of attack (degrees)	
	With suction	Without suction		With suction	Without suction		From measured model motions	From measured model motions
5.0	2.70	2.90	1.78	5.20	8.00	2.9	16.6°	11.7
6.66	3.10	2.62	2.36	7.10	7.95	4.0	18.9	15.6
8.33	3.50	2.87	2.94	7.90	7.90	5.1	21.2	19.5
10.0	3.98	3.30	3.54	8.90	8.90	6.2	24.35	23.4
11.65	4.30	4.10	4.12	10.40	10.65	7.3	28.3	27.3
13.35	5.00	4.85	4.72	10.9	12.00	8.4	32.7	31.2
15.00	5.80	5.55	5.30	12.4	13.20	9.5	36.1	35.1
16.69	5.95	6.05	5.88	15.0	14.0	10.6	38.6	39.0
18.35	5.95	6.45	6.48	15.7	14.4	11.7	40.3	42.9
20.0	5.95	6.70	7.06	16.7	16.2	12.8	42.3	46.8

*Based upon the assumption that the slope of the lift curve line is constant for all fin angles of attack.

- Note: (1) No transverse bow vibrations were recorded on ships double wave heights below 11.63 Ft.
 (2) Minor transverse bow vibrations were recorded at ship double wave heights 13.35 and above.
 (3) Boundary layer suction did not reduce the vibrations observed.

TABLE XXXIII

Summary of descriptive data for NACA0018 airfoils used in this thesis

	<u>Aspect ratio (effective)</u>	<u>Thickness chord</u>	<u>Computed $\left(\frac{\partial C_L}{\partial \alpha}\right)_{\alpha=0}$</u>	<u>Half span</u>	<u>Chord</u>	<u>Proj.area</u>	<u>Chord length suction taken from LE</u>
Small fin	4	18%	3.93	2.8 in	1.4in.	7.83 in. ²	0.6 in.
Large fin	2	18%	2.98'	4 "	4 "	32 "	1.45 "

	<u>Max. suction rate</u>	<u>Position installed</u>	<u>Construction material</u>
Small fin	0.6 GPM	At baseline	Brass stock + brass sheet
Large fin	1.35 GPM	3 in. below baseline	Plexiglass stock + brass sheet

TABLE XXXIV

Summary of descriptive data for model and ship ($\lambda = 100$)

	<u>Model</u>	<u>Ship</u>
Length LWL	4.81 Ft.	481.9 Ft.
Beam (molded)	8.29 in.	69 Ft.
Draft (full load)	3.44 in.	28.67 Ft.
Wetted surface	4.402 Ft. ²	44036 Ft. ²
Displacement (full load)	39.21 Lbs.	17,800 Tons
Designed speed	1.65 Kts.	16.5 Kts.
Maximum speed	1.75 Kts.	17.5 Kts.
Block coefficient	0.6623	0.6623
Prismatic coefficient	0.6770	0.6770
Resonant frequency of bow	23 vib/sec	2.2 vib/sec
Fin Reynold's number @59°F		
Effective AR = 4.0	1.765×10^4 (FW)	1.69×10^6 (SW)
Effective AR = 2.0	5.05×10^4 (FW)	4.84×10^6 (SW)

B. Adjustment of radius of gyration of the model

The radius of gyration of the model was selected to be 25 per cent of the ships length. This was because, in the absence of specific information concerning the actual distribution of weights on the ship prototype, experience has shown that for ships of this type, the computed radius of gyration lies between .23L and .27L. Therefore, a selected value of .25L was considered reasonable.

After the model had been weighed and trimmed, the radius of gyration could be adjusted by moving fore and aft equal ballast weights longitudinally equal distances from the center of gravity. The method used was as follows:

The model was suspended fore and aft by two springs of equal length and equal spring constants.

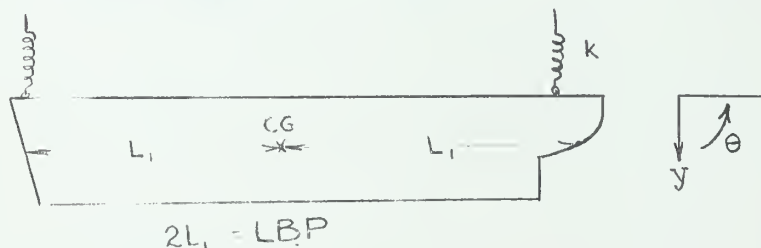


FIGURE XXXII. Description of notation in the calculation of model radius of gyration

The equation of vertical motion, neglecting damping is:

$$m \frac{d^2 y}{dt^2} + 2ky = 0$$

The equation of rotational motion about the CG is:

$$J \frac{d^2\theta}{dt^2} + 2kL_1^2 \theta = 0$$

Changing to complex notation:

$$-m\omega_y^2 y + 2ky = 0$$

$$-J\omega_\theta^2 \theta + 2k\theta L_1^2 = 0 \quad L_1 = \frac{1}{2}L$$

$$\frac{m\omega_y^2}{J\omega_\theta^2} = \frac{1}{L_1^2}$$

$$\text{Radius of gyration } \bar{r} = \sqrt{\frac{J}{m}} = \frac{1}{4}L = \frac{1L_1}{2}$$

$$\frac{\omega_y^2}{\omega_\theta^2} = \frac{J}{m} \frac{L}{L_1^2}$$

$$\frac{f_y^2}{f_\theta^2} = \frac{J}{m} \frac{1}{L_1^2} = \bar{r}^2 \frac{1}{L_1^2}$$

$$\frac{f_y^2}{f_\theta^2} = 1/4$$

$$\frac{f_y}{f_\theta} = 1/2$$

where f_y = frequency of heave

f_θ = frequency of pitch

$L_1 = 1/2 \text{ LWL}$

Consequently, when the frequency of heave was equal to 1/2 the frequency of pitch, the radius of gyration was 25% LWL.

C. Sample calculation of lift coefficient

This calculation is for the AR = 2 fin with boundary control suction at the rate of 2.06 GPM an area. Suction was taken over a chord distance 1.45 in. from the leading edge.

TABLE XXXV

Strain readings and resultant lift coefficients

<u>Angle of attack</u>	<u>Readings in microinches/inch</u>		<u>Average reading</u>	<u>Hose correction</u>	<u>Corrected reading</u>	<u>Lift</u>	<u>CL</u>
0	6	6	6	0	6	0.0432	0.0583
5	35	34	34.5	-6.5	28.0	0.202	0.272
10	64	64	64	-12.0	52.0	0.374	0.505
15	104	104	104	-18.5	85.5	0.616	0.831
20	124	131	127.5	-24.5	103.0	0.740	1.005
25	119	119	119	-30.5	88.5	0.637	0.860
30	124	119	121.5	-35.0	86.0	0.619	0.835
35	104	104	104	-38.0	66.0	0.475	0.641
40	105	112	108.5	-37.0	71.5	0.515	0.695
45	109		109.0	-32.0	77.0	0.555	0.750

In Table XXXV the strain was read on the Baldwin Strain Indicator as the fin angle of attack was increased from 0° to 45° and also as the angle was decreased from 45° to 0°. The results of the two runs were then averaged. This reading still had to be corrected for the influence of the steel tube which was tied to the aluminum bar. This correction was obtained by changing the fin angle of attack by 10° increments with the fin in water and then plotting the results (Figure VI). With the corrected readings the strain gage calibration curve was entered and the lift was obtained. The calibration curve was obtained by hanging weights on the bar in air and observing the strain indicated for a known weight. With the known lift at each angle of attack C_L was obtained using Equation (15).

For an angle of attack equal to 20°, the readings in microinches per inch were 124 and 131. The average reading was 127.5 microinches per inch.

The hose correction from Figure VI at 20° is -24.5. Therefore, the corrected reading is $127.5 - 24.5 = 103$.

Referring to Figure VI the slope is:

$$\frac{280 \text{ microinches/inch}}{2 \text{ lbs.}} = \frac{140 \text{ microinches}}{\text{in.lb.}}$$

Therefore:

$$\frac{103}{140} = .740 \text{ lbs.}$$

$$C_L = \frac{L}{\frac{1}{2}\rho AV^2} \quad (15)$$

$$L = .740 \text{ lbs.}$$

$$\rho = 1.93 \frac{\text{lb. sec.}^2}{\text{ft.}^4}$$

$$A = \frac{32 \text{ in.}^2}{144 \text{ in.}^2/\text{ft.}^2} = .222 \text{ ft.}^2$$

$$V = 1.857 \text{ ft./sec.}$$

Substituting and solving:

$$C_L = \frac{.740 (2)}{(1.93)(.222)(1.857)^2} = 1.005$$

D. Sample calculation of hydrodynamic fin angle of attack from ship motions

The sample calculation made here is for the AR = 2.0 finned model, scaled to prototype dimensions, operating in waves for $\lambda/L = 1.25$ and a double wave height of 1.0 inches. For the prototype this wave height is equivalent to a single amplitude value of 4.166 Ft.

From the theoretical calculations for a $\lambda/L = 1.25$ and a single wave height amplitude = 8.33 Ft. the following information is available:

$$\theta = 2.95^\circ = 0.0515 \text{ radians; phase} = 22.36^\circ$$

$$z = 5.20 \text{ Ft.; phase} = -68.82^\circ$$

$$V_w = 2.73 \text{ Ft./sec.; phase} = 249.11^\circ$$

If it is assumed that heave and pitch amplitudes at constant speeds vary linearly with wave height and that the phase relationships are unchanged, for a 4.166 Ft. wave the above values become:

$$\theta = \frac{(4.166)(2.95^\circ)}{8.33} = 1.47 = 0.0257 \text{ radians; phase} = 22.36^\circ$$

$$z = \frac{(4.166)}{(8.33)} (5.20) = 2.60 \text{ Ft.; phase} = -68.82^\circ$$

$$V_w = \frac{(4.166)}{(8.33)} (2.763) = 1.38 \text{ Ft.; phase} = 249.11^\circ$$

Next it is necessary to determine the hydrodynamic angle of attack by vectorially adding $\theta - \frac{\dot{\theta}_1}{V_s} - \frac{\dot{z}}{V_s} + \frac{V_w}{V_s}$ taken from equation (7) where

$$\theta = 0.0257 \text{ radians; phase} = 22.36^\circ$$

$$\begin{aligned} \tan^{-1} - \frac{\dot{\theta}_1}{V_s} &= \tan^{-1} - \frac{\theta \omega_e 1}{V_s} = \tan^{-1} - \frac{(0.0257)(0.777)(240.9)}{18.579} \\ &= \tan^{-1} - 0.258 = -14.47^\circ = -0.253 \text{ radians} \\ \text{phase} &= 90^\circ + 22.36^\circ = 112.36^\circ \end{aligned}$$

$$\begin{aligned} \tan^{-1} - \frac{\dot{z}}{V_s} &= \tan^{-1} - \frac{z \omega_e}{V_s} = \tan^{-1} - \frac{(2.60)(0.777)}{18.579} = \tan^{-1} - 0.109 \\ &= -6.23^\circ = -0.110 \text{ radians} \\ \text{phase} &= 90^\circ - 68.82^\circ = 21.18^\circ \end{aligned}$$

$$\begin{aligned} \tan^{-1} \frac{V_w}{V_s} &= \tan^{-1} \frac{1.38}{18.579} = \tan^{-1} 0.0743 \\ &= 4.25^\circ = 0.745 \text{ radians} \\ \text{phase} &= 249.11^\circ \end{aligned}$$

These four vectors are plotted and added graphically in Figure V. The resulting hydrodynamic angle of attack = 15.1°.

Because of the linearity of model motions with wave height, this procedure can be repeated for any wave height desired. The results are also plotted on this figure.

The values of hydrodynamic angles of attack for the measured motions are also plotted in the same figure. For these calculations the measured values of heave and pitch were used, although the phase relationships were assumed to be the same as the computed values.

E. Sample calculation of bow immersion

Wave height at which bow immerses for AR2 fin operating in regular waves 600 feet long at a ship speed equal to 11 knots.

The model depth at the bow scaled to ship size was determined to be 50.4 feet.

The freeboard is equal to the depth minus draft:

$$\text{Frbd.} = D - H = 50.4 - 28.67 = 21.73 \text{ feet}$$

To determine the wave height (h) at which the bow will immerge is computed by equation (11)

$$\bar{h}_B - \bar{\theta}_1 - \bar{z} = H_B$$

$$\text{solved for } (H_B) = 21.73 \text{ feet}$$

where \bar{h}_B , $\bar{\theta}_1$ and \bar{z} are the instantaneous drafts at bow due to wave height, pitch, and heave respectively, measured from the load waterline.

For simplicity, any value of wave height can be selected and the resulting three components added. Since the draft at the bow is a linear function of wave height, the original wave height selected can be modified to balance the above equation.

Therefore, for $h = 8.33$ feet with the wave crest at station 11,

$$h_B = 8.33 \text{ ft. phase } \frac{2\pi x}{\lambda} = 159^\circ$$

From measurements:

$$\theta = .0523 \text{ radians} \quad \text{phase} = 22.36^\circ$$

$$\theta_1 = (.0523)(240.9) = 12.61 \text{ ft.} \quad \text{phase} = 22.36^\circ$$

$$z = 7.25 \text{ ft.} \quad \text{phase} = 68.82^\circ$$

The above three vectors added in equation (11). We find $H_B \text{ max} = 22.6 \text{ Ft.}$

$$\text{The bow will immerge when } h = (8.33) \frac{21.73}{22.6} = 8.0 \text{ Ft. or}$$

$$2h = 16 \text{ ft.}$$

The wave height of fin emergence can be computed in a similar way except

that $|H_B|$ = the load waterline draft of the ship = 28.67 ft.

APPENDIX C

SUPPLEMENTARY DISCUSSION

A. Boundary layer separation

Reference (8) discusses the influence of Reynolds number on the boundary layer separation by an airfoil. Reference (16) discusses the modifications of the boundary layer that result from using suction slots at various locations on an airfoil surface. The tests made in this thesis were conducted at Reynolds numbers below the critical value for the NACA 0018 fin of 1×10^6 . At these low Reynolds numbers, at low angles of attack, the flow over most of top surface is laminar. As the angle of attack is increased, the pressure distribution over the fin chord is such that it decreases to a minimum at a point near the leading edge after which it again increases when proceeding toward the trailing edge. This increasing pressure gradient causes the water in the laminar boundary layer to fail to flow with consequent separation and reduction in fin lift. The point at which this occurs, called the laminar separation point, is closely behind the point of minimum pressure.

At very low Reynolds numbers the region behind the point of ~~turbulent~~ ^{laminar} separation is called a transition region.

In the tests made without suction, laminar separation at low angles of attack had the effect of reducing the slope of the lift curve. As the angle of attack increased the point of laminar separation moved forward further reducing the slope of the lift curve until finally the angle of attack was sufficient for the laminar separation point to be almost at the leading edge. At this point the lift decreased.

Applying suction to the leading surface resulted in pumping off the laminar boundary layer in the area to which suction was applied. This delayed laminar separation in this area and reduced the transition region. The result was that suction straightened the slope of the lift curve and increased the angle of breakdown until the suction rate was no longer sufficient to prevent laminar separation. The rounding of the lift curve was caused by laminar separation occurring near to but a little behind the leading edge. As the angles of attack increased, the separation point moved forward until the lift decreased as before. Properly controlled suction applied to the selected areas at the trailing as well as the leading edge could be expected to delay laminar separation until the separation point was at the leading edge after which a sharp break in the lift curve could be expected.

At Reynolds numbers above the critical range, which would be expected for a ship fin, a point of turbulent separation could be expected near the trailing edge. Behind this point a turbulent boundary layer would exist which would have greater resistance to separation than does the laminar boundary layer. In this case, as the Reynolds number is increased, the point of turbulent separation would move forward, thus decreasing the transition region with resultant increase in lift and angle of breakdown. Finally at sufficiently high Reynolds numbers, the turbulent separation point would occur at the same point as the laminar separation point. This causes a very sharp break in the lift curve.

B. Vortex ventilation

In the pitching cycle when the bow is pitching down, the effective angle of attack for the fin is large. Accompanying this high angle of

attack are vortices and flow separation. Since the fin is near the surface (or has actually penetrated the surface) in the above condition, air enters the vortices and forms a fully ventilated bubble on the low pressure surface of the fin. This bubble is an air bubble surrounded by a film of water in such a manner that the water does not touch the upper surface of the fin.

At much lower angles of attack and speeds, these air bubbles would form in the vortices trailing the fin. However as speed and angle of attack increase the bubbles travel forward along a helical path inside the vortices until they reach the fin when flow separation takes place. The resultant full bubble formation causes a large reduction in the lift of the fin. Figure XIX shows the fully developed bubble on the fin which has been attributed to vortex ventilation.

If boundary layer separation does not occur, though vortex ventilation results in the formation of air bubbles aft of the fin, there is no appreciable loss of lift. Therefore boundary layer control would reduce the adverse effects of vortex ventilation if flow separation could be eliminated.

APPENDIX D
BIBLIOGRAPHY

- (1) Abbot, I.H., von Doenhoff, A.E., and Stivers, L.S., Jr., "Summary of Airfoil Data", U.S.N.A.C.A. Report No. 824, 1945
- (2) Abkowitz, M.A., "Seakeeping Considerations in Design and Research", N.E. Section, SNAME, vol. 65, 1957
- (3) Abkowitz, M.A., Ship Behavior at Sea, "Anti-Pitching Fins", Stevens Institute of Technology, Second Summer Seminar, June 16 thru 20, 1958, pp. 25-28
- (4) Abkowitz, M.A. and Paulling, J.R., Jr., "The Ship Model Towing Tank at M.I.T.", Transactions, SNAME, vol. 61, 1953
- (5) Dabovich, M.R., "Activated Anti-Pitching Fins", S.M. Thesis, Department of Naval Architecture and Marine Engineering, M.I.T., 1958
- (6) Edstam, V.B. and Vytlačil, N., "Hydrodynamic Effect of a Bow Hydrofoil on Three Vessel Types", S.M. Thesis, Department of Naval Architecture and Marine Engineering, M.I.T., 1955
- (7) Eshbach, O.W., Handbook of Engineering Fundamentals, 2nd Edition, Section 7, Wm. Wiley and Sons, N.Y., 1952
- (8) Jacobs, E.N., and Sherman, A., "Airfoil Section Characteristics as Affected by Variations of the Reynolds Number", U.S.N.A.C.A. Report 586, 1937
- (9) Korvin-Kroukovsky, B.V., "Investigation of Ship Motions in Regular Waves", Transactions, SNAME, vol. 63, 1955
- (10) Korvin-Kroukovsky, B.V. and Jacobs, W.R., "Pitching and Heaving Motions of a Ship in Regular Waves", Transactions, SNAME, vol. 65, 1957
- (11) Lewis, F.M., "Propeller Testing Tunnel at the Massachusetts Institute of Technology", Paper presented at the Spring meeting of SNAME, held at M.I.T., May, 1939
- (12) Lewis, E.V. and Jacobs, W.R., "Preliminary Study of the Influence of Controlled Fins on Ship Pitching and Heaving", E.T.T. Note 379, February 8, 1957
- (13) Mandel, P., "Some Hydrodynamic Aspects of Appendage Design", Transactions, SNAME, vol. 61, 1953
- (14) Moyer, LT. D.R., U.S.N. and Michaels, Lt. R.J., U.S.N., "Hydrodynamically Similar Roll Stabilization Fins for Ship Model Tests", S.M. Thesis, Department of Naval Architecture and Marine Engineering, M.I.T., 1958

BIBLIOGRAPHY (Continued)

- (15) Paulling, J.R., Jr., "Model Seaworthiness Testing Technique and the Effect of Anti-Pitching Fins", S.M. Thesis, Department of Naval Architecture and Marine Engineering, M.I.T., 1953
- (16) Racisz, S.F., "Experimental Investigation of the Effectiveness of Various Suction-Slot Arrangments as a Means for Increasing the Maximum Lift of the NACA 653-018 Airfoil Section", U.S.N.A.C.A. RM L50A10, 1950
- (17) Wadlen, K.L., Ramsen, J.A. and Vaughan, V.L., Jr., "The Hydrodynamic Characteristics of Modified Rectangular Flat Plates Having Aspect Ratios of 1.00, 0.25, and 0.125 and Operating Near a Free Water Surface", U.S.N.A.C.A. Report 1246, 1955
- (18) Weinblum, G. and St. Denis, M., "On the Motions of Ships at Sea", Transactions, SNAME, vol. 58, 1950
- (19) Wiener, Z.B., "Report of Sea-Keeping Tests Done at the Towing Tank of Massachusetts Institute of Technology", S.M. Thesis, Department of Naval Architecture and Marine Engineering, M.I.T., 1958



thesM64

Boundary layer suction to control bow vi



3 2768 001 89122 9

DUDLEY KNOX LIBRARY